THE UNIVERSITY OF
SYDNEY

THE PHYSICS OF WATER LEAKS AND WATER NANOFLOWS

by

Wenwen Lei

A thesis submitted in
fulfilment of the requirements
for the degree of
Doctor of Philosophy

Faculty of Science
The University of Sydney
March, 2015

Abstract

The encapsulation of devices sensitive to moisture is necessary to prolong the operational lifetimes under adverse environmental conditions. Active implantable medical devices, solar cells, and organic light emitting diodes (OLEDs) have particularly stringent requirements on their encapsulations. Quantifying the flow of moisture is important in the design and verification of encapsulations for devices operating in adverse environments.

Flows of a wide variety of gases have been studied in the years since the pioneering paper of Knudsen appeared in 1909, with one important exception: water vapour, the flow of which has scarcely received any attention. Before we study flows of water vapour, nitrogen as the majority constituent of air and representative of ideal gas is selected to be a reference for water vapour. Theoretical predictions of flows in tubes are still developing until the present time. A convenient one is named *extended Navier-Stokes equations* which have only one equation for all flow regimes with one empirical parameter, approaching the classical Navier-Stokes equations at small Knudsen number (*Kn*) and the Smoluchowski extension of the Knudsen equation at large *Kn*. Here we use the extended Navier-Stokes equations, as developed by Cha and McCoy in 1971, for predicting flow rates of nitrogen and water vapour through a 25 μm diameter silica glass cylindrical tube. In this thesis, flow rates of nitrogen and water are both under assumptions of isothermal conditions.

A recent unexpected finding from Holt et al. concerning ultra-fast water and air flows in carbon nanotubes due to large slip length and atomically smooth walls is significant. In contrast, Gruener and Huber did not obtain ultra-fast nitrogen flow rates in silicon nanotubes. This leaves us with important questions concerning the main factors that affect

flows in tubes. Liquid water has enhanced flow rates in nanotubes, but what about for water vapour? Do the enhanced flow rates only occur in nanotubes? In order to test the enhanced flow rates in another material, here we first measure nitrogen flow rates through silica cylindrical microtubes across a wide range of *Kn* (0.0048 ~ 12.4583) using a two-chamber method. These measurements enable the evaluation of the tangential momentum accommodation coefficient (TMAC) α defined by Maxwell which describes the collision situations between molecules of fluid and walls. This is the first study for nitrogen flows through a cylindrical microtube across all flow regimes. Smoluchowski's equation relies on the TMAC definition of Maxwell, recently challenged by Arya et al. We find that the nitrogen flow obeys the Cha and McCoy equation with a large value of α, unlike carbon nanotubes which show flows consistent with a small value of α. Silica microtubes are therefore not atomically smooth. We find the flow at small *Kn* has α = 0.91 and at large *Kn* has α close to one, consistent with the redefinition of accommodation coefficient by Arya et al., which also resolves a problem in the literature where there are many observations of α of less than one at small *Kn* and many equal to one at large *Kn*.

Although the silica microtubes are not atomically smooth, we still obtain fast transport of water vapour compared to the predictions from the equation of Cha and McCoy over a restricted range of pressures using the two-chamber method and a mass loss method. We attribute the excess flows to two effects. One is that a thin adsorbed layer of chain-like water on the walls reducing the TMAC at lower inlet pressures, an effect recently found for humid nitrogen flows over silica. The other is due to liquid or two-phase flow existing

in the tube for inlet pressure close to saturation pressure. A theory for the effect is developed using an approximation to the Langmuir adsorption.

In practice, interdiffusive flow of moisture in a background of air at atmospheric pressure occurs more commonly. However, there is no study of mass flow rates under these conditions. In this thesis, we measure the interdiffusive flow rates of water and water vapour in the same silica microtubes with and without air at atmospheric pressure using mass loss method and compare experimental results with ideal gas interdiffusive flow theory. We find interdiffusive flows of water vapour in air agree with the theory except for the case where water vapour partial pressures are close to the saturation pressure. When liquid is present, it causes an enhancement of the interdiffusive flow by up to three orders of magnitude. The flow enhancement is attributed to two phase flows that have been observed in silica tubes of similar size.

Using the best available theories we predict the dominant types of flow as a function of channel diameter and we make recommendations on the testing for moisture hermeticity in devices requiring high performance moisture barriers.

Acknowledgements

First I would like to express my deepest appreciation to my supervisor Professor David McKenzie, for his dedicated supervision and endless support and encouragement. I have been immeasurably fortune to have a supervisor who provided generously of his time and expertise, who edited my thesis and articles so carefully and patiently and who released my huge burden on tuition fees by providing financial support. I am most grateful to have had his talent, thoughts, humour and kindness. I could not have imagined completing my PhD without his guidance and support.

To my associate supervisors, Professor Marcela Bilek I want to thank her to provide me the chance to study in University of Sydney and the help for arguing for the scholarship application; Dr. Yongbai Yin who helped me on setting up my experimental apparatus and discussed with me for better understandings of problems. I also want to acknowledge Dr. Michelle Rigozzi who shared a lot of useful study materials, gave many valuable discussions and encouraged me with her passion and earnest. For building my experimental apparatus, I would like to thank Mr. David McFall for making our design come true, Mr. Chulatunga Daluwatu for providing Baratron gauges which are necessary for my experiments, Dr. Cenk Kocer for discussing testing methods and providing gauges and valves for my system. I would also like to thank the Workshop in School of Physics for making small elements and solving problems for my experimental apparatus.

On a personal note I would like to thank my family who support me to make my dream come true. Their love, understanding and encouragement are important for me. I would also thank all my friends accompanying with me during these years: the spirit supports and helps from Xinying Cheng, the talking, having dinners and shopping with Heather Main, the helps on Matlab from Wenliang Lu, the helps and cares from Thao Tran, Kai Hu, Antti Aronen, Nicole Fong, Elena Kosobrodova, Kosta Tsoutas and also all the other people who have helped me in the Physics building. Thank you all to make my study and life in Australia wonderful.

Declaration of originality

This thesis contains no material which has been presented for a degree at this or any other university and, to best of my knowledge and belief, contains no copy or paraphrase of work published by another person, except where duly acknowledged in the text.

Wenwen Lei

Publications

1. Lei, W., McKenzie, D., Revisiting Maxwell's tangential momentum accommodation coefficient A study of nitrogen flow in a silica microtube across all flow regimes, *Ann. Phys.*, 351, 828-836, 2014.
2. Lei, W., McKenzie, D., Enhanced water vapor flow in silica microtubes explained by Maxwell's tangential momentum accommodation and Langmuir's adsorption, *Phys. Rev. Lett.*, 2015 (submitted).
3. Lei, W., Svehla, M., Fong, N., McKenzie, D., The missing link in measuring water leaks in micro- and nano-channels, Science, 2015 (submitted).

Table of Contents

Chapter 1 Introduction

Gaseous and liquid flows through tubes have been studied for more than two hundred years. Many famous names are associated with this field, including Poiseuille, Graham, Maxwell, Stokes, Boltzmann, Knudsen, Smoluchowski and others. Nowadays, the prevention of moisture penetration through barriers is more and more important to ensure long enough lifetimes for devices. Food packaging is a well known application in which the environmental moisture penetration through the barrier is prevented. Sensitive food products require a water vapour transmission rate (WVTR) of less than 100 $g/m^2/day$ [1]. The WVTR can be measured using commercial equipment for water vapour transmission rate testing, including the apparatus manufactured by MOCON [2]. Electrical and electronic devices demand much higher moisture barrier performance. Example devices are organic light emitting diodes (OLEDs), solar cells and active implantable medical devices that have electronic components. The WVTR of OLED encapsulation needs to be lower than 10^{-6} $g/m^2/day$ to guarantee a 10 year lifetime [3]. Implantable medical devices, such as Cochlear implants, demand even better moisture barriers to enable the devices to work well for the normal lifetime of a human. Electronic devices are very sensitive to moisture, which presents a challenge to develop new materials with a high barrier performance and low cost. In order for industry to guarantee the performance it is essential to develop a sensitive, accurate and convenient measurement method for a very low WVTR. Therefore, it is important to understand the behaviour of water vapour and liquid water as they flow through tubes and permeate through materials.

This thesis reports an investigation of the flow rates of noncondensable single phase gases and condensable single/two-phase vapours through silica microtubes, in addition to theories for predicting gas and liquid flows in micro- and nano-tubes. Chapter 2 reviews the history and development of fluid flows during 200 years in brief and points out where there is a lack of understanding of water vapour flows.

Chapter 3 presents the basic definitions and equations of fluid flows. A useful dimensionless number, the Knudsen number [4], is introduced to define the flow regimes (continuum, slip, transition and molecular flow regimes).

In Chapter 4, nitrogen flow rates were first studied through microtubes theoretically and experimentally as an example of noncondensable gas. Although there are many studies of a wide variety of gases, this is the first study that measures the flow of nitrogen through a cylindrical microtube over all flow regimes. The Maxwell tangential momentum accommodation coefficient (TMAC) is obtained from the experimental data and revisited based on a recent study by Arya et al. [5].

In Chapter 5, the measurement of water vapour flows in silica microtubes is undertaken at the first time. This is essential knowledge for the quantification of moisture penetration. Two measurement methods which are two-chamber method and mass loss method agree well. Enhanced water vapour transport is found due to either variable TMAC caused by adsorption of ice-like layers or two-phase/liquid flows arising from the inlet pressure at the tube that is near the saturation pressure of water vapour. A theory for TMAC of water on silica surface is proposed based on the adsorption isotherms of water. This work presents a solution for the difficulty raised by Seo et al. [6] in the understanding of the behaviour of nitrogen colliding with a thin water layer adsorbed on a silica surface.

Chapter 6 provides the theoretical and experimental results of interdiffusive flow which is a practical case since devices requiring protection usually operated in a background of air. The theory of interdiffusive flow has been developed recently, while the experimental results of water diffusing into atmospheric air through microtubes have not been reported to my knowledge. The interdiffusive water vapour flow rate in air in a 25 μm tube is predicted to be approximately three orders of magnitude lower than the flow rate for water vapour only without air. This prediction is in agreement with experiment for small vapour pressures while enhanced interdiffusive flow rates of water vapour are found to be due to two-phase/liquid flows when the inlet vapour pressure at the tube is near the saturation pressure of water.

Chapter 7 predicts the mass flow selectivity for helium, nitrogen and water vapour from the equation of Cha and McCoy and liquid water from the Poiseuille law and makes recommendations on moisture hermeticity testing of encapsulations for industry. It is concluded that helium leak testing, the most commonly used method in industry cannot predict water leak rates directly. This chapter also predicts the flow modes and their mass conductance as a function of tube diameter. Surface flow contributes significantly to flow rates only for very small nanotubes and liquid flow becomes dominant as diameter increases to approximately 40 nm.

REFERENCES

1. Kääriäinen, T.O., et al., *Atomic Layer Deposition on Polymer Based Flexible Packaging Materials: Growth Characteristics and Diffusion Barrier Properties.* Thin Solid Films, 2011. **519**(10): p. 3146-3154.

2. MOCON, *Aquatran Model 2 Brochure.* 2013.

3. Martínez-Landeros, V.H., et al., *Permeation Studies on Transparent Multiple Hybrid SiO_2-PMMA Coatings-Al_2O_3 Barriers on PEN Substrates.* J. Sol-Gel Sci. Technol. , 2011. **59**(2): p. 345-351.

4. Knudsen, M., *The laws of molecular and viscous flow through tubes (in German).* Ann. Phys. (Berlin), 1909. **28**: p. 75-130.

5. Arya, G., H.-C. Chang, and E. Maginn, *Knudsen Diffusivity of a Hard Sphere in a Rough Slit Pore.* Phys. Rev. Lett., 2003. **91**: p. 026102.

6. Seo, D., D. Mastropietro, and W.A. Ducker, *Gas flows near solids coated with thin water films.* J. Phys. Chem. C, 2013. **117**: p. 6235-6244.

Chapter 2 Previous Studies

2.1 Theories of Flows in a Tube

The first study on pressure driven viscous flow through tubes was done by Jean Louis Marie Poiseuille, a French anatomist. He devised the well known Poiseuille law for the flow rate in a cylindrical tube with an assumption of the flow velocity being zero at the walls [1]. For this no-slip boundary condition, the dominant forces are the viscous drag forces and the forces due to the pressure gradient in the tube. The Poiseuille law is applicable to liquid flow as well as to dense gaseous flow. For relatively dense gaseous flow, the Poiseuille equation can be derived from the famous Navier-Stokes equations with the help of the ideal gas law. However, when the mean free path of the gas becomes comparable with the dimensions of the tube, friction forces at the walls of the tube become more important than the viscous drag in the fluid. In this case, the Poiseuille law has to be corrected in order to provide accurate flow rates. Maxwell proposed boundary conditions at the walls that include a TMAC [2]. This allows the Poiseuille law to work in the slip flow regime with only one correction factor (first boundary conditions). For dilute gases, Knudsen had completed a theoretical and experimental investigation of flows in cylindrical tubes at low pressures in 1909 in which he derived the equation that bears his name for both cylindrical and rectangular tubes [3]. Knudsen assumes all the incident molecules diffuse after collision with the walls, which applies in most cases but shows limits in special cases where the walls are exceptionally smooth. The year after Knudsen's important paper, Smoluchowski [4] extended his equation by using Maxwell's

definition for TMAC which allows molecules to have either a diffuse or a specular reflection after collision.

For the intermediate transition flow regime, the Navier-Stokes equations with first order boundary conditions break down as Knudsen diffusion becomes more and more dominant, requiring higher order boundary conditions such as the Burnett and Woods equations. The Burnett and Woods equations are derived from the Boltzmann equation based on the Chapman-Enskog expansion of the velocity distribution function [5]. The Boltzmann equation is in turn derived from the Liouville equation [6], as a basic equation in fluid mechanics, and not only provides higher order boundary conditions but also predicts accurate flow rates of gases in arbitrary complex geometries for all flow regimes.

However, the Boltzmann equation is difficult to solve, encouraging the development of several approximate forms, for example, the linearised Boltzmann equation [7] and the Bhatnagar-Gross-Krook (BGK) equation [8-11] which may also be linearised. A combination of the Navier-Stokes equations and the Boltzmann equation was used for rectangular and elliptical tubes by Sharipov et al. [12-15]. There is another branch of theories named *extended* Navier-Stokes equations which have only one equation with an empirical parameter to match the behaviour of dense and dilute gases. The extended Navier-Stokes equations trend to the classical Navier-Stokes equations (the Poiseuille law) at high pressures and to the Knudsen equation at low pressures. Cha and McCoy [16] derived an extended Navier-Stokes equation for a cylindrical tube which works very well for various gases, such as nitrogen, air and carbon dioxide. Recently, Dongari et al. [17] devised an extended Navier-Stokes equation for a rectangular tube and showed that the extended Navier-Stokes equation predicts flow rates even better than the Boltzmann

equation does when compared with simulation methods such as the Direct Simulation Monte Carlo (DMSC) method. Extended Navier-Stokes equations are more convenient than other theories to be used owing to their closed analytical form.

For the derivation of the theories above, there are two useful works: the book of Karniadakis et al. [18] and the review of Sharipov [11]. The book by Karniadakis focuses on simulations for gas flow through two parallel plates for pressure driven flow (flow driven by pressure difference) and for liquid transport driven by surface tension and electrokinetic forces. The review of Sharipov provides numerical and analytical models on mass flow rate and heat flux but does not compare with experiment.

The translation of the theories above to the study of the hermeticity of encapsulations has led to an emphasis on ideal gas behaviour [19, 20], even for water permeation [21]. The flow of condensable gases and vapours such as carbon dioxide and organic vapours which may show strong departures from ideal gas behaviour in porous media has been reviewed by Choi et al. [22] but a discussion of water vapour flows is lacking. Reviews of the literature covering specifically moisture permeation rates have been limited to summaries of measurements of permeabilities rather than attempts to relate moisture permeability to theories based on microstructural properties.

2.2 Experimental Methods for Measuring Flow and Permeation

Measurement of gaseous flow rate in microtubes has been mainly studied in recent years. For gaseous flow rates under isothermal condition, the most common method is a two-chamber method for which the two chambers with set pressures are connected with a microtube. It is also named “constant volume technique” which has been used for

testing flow rates of nitrogen, helium, argon and carbon dioxide [23-26]. For condensable vapour flow rates, permeation rates are measured by gravimetric testing in which the mass of accumulated water is measured by weighing a test cell containing a water absorbing material such as a desiccant before and after a known exposure time to water vapour [27-29]. However, such tests are time consuming and not readily compatible with routine testing for performance compliance during manufacture. For this reason, testing for water penetration under accelerated conditions may be carried out in equipment such as that produced by MOCON [30]. In the MOCON equipment, water molecules are detected by their effect on electrical conductivity using a coulometric cell. While this method is more convenient than the gravimetric test, there remain significant time delays associated with the response time of the sensor and the time for the water background to come into equilibrium with and be cleared from the interior of the equipment. Mass spectrometry is a method of detecting and quantifying the partial pressures of gases present in a chamber that has been used for measuring water vapour permeation rates [31]. Mass spectrometry has an excellent sensitivity and offers some advantages in response time and sensitivity. However, it is still subject to the time delays in the system that result from the need for the flow rates to come to equilibrium and the need for residual or background water to be cleared from the system. The use of isotopically modified water with mass 20 such as H_2O^{18} [31] and heavy water D_2O^{16} are of considerable value in minimising the background of adventitious water vapour. There is a new WVTR testing system using mass spectrometer appearing in 2013, Vacutran [32]. In its brochure, it is said that "Vacutran enables WVTR measurement of barrier layers to better than 10^{-6} g/m^2/day". However, the service of Vacutran was stopped in the market place in 2014 and the technique has to be restudied. Nowadays, obtaining a better WVTR testing

limit than MOCON still has challenges. In addition, it is surprising that there is no measurement or theory applicable to water vapour flow rate measurement.

2.3 Flows in Nanotubes Challenge Classical Theories

The subject of water flows and permeation has received a resurgence of interest as part of a trend in which phenomena traditionally studied by observation on the macroscopic scale are now being viewed on the nanometre scale where new and often unexpected findings are being made. The availability of atomistic and molecular simulations has assisted this trend and has delivered valuable insights. The design of microfluidic devices requires an understanding of flow in small tubes and is an active field of research. As the dimensions of the tubes are reduced to achieve miniaturisation of the devices, the flow becomes dependent on the boundary conditions at the walls so that the permeability of the walls to the (usually aqueous) fluids becomes important (see for example [33]). An emerging field that relies on the permeation of fluids is that of drug delivery by means of particles, especially nanoparticles. These drug delivery particles are required to control the drug release to provide local administration of the drug [34].

Recent unexpected findings have challenged our understanding of flows in small tubes at low pressures [35-38] (shown in Figure 1(a)), for example, Holt et al. [35] found maximum enhancements of 2.1 for polycarbonate (PC) and 120 for double-walled carbon nanotubes (DWNTs) for air flow rate over Knudsen equation and the enhancements of 3.7 for PC and 8400 for DWNTs for liquid water permeability over Poiseuille law. Our understanding of the flow of condensable vapours in membranes has also been challenged in membranes with layered microstructures (see for example the work of Nair et al. [39] in which the flow of water is observed to be up to almost ten orders of magnitude higher

than the flow of helium, shown in Figure 1(b)). Such findings have outlined the need for deeper understanding in these fields and have driven a resurgence of interest into what seemed only a few years ago to be a mature research field with no surprises.

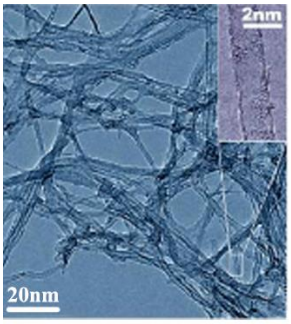

Membrane	Maximum enhancement over Knudsen equation (air)	Maximum enhancement over Poiseuille law (water)
DWNTs	120	8400
Polycarbonate	2.1	3.7

(a)

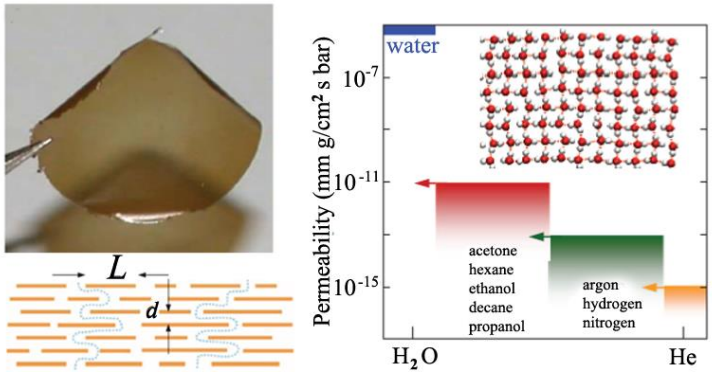

(b)

Figure 1 Reproduced pictures (a) from Holt et al. [35] and (b) from Nair et al. [39]. (a) The left picture is a transmission electron microscopy (TEM) picture of the grown DWNTs used by Holt et al. and the right table shows the enhancements for permeability of air over Knudsen model. (b) The left upper picture is a picture of a 1 μm thick graphene oxide (GO) film peeled off of a Cu foil and the lower one is a schematic view for possible permeation through the laminates with *L* (sizes of crystals of the GO film) over *d* (distance between the laminates) of 1000 approximately. The right picture shows the permeability of GO film with respect to water and various small molecules (argon, hydrogen and nitrogen) and other organic molecules (acetone, hexane, ethanol, decane and propanol) with an inset picture showing the schematic representation of the structure of monolayer water inside a graphene tube with $d = 7$ Å.

REFERENCES

1. Poiseuille, J.L.M., *Recherches Expérimentales sur le Mouvement des Liquides dans les Tubes de Trés Petits Diamétres (in French).* Compt. Rend. , 1841. **12**: p. 112-115.
2. Maxwell, J.C., *On stresses in rarified gases arising from inequalities of temperature.* Phil. Trans. R. Soc. Lond., 1879. **170**: p. 231-256.
3. Knudsen, M., *The laws of molecular and viscous flow through tubes (in German).* Ann. Phys. (Berlin), 1909. **28**: p. 75-130.
4. Smoluchowski, M., *To the kinetic theory of transpiration and diffusion of dilute gases (in German).* Ann. Phys. (Berlin), 1910. **33**: p. 1559-1570.
5. Burnett, D., *The Distribution of Molecular Velocities and the Mean Motion in A Non-Uniform Gas.* Proc. London Math. Soc., 1935. **39**(2): p. 385-435.
6. Cercignani, C., *The Boltzmann Equation and Its Applications (Applied Mathematical Sciences).* 1988, USA: Springer-Verlag.
7. Loyalka, S.K. and S.A. Hamoodi, *Poiseuille Flow of A Rarefied Gas in A Cylindrical Tube: Solution of Linearized Boltzmann Equation.* Phys. Fluids A, 1990. **2**(11): p. 2061-2065.
8. Cercignani, C., *Cylindrical Poiseuille Flow of a Rarefied Gas.* Phys. Fluids, 1966. **9**(1): p. 40-44.
9. Valougeorgis, D. and J.R. Thomas Jr, *Exact Numerical Results for Poiseuille and thermal Creep Flow in A Cylindrical Tube.* Phys. Fluids, 1986. **29**: p. 423-429.
10. S.S.Lo and S.K.Loyalka, *An Efficient Computation of Near-Continuum Rarefied Gas Flows.* J. Appl. Math. Phys., 1982. **33**: p. 419-424.

11. Sharipov, F., *Data on Internal Rarefied Gas Flows.* J. Phys.Chem. Ref. Data, 1998. **27**(3): p. 657-706.

12. Sharipov, F. and D. Kalempa, *Velocity Slip and Temperature Jump Coefficients for Gaseous Mixtures. I. Viscous Slip Coefficient.* Phys. Fluids, 2003. **15**(6): p. 1800-1806.

13. Sharipov, F., *Transport Phenomena through Gaseous Mixtures in Microchannels*, in *Fifth International Conference on Nanochannels, Microchannels and Minichannels*. 2007, ASME: Puebla, Mexico.

14. Sharipov, F., *Rarefied Gas Flow through a Long Rectangular Channel.* J. Vac. Sci. Technol. A, 1999. **17**(5): p. 3062-3066.

15. Graur, I. and F. Sharipov, *Gas Flow through An Elliptical Tube over the Whole Range of the Gas Rarefaction.* Eur. J. Mech. B-Fluid 2008. **27**: p. 335-345.

16. Cha, C.Y. and B.J. McCoy, *Application of third-order constitutive relations to Poiseuille flow of a rarefied gas.* J. Chem. Phys., 1971. **54**: p. 4373-4383.

17. Dongari, N., A. Sharma, and F. Durst, *Pressure-Driven Diffusive Gas Flows in Micro-Channels: From the Knudsen to the Continuum Regimes.* Microfluidics Nanofluidics, 2009. **6**(5): p. 679-692.

18. Karniadakis, G., A. Beskok, and N. Aluru, *Microflows and Nanoflows from fundamental to simulation*. 2005, USA: Springer Science+Business Media, Inc.

19. Greenhouse, H., *Hermeticity of Electronic Packages*. 2 ed. 2012, UK: Elsevier.

20. Dushmann, S., *Scientific Foundations of Vacuum Technique*. 2 ed. 1962, USA: John Wiley&Sons, Inc.

21. Vanhoestenberghe, A. and N. Donaldson, *The Limits of Hermeticity Test Methods for Micropackages.* Artif. Organs, 2011. **35**(3): p. 242-244.

22. Choi, J.-G., D.D. Do, and H.D. Do, *Surface diffusion of adsorbed molecules in porous media: monolayer, multilayer, and capillary condensation regimes.* Ind. Eng. Chem. Res., 2001. **40**: p. 4005-4031.

23. Hadj Nacer, M., et al., *Gas Flow through Microtubes with Different Internal Surface Coatings.* J. Vac. Sci. Technol. A, 2014. **32**(2): p. 021601.

24. Hadj Nacer, M., et al., *Experimental study of the gas flows through channels with circular cross sections.* J. Phys. Conf. Ser., 2012. **362**: p. 012025.

25. Ewart, T., et al., *Mass flow rate measurements in gas micro flows.* Exp. Fluids., 2006. **41**: p. 487-498.

26. Ewart, T., et al., *Mass flow rate measurements in a microchannel, from hydrodynamic to near free molecular regimes.* J. Fluid Mech., 2007. **584**: p. 337-356.

27. Choi, B.I., et al., *Determining Ultra-Low Moisture Permeation Measurement for Sealants on OLED Encapsulation.* J. Korean Phys. Soc., 2013. **61**(12): p. 2032-2035.

28. Carcia, P.F., et al., *Ca Test of Al_2O_3 Gas Diffusion Barriers Grown by Atomic Layer Deposition on Polymers.* Appl. Phys. Lett., 2006. **89**: p. 031915.

29. Miguel, O., M.J. Fernandez-Berridi, and J.J. Iruin, *Survey on Transport Properties of Liquids, Vapours, and Gases in Biodegradable Poly(3-hydroxybutyrate) (PHB).* J. Appl. Polym. Sci., 1997. **64**(9): p. 1849-1859.

30. MOCON, *Aquatran Model 2 Brochure.* 2013.

31. Zhang, X.D., et al., *Measurement of Reactive and Condensable Gas Permeation Using a Mass Spectrometer.* J. Vac. Sci. Technol. A, 2008. **26**(5): p. 1128-1137.

32. Vacutran, *VG Scienta Vacutran Brochure.* 2013.

33. Randall, G.C. and P.S. Doyle, *Permeation-Driven Flow in Poly(Dimethylsiloxane) Microfluidic Devices.* Proc. Natl. Acad. Sci. USA, 2005. **102**(31): p. 10813-8.

34. De Jong, W.H. and P.J. Borm, *Drug Delivery and Nanoparticles-Applications and Hazards.* Int. J. Nanomedicine, 2008. **3**: p. 133-149.

35. Holt, J.K., et al., *Fast mass transport through sub-2-nanometer carbon nanotubes.* Science, 2006. **312**: p. 1034-1037.

36. Schoch, R., J. Han, and P. Renaud, *Transport Phenomena in Nanofluidics.* Rev. Mod. Phys., 2008. **80**: p. 839-883.

37. Majumder, M., N. Chopra, and B. J.Hinds, *Mass transport through carbon nanotube membranes in three different regimes: Ionic diffusion and gas and liquid flow.* ACS Nano, 2011. **5**: p. 3867-3877.

38. Joseph, S. and N.R. Aluru, *Why are carbon nanotubes fast transporters of water?* Nano Letters, 2007. **8**: p. 452-458.

39. Nair, R.R., et al., *Unimpeded permeation of water through helium-leak-tight graphene-based membranes.* Science, 2012. **335**: p. 442-444.

Chapter 3 Theoretical Basis

In this chapter, we first introduce basic definitions for fluid through tubes and then porous medium and membranes, including mass, molar, volume and particle number flow rates through tubes and permeability, permeance and water vapour transmission rate through a material. Two important constants were given: Reynolds number which determines whether the flow is laminar flow and Knudsen number which determines flow regimes. Under the condition of laminar flow, we show brief derivations of several useful equations (Knudsen equation, Boltzmann and its related equations and Navier-Stokes equations) for predicting flow rates in various flow regimes. The guide for this chapter is shown as below.

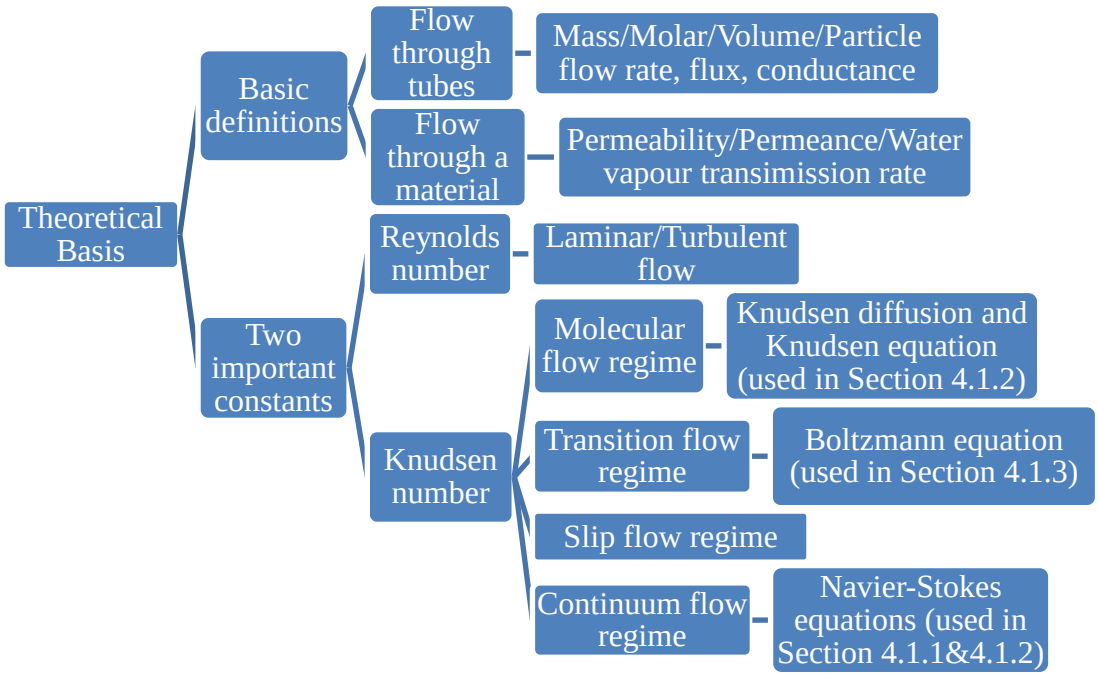

Figure 2 A guide for basic definitions in Chapter 3.

3.1 Basic Definitions and Regimes of Flow

3.1.1 Mass, Volume and Particle Number Flow Rates, Fluxes and Conductance

Quantities that are basic to the quantification of a flow are the flow rate and the flux. The flow rate is the quantity of flow per unit time and a flux is defined as the flow rate divided by the area of the conducting aperture. Some authors have tended to emphasise mass flow rate [1] while others use volume [2] and particle number (or molar) flow rates. The mass flow rate $\dot{m}$ in kg/s will be used in this thesis as the normal outcome of a calculation or measurement on a single tube or of permeation through a material medium. The mass flux is defined by:

$$\frac{\dot{m}}{A} \tag{1}$$

where A is the cross sectional area of the aperture defining the boundaries of the flow. Another convenient outcome of calculation or measurement is the mass conductance:

$$C = \frac{\dot{m}}{\Delta P} \tag{2}$$

where $\Delta P = P_i - P_o$ is the pressure difference across the tube defined as the difference in the pressures of the fluid on the inlet (P_i) and the outlet of the tube (P_o). Conductance is useful for comparing flow rates under various pressure differences.

The particle number flow rate and molar flow rate are often convenient for determining the effects on the contents of packages or encapsulations and are useful when comparing two different gases or vapours. The mass flow rate is readily converted to particle number flow rate using the conversion:

$$\dot{n} = \dot{m}/m_m \tag{3}$$

where $\dot{n}$ is the number of particles flowing per second and m_m is the molecular mass. The particle flow rate is converted to a molar flow rate by dividing the Avogadro's number 6.023×10^{23}.

The volume flow rate (m^3/s) is related to the mass flow rate by:

$$\dot{V} = \dot{m}/\rho \tag{4}$$

where ρ is the density of the fluid in kg/m^3. The flow velocity averaged over the cross section $\bar{v}$ is given by:

$$\bar{v} = \frac{\dot{V}}{A} \tag{5}$$

Particle, molar and volume conductances are obtained using a similar conversion method with Eq.(2). In cases where there are two species present, labelled 1 and 2, the composition of the fluid under flow is described by the contributions of each to the total particle concentration, the particle number per unit volume:

$$c = \frac{n}{V} = \frac{n_1}{V} + \frac{n_2}{V} = c_1 + c_2 \tag{6}$$

In the case where species are gases, it is usual to write the total pressure P_T as the sum of the two partial pressures P_1 and P_2:

$$P_T = P_1 + P_2 \tag{7}$$

and for ideal gases the equation of state applies:

$$PV = nk_BT \tag{8}$$

where V is the volume, n is the number of particles, k_B is the Boltzmann constant and T is temperature in Kelvin. Eqs.(7) and (8) can be used to relate the particle concentrations to partial pressure for ideal gases:

$$c_1 = \frac{P_1}{k_B T}, c_2 = \frac{P_2}{k_B T} \tag{9}$$

3.1.2 Diffusion Coefficients, Permeability, Permeance and Water Vapour Transmission Rate

The permeation process usually does not consider the boundaries of the medium to influence the permeation rate. Here we follow the ASTM standard definitions of permeability, permeance and WVTR, but will express them in SI units. The lateral boundaries of the medium under consideration are normally considered distant and cause no perturbation of the flow, as in a thin membrane covering an aperture. We will use axes in which the flow is directed along x. The particle number flow rate under steady state conditions through a medium with a defined aperture A (particle flux) is frequently observed to be proportional to the particle concentration gradient of permeant across the medium, a result originally arrived at by Fick from a consideration of diffusive processes and named Fick's law [3]:

$$\frac{\dot{n}}{A} = -D_F \frac{\partial c}{\partial x} \tag{10}$$

where D_F is the Fick's law diffusion coefficient. For a gas diffusing in a volume where the boundaries are distant, D_F is derivable from kinetic theory [4]:

$$D_F = \frac{1}{3} \lambda \bar{u}_m \tag{11}$$

where $\bar{u}_m$ is the mean molecular speed, and λ is the mean free path which is given for an ideal gas by [4]:

$$\lambda = \frac{k_B T}{\sqrt{2}\pi P {d_m}^2} \tag{12}$$

where d_m is the diameter of molecules.

Wroblewski [5] further developed Fick's law and related the mass flux to a pressure gradient:

$$\frac{\dot{m}}{A} = P_{mass} \frac{\Delta P}{l} \tag{13}$$

where P_{mass} is the mass *permeability* (kg/m/Pa/s) of the medium to the permeant under study, l is the thickness of the medium and ΔP is the pressure difference across the medium. In the special case where the medium under permeation is another ideal gas, the concentration of the permeant is continuous across the boundaries, but in general for other media there is a discontinuity in the concentration on passing from the outside to the inside of the medium. It is possible to assign volume, particle number and molar permeabilities of a membrane by changing the mass flux to volume, particle number and molar fluxes respectively.

Mass *permeance* in units of kg/Pa/m^2/s is the mass permeability divided by the thickness of the test piece. In the special case of water permeation through a membrane, a quantity termed WVTR is defined as the mass transfer rate of water vapour per unit area of membrane (kg/m^2/s) under known conditions of water vapour pressure on each side of the membrane. Following this definition, WVTR is the product of the permeance of the

material to water vapour multiplied by the difference in water vapour pressure just outside the inlet and outlet surfaces of the test piece.

To describe the permeation process in a material membrane, the solution-diffusion model, originating in the work of Graham in 1866 [6], proposes that the flow through a membrane is established in three steps. First, the permeant dissolves in the surface of the material to give an internal concentration that is dependent on the pressure just outside the input surface (assuming, for now, the linear relation known as Henry's law which does not always apply):

$$c_i = P_i S_H \tag{14}$$

where S_H is the Henry law solubility and c_i is the internal concentration in the inlet side of the membrane. Second, the concentration gradient of the permeant inside the membrane is established by diffusion over time to a steady state level also determined by the conditions at the outlet side, in turn determined by the external pressure of the permeant just outside the outlet surface of the membrane, P_o. Finally, the evaporation of the permeant from the outlet surface of the membrane, where again the external pressure, is related to the internal concentration at the outlet side of the membrane by the Henry's law solubility.

From Eqs.(10) and (14) we write the mass flux as:

$$\frac{\dot{m}}{A} = -D_F \frac{\partial c}{\partial x} = D_F S_H \frac{P_i - P_o}{l} \tag{15}$$

So that from Eq.(13):

$$P_{mass} = S_H D_F \tag{16}$$

In some of the literature on membranes, the term *permeation coefficient* is used instead of permeability [7]. In polymers, the Fick's law diffusion coefficient is often referred to simply as the *diffusivity*. An analogy can be made with the electrical *conductivity* of a medium where the mass flux is analogous to the current density and the pressure is analogous to *electrical potential*.

In the case where Henry's law applies, the relation Eq.(16) may be used to obtain any of three variables in it when the other two are known. The solubility can be determined separately by the total permeant uptake when the medium is immersed in permeant. In the case of water, a *water absorbance* is often measured in this way as a mass of water per unit mass of medium.

Flow in porous medium is different from the flow in permeable membranes. A *porous* medium is one having interconnected void spaces that can be filled with liquid or gas. The geometry of the pores may be complex, leading to flow tubes with both constrictions and tortuosity. The nature of the interconnectivity may also be complex, with divergent and convergent connections. The simplest case is for ideal gas flows through a porous medium, in which case the concentration of the gas is continuous on entering the medium (corresponding to a Henry's law solubility of unity). For condensable gas flows there will be a concentration increase on entering the medium when condensation occurs on the surface of the pores. The proportionality of the flow rate to the pressure difference ΔP across the medium often applies in viscous flows through porous media where it is referred to as Darcy's law. For our purposes, a viscous flow is one in which the viscosity of the permeant is a well defined quantity. When written as an expression for the volume flow rate [8] Darcy's law is:

$$\dot{V} = -P_{volume} A \frac{\Delta P}{l} = -\frac{k\, A}{\mu} \frac{\Delta P}{l} \tag{17}$$

where P_{volume} is the volume permeability (m^2/s/Pa), k is the *intrinsic Darcy's law permeability* of the porous medium (m^2) and μ is the dynamic viscosity. For an ideal gas of elastic hard spheres, μ has the value [9]:

$$\mu = \frac{5}{16 d_m^2} \left(\frac{k_B T m_m}{\pi} \right)^{\frac{1}{2}} \tag{18}$$

Eq.(18) predicts viscosity of nitrogen well (for nitrogen at 25°C, μ = 1.73 × 10^{-5} kg/m/s from Eq.(18) and 1.78 × 10^{-5} kg/m/s from the database of National Institute of Standards and Technology (NIST) [10]), but fails for water vapour. Water is a polar molecule and it is not well approximated as an elastic hard sphere. In this thesis, we use the dynamic viscosity of water vapour at 25°C obtained from NIST database [10] which is about 9.87 × 10^{-6} kg/m/s.

Note that when Eq. (17) applies, the intrinsic Darcy's law permeability is a property of the porous medium and not of the permeant since the properties of the permeant enter through the viscosity. In this respect, the intrinsic Darcy's law permeability differs from the more common mass and volume permeability definitions given above. The permeation process in a porous medium is frequently more complex than Darcy's law suggests, especially for condensable permeants such as water vapour. It is therefore important to distinguish between gases that do not condense on the surface of a tube and vapours that condense to form a liquid layer.

We divide flows into cases where there is a single species and cases where there are multiple species. For two component flows, Landau and Lifshitz [11] have given a useful

breakdown of the flux of one species in a two component flow. If species 1 is considered as the permeant of interest then its particle flux is given by:

$$J_1 = -[D_{12}\frac{\partial c_1}{\partial x} + D_T c_1 \frac{\partial T}{\partial x} + D_F \frac{c_1}{c_T}\frac{\partial c_T}{\partial x}] \quad (19)$$

where D_{12} is the *mutual Fick's law interdiffusion* coefficient of species 1 in species 2 describing the "interdiffusive" component of the flow. D_T is the "thermodiffusion" coefficient describing temperature driven flow and D_F is the Fick's law diffusion coefficient describing the flow of both species together. Eq.(19) is a statement that the fluxes are independent and additive. For example, the interdiffusive flux and total flux can occur together. A two component flow is entirely interdiffusive if there are only partial pressure gradients and no total pressure gradient.

3.1.3 Dimensionless Constants of Flow in a Tube

The *Reynolds number* is useful in determining whether a viscous flow is turbulent or laminar and for a flow having a fluid velocity $\bar{v}$ is defined by:

$$Re = \frac{\rho \bar{v} d_h}{\mu} \quad (20)$$

where d_h is the hydraulic diameter of the tube defined by:

$$d_h = \frac{4A}{p_w} \quad (21)$$

where p_w is the wetted perimeter of the tube. Laminar flows are described by streamlines representing the vector direction of the flow.

The *Knudsen number* is useful in defining flow regimes [12] and is defined as:

$$Kn = \frac{\lambda}{l_0} = \frac{k_B T}{4\sqrt{2}\pi {r_m}^2 \mathrm{P} l_0} \tag{22}$$

where l_0 is a characteristic dimension of the tube for which it is common practice to use the diameter $2r_c$ for a circular tube or the smallest separation of the walls for a rectangular tube and r_m is the radius of molecule. The flow regimes are defined by the following ranges of Kn:

- For $0 < Kn \leq 0.01$, we define the continuum flow regime (also called hydrodynamic flow or viscous flow). The classical Navier-Stokes equations with no-slip boundary conditions are usually valid for this flow regime.

- For $0.01 < Kn \leq 0.1$, we define the slip flow regime. In this flow regime, a sublayer, known as the Knudsen layer, exists between the bulk of the fluid and the surface which has a thickness of the order of the mean free path. The majority of the flow is governed by the classical Navier-Stokes equations, while the flow in the Knudsen layer, which usually covers much less than 10% of the tube width or diameter, can be neglected. It is more accurate to use Maxwell's velocity slip boundary conditions (first order boundary conditions) as a correction factor added to the classical Navier-Stokes equations.

- For $0.1 < Kn \leq 10$, we define the transition flow regime. In this flow regime, the classical Navier-Stokes equations require higher-order boundary conditions to give accurate flow rates. A simplified form of the

Boltzmann equation known as the Bhatnagar-Gross-Krook (BGK) equation is one approach for modelling flow in this flow regime.

- For $Kn > 10$, we define the free molecular flow regime. In this flow regime, intermolecular collisions are assumed to be negligible in determining the gas dynamics. The BGK equations are also used to model flow in this flow regime [1, 13].

3.2 KNUDSEN DIFFUSION AND THE KNUDSEN EQUATION

The diffusion of a single component gas in a conduction tube was first studied quantitatively by Knudsen [14] who derived a value for the diffusion coefficient under molecular flow conditions in which collisions with the walls are dominant over intermolecular collisions, a process termed *Knudsen diffusion*. Knudsen's expression for the Knudsen diffusion coefficient D_K is analogous to that for the Fick's law diffusion coefficient (Eq.(11)) where the mean free path is replaced by a path length determined by the tube dimensions:

$$D_K = \frac{1}{3}\bar{u}_m H \tag{23}$$

where *H* is a shape dependent length equal to the diameter $2r_c$ for a cylindrical tube. The Knudsen diffusion coefficient is readily related to the mass flow rate in the tube by invoking the ideal gas law Eq.(8), so that the particle flux is related to the pressure gradient along the diffusion direction *x* by:

$$\frac{\dot{n}}{A} = \frac{\dot{n}}{\pi r_c^2} = \frac{D_K}{k_B T}\frac{dP}{dx} \tag{24}$$

The mass flow rate is:

$$\dot{m} = m_m \dot{n} = \frac{\pi r_c^2 m_m D_K}{k_B T} \frac{dP}{dx} \tag{25}$$

Evaluating D_K from kinetic theory using the result of $\bar{u}_m$ given by Loeb [3]:

$$\bar{u}_m = \sqrt{\frac{8 k_B T}{\pi m_m}} \tag{26}$$

We obtain the Knudsen equation for the mass flow rate in the molecular flow regime:

$$\dot{m} = \frac{4\sqrt{2\pi} r_c^3}{3} \sqrt{\frac{m_m}{k_B T}} \frac{dP}{dx} \tag{27}$$

The Knudsen equation works well for the flow at low pressures. There is an implicit assumption that the collisions with the walls of a tube are similar to collisions between molecules in the sense that the momentum of a molecule in the direction of flow is not preserved after the collision. This corresponds to an assumption of diffuse reflection at the walls, to be discussed later. Soon after Knudsen's paper appeared, Smoluchowski [15] provided a generalisation of the Knudsen result for the case where a fraction α (TMAC) of the collisions with the walls are diffuse and the remainder specular. Smoluchowski's result is the same as Knudsen's in the limit of TMAC α approaching unity:

$$\dot{m} = \frac{4\sqrt{2\pi} r_c^3}{3} \sqrt{\frac{m_m}{k_B T}} \frac{dP}{dx} \frac{2 - \alpha}{\alpha} \tag{28}$$

3.3. The Boltzmann and Related Equations

A general starting point for the understanding of gas flows under a wide variety of conditions is the Boltzmann equation, derived by Ludwig Boltzmann in 1872. The Boltzmann equation is the fundamental equation governing flow in regimes from a moderately dense gas or vapour to a rarefied gas or vapour. For dense gases and vapours,

it is more convenient to consider the gas as a homogeneous viscous fluid and to use the classical Navier-Stokes equations as the starting point.

To determine the mass flow rate of a gas crossing an area on the $y - z$ plane, the integrated value of the product of the macroscopic observables density ρ and fluid velocity u over the cross section of the conduction tube is needed:

$$\dot{m} = \iint_{cross\ section} \rho(y,z)u(y,z)dydz \tag{29}$$

The functions ρ and u are in principle determined by the underlying equations of motion for the individual molecules, which can be described classically by Newton's laws. By working within certain simplifying assumptions, it is possible to write averaged equations of motion that are much simpler to solve than the individual equations for each particle and in some limits give rise to the macroscopic fluidic dynamic descriptions. A generalized form of the Boltzmann equation has been derived from the Liouville equation [16] for the time evolution of the phase space distribution function $f(\boldsymbol{r}, \boldsymbol{v}, t)$ that describes the probability of there being a particle in a given phase space volume $d^3\boldsymbol{r}d^3\boldsymbol{v}$ at time t, where $\boldsymbol{r}$ is the position of a particle and $\boldsymbol{v}$ its velocity. The particles are assumed identical and uncorrelated (molecular chaos) with no internal degrees of freedom.

Macroscopic properties are obtained by taking velocity moments of the distribution function. The quantities needed for calculating the mass flow rate in Eq.(29) are defined using the distribution function as:

Particle number: $$n = \int f(\boldsymbol{r}, \boldsymbol{v}, t)d\boldsymbol{v} \tag{30}$$

Density: $$\rho(\boldsymbol{r}, t) = m_m \int f(\boldsymbol{r}, \boldsymbol{v}, t)d\boldsymbol{v} \tag{31}$$

Bulk velocity: $$\boldsymbol{u} = \frac{1}{n}\int \boldsymbol{v} f(\boldsymbol{r}, \boldsymbol{v}, t) d\boldsymbol{v} \tag{32}$$

The Boltzmann equation is the following governing equation for the probability distribution function *f*:

$$\frac{\partial f}{\partial t} + \boldsymbol{v} \cdot \frac{\partial f}{\partial \boldsymbol{r}} + \boldsymbol{F} \cdot \frac{\partial f}{\partial \boldsymbol{v}} = Q \tag{33}$$

The first term gives the rate of change of the number of molecules at $\boldsymbol{r}$ having velocity $\boldsymbol{v}$ in the phase space; the second term describes molecules passing through a fluid volume at $\boldsymbol{r}$ with velocity $\boldsymbol{v}$; the third term describes molecules at $\boldsymbol{r}$ passing through velocity space under the influence of the external force $\boldsymbol{F}$. For steady flows, in which *f* has no explicit dependence on time, the first term vanishes and for flows in the absence of external forces, the third term vanishes. The term on the right hand side represents the effect of collisions between molecules, where Q is an operator acting on the velocity distribution function f before and after a collision. To find an expression for Q, further assumptions must be made. First, we discuss the case where there are no boundaries and assume that the only collisions that take place are between molecules. Furthermore, these collisions are assumed to be binary collisions only, an assumption that applies provided the gas is sufficiently dilute. Q is expressed by the integral giving the operator that gives the change in the number of particles with velocity $\boldsymbol{v}$ as a result of a collision between two particles of velocity $\boldsymbol{v}$ and $\boldsymbol{v}_*$:

$$Q = \int_{R^3}\int_0^{4\pi} |\boldsymbol{v} - \boldsymbol{v}_*|\, I(|\boldsymbol{v} - \boldsymbol{v}_*|, \Omega)[f(\boldsymbol{r}, \boldsymbol{v}_*) f(\boldsymbol{r}, \boldsymbol{v}) - f(\boldsymbol{r}, \boldsymbol{v}_*') f(\boldsymbol{r}, \boldsymbol{v}')] d\Omega d\boldsymbol{v}_* \tag{34}$$

where $I(|\boldsymbol{v} - \boldsymbol{v}_*|, \Omega)$ is the differential cross section of the collision, where the relative velocity changes from the incident direction to the element of the solid angle $d\Omega$ as a

result of collision. R^3 is the domain of integration over all velocities. It considers two particles colliding, starting with velocities $\boldsymbol{v}$ and $\boldsymbol{v}_*$ and leaving the collision elastically with velocities $\boldsymbol{v}'$ and $\boldsymbol{v}'_*$**.** The terms subtracted from one another in the square brackets have the form "the number of particles scattered in, minus the number of particles scattered out"; some particles that had velocity $\boldsymbol{v}$ will be scattered through collisions to having new velocities, while other particles will join the group of particles with velocity $\boldsymbol{v}$ after colliding. Here we consider only isothermal cases.

When considering flow in a tube, collisions with the boundary must be included in the collision term. Maxwell derived a form of the scattering term that includes an accommodation coefficient that describes two cases of collisions, diffusive and specular. An accommodation coefficient of unity describes the case where all molecules are diffusely reflected and a value of zero describes the case where all molecules are specularly reflected, that is the momentum parallel to the surface is unchanged after the collision. For more details of the derivation of the equations in this section the reader is referred to the book of Karniadakis [17].

The Boltzmann equation is difficult to solve because of its six dimensional phase space. A popular approach that applies to the case of a relative dense particle system is named the Chapman-Enskog method for which the phase space distribution function f takes the form below including terms up to Kn^2:

$$f = f^0 + f^1 + f^2 = f^0(1 + aKn + bKn^2) \qquad (35)$$

where a and b are functions of fluid density, temperature and velocity, and f^0 is the absolute Maxwellian distribution function for an equilibrium state and:

$$f^0 = n_0 \left(\frac{m_m}{2\pi k_B T}\right)^{3/2} \exp(-\frac{m_m}{2k_B T}\boldsymbol{v}^2) \tag{36}$$

where n_0 is the equilibrium number density.

For a rarefied gas or vapour, approximate forms of the Boltzmann equation have been applied such as the linearised Boltzmann equation (LBE) [18, 19] and the Bhatnagar-Gross-Krook (BGK) equation [2, 20-22] which may also be linearised. In the LBE and BGK equations, linearizing is carried out by writing the velocity distribution function as a perturbation expansion:

$$f = f^0[1 + \mathrm{h}(\boldsymbol{r}, \boldsymbol{v}, t)] \tag{37}$$

using a perturbation distribution function $\mathrm{h}(\boldsymbol{r}, \boldsymbol{v}, t)$ [23]. These approaches differ in the form of the collision term in the Boltzmann equation, as shown in Table 1 for the case of steady flows. In this table, f_{loc} is the local Maxwellian distribution function:

$$f_{loc} = n \left(\frac{m_m}{2\pi k_B T}\right)^{3/2} \exp[-\frac{m_m(\boldsymbol{v} - \boldsymbol{u})^2}{2k_B T}] \tag{38}$$

where $n = n(\boldsymbol{r}, t)$ is the local number density depended on the spatial coordinates and time.

Table 1 Approximate forms of the governing equations for the phase space distribution function *f* in the Boltzmann equation with the corresponding forms of the collision terms and the governing equation for steady flows.

Name	**Collision term**	**Governing equations**
BGK equation	$Q_{BGK} = \frac{1}{\tau}(f_{loc} - f)$	$\boldsymbol{v} \cdot \frac{\partial f}{\partial \boldsymbol{r}} = \frac{1}{\tau}(f_{loc} - f)$
Linearised Boltzmann equation	$Q_{LBE} = \int_{R^3}\int_{S^+} f^0(\boldsymbol{v}_*) \times (\mathrm{h}' + \mathrm{h}'_* - \mathrm{h} - \mathrm{h}_*) dn d\boldsymbol{v}_*$	$\frac{\partial \mathrm{h}}{\partial t} + \boldsymbol{v} \cdot \frac{\partial \mathrm{h}}{\partial t} = Q_{LBE}$

As in the Knudsen equation, the boundary condition at the walls is usually assumed to be fully diffuse reflection, which imposes a condition on the perturbation function at the walls. The above form of the BGK equation was used by Cercignani and Daneri in a conceptually simple approach using a discrete ordinate method [2]. It has been estimated that the difference of the mass flow rate between parallel plates calculated by solving the BGK equation and that obtained by solving the full Boltzmann equation for the isothermal flow in a rectangular tube is only about 2% [20].

3.4 NAVIER-STOKES EQUATIONS

The Navier-Stokes equations were first derived by the French mathematician L. M. H. Navier in 1822 and then further developed by the English mechanician Sir G. G. Stokes in 1845. These equations apply to the single phase viscous flow of fluids including liquids as well as vapours and gases in the continuum flow regime. While some researchers have focused on the derivation of the Navier-Stokes equations from the Boltzmann equation [24-26], we obtain the Navier-Stokes equations more simply from *Cauchy's equation of motion*, which is based on Newton's second law:

$$\left(\boldsymbol{g} - \frac{\partial \boldsymbol{u}}{\partial t}\right)\rho + \nabla \cdot \boldsymbol{\sigma} = 0 \qquad (39)$$

This equation is valid for both compressible and incompressible fluids in the presence of the gravitational acceleration $\boldsymbol{g}$. By expressing Eq.(39) in Cartesian coordinates and evaluating the contributions to the total stress tensor $\boldsymbol{\sigma}$ from pressure gradients and shear stresses and then relating the shear stresses to the rate of strain tensor (using the fluid constitutive relations), we obtain the compressible Navier-Stokes equations [27]. For which the x component is:

$$\frac{\partial u_x}{\partial t} + u_x\frac{\partial u_x}{\partial x} + u_y\frac{\partial u_x}{\partial y} + u_z\frac{\partial u_x}{\partial z} = g_x - \frac{1}{\rho}\frac{\partial P}{\partial x} + \frac{\mu}{\rho}\cdot\left(\frac{\partial^2 u_x}{\partial x^2} + \frac{\partial^2 u_x}{\partial y^2} + \frac{\partial^2 u_x}{\partial z^2} + \frac{\partial D_v}{\partial x}\right) \quad (40)$$

with corresponding equations for the *y* and *z* components. As in previous sections, the *x* direction is the direction of flow. D_v is a volumetric dilation and in the case of *incompressible* flow, $D_v = 0$. In vector notation for the incompressible case the equations are:

$$\underset{\text{I.}}{\frac{\partial \boldsymbol{u}}{\partial t}} + \underset{\text{II.}}{(\boldsymbol{u}\cdot\nabla)\boldsymbol{u}} = \underset{\text{III.}}{\boldsymbol{g}} - \underset{\text{IV.}}{\frac{1}{\rho}\nabla P} + \underset{\text{V.}}{\frac{\mu}{\rho}\nabla^2\boldsymbol{u}} \quad (41)$$

In the case where the flow velocity depends only on a single spatial variable, the flow is termed *one dimensional*. The terms numbered in Eq.(41) with Roman numerals have the meanings shown in Table 2. The meanings of *steady flow* and *uniform* flow are also defined in Table 2. In *parallel* flow the velocity is in one direction at all positions and times. Table 3 gives the special conditions for incompressible flows that lead to related governing equations that are special cases of Eq.(41), well known in fluid mechanics.

A well known equation named after Poiseuille which predicts the flow rate of liquid in tubes can be derived from a special condition of the Navier-Stokes equations, the Stokes equation:

$$\dot{m}_P = \frac{\pi {r_c}^4 \Delta P \rho}{8\mu L} \quad (42)$$

where *L* is the tube length.

The classical Navier-Stokes equations have been extended to cover all flow regimes by ensuring that the expressions approach the Knudsen flow Eq.(27) at large *Kn*. An

empirically determined parameter is usually needed to achieve a smooth dependence on *Kn* for intermediate values of *Kn* [17, 28]. In one approach, the matching process is formalised by adding an additional diffusive mass flow rate term to the Navier-Stokes equations based on Fick's law [29-31]. The resulting extended Navier-Stokes equations provide agreement with experimental data of helium, argon, nitrogen and carbon dioxide over a wide range of Knudsen numbers across all flow regimes.

The available theories for describing single non-condensing gas or vapour flow without special conditions have been summarized diagrammatically by Bird [32] as a function of *Kn*. An updated summary of Bird's diagram is shown in Figure 3.

Table 2 The meaning of the terms in the incompressible Navier-Stokes equations, Eq.(41).

Term No.	**Meaning of the terms**
I.	The temporal change in momentum at a fixed control volume in the flow. For a steady flow, in which the velocities at each position in the flow are independent of time, this term is zero. All steady flows are laminar.
II.	The convective change in momentum of the fluid, which describes the rate at which momentum in convected away from a control volume in the flow. Uniform flow, as for example in a tube with dimensions independent of position, has no convective acceleration.
III.	The body forces acting on the fluid. The example used is gravity.
IV.	The force arising from pressure gradients.
V.	The acceleration (deceleration) due to the frictional resistance (viscosity) of the fluid.

Table 3 Special conditions applying to the Navier-Stokes equations (Eq.(41)) lead to the other principal equations of fluid flow, with the applications listed.

Name	**Formula**	**Special Conditions on the Terms**	**Application**
Euler's equation	$\frac{\partial \boldsymbol{u}}{\partial t} + (\boldsymbol{u} \cdot \boldsymbol{\nabla})\boldsymbol{u} = \boldsymbol{g} - \frac{1}{\rho}\boldsymbol{\nabla} P$	V. $= 0$	Inviscid and incompressible flow.
Bernoulli's equation	$\frac{\rho u^2}{2} + P + \rho g z = constant$ (integral form of Euler's equation)	I. $=$ V. $= 0$	One dimensional, steady, inviscid and incompressible flow.
Parallel flow	$\frac{\partial u}{\partial t} = -\frac{1}{\rho}\nabla P + \frac{\mu}{\rho}\nabla^2 \boldsymbol{u}$	II. $=$ III. $= 0$	Uniform, incompressible flow with velocity in one direction in a horizontal tube or in zero gravity conditions.
Stokes flow	$\frac{1}{\rho}\nabla P = \boldsymbol{g} + \frac{\mu}{\rho}\nabla^2 \boldsymbol{u}$	I. $=$ II. $= 0$	Steady, parallel flow. The advective inertial forces are small compared with viscous forces.

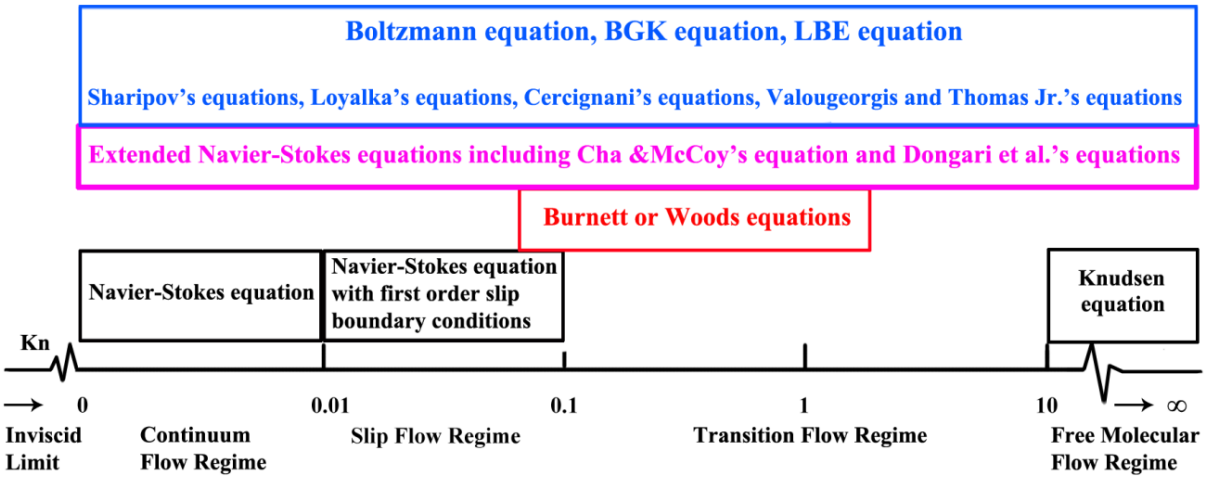

Figure 3 The Knudsen number *Kn* ranges defining flow regimes. Also shown is a selection of equations for predicting flow rates (adapted from Bird [32]) with their regimes of applicability. There are three types of theory covering the values of *Kn* between the slip flow regime and the molecular flow regime, those using higher order boundary conditions (red box) [33, 34], those requiring an empirical parameter (pink box) [28, 31] and those arising from an approximate solution of the Boltzmann equation (blue box) [2, 18, 22, 35].

REFERENCES

1. Sharipov, F., *Rarefied Gas Flow through a Long Rectangular Channel.* J. Vac. Sci. Technol. A, 1999. **17**(5): p. 3062-3066.
2. Cercignani, C. and A. Daneri, *Flow of a Rarefied Gas between Two Parallel Plates.* J. Appl. Phys., 1963. **34**(12): p. 3509-3513.
3. Fick, A., *Ueber Diffusion (in German).* Ann. Phys. (Berlin), 1855. **170**: p. 59-86.
4. Loeb, L.B., *The Kinetic Theory of Gases*. 3 ed. 1961, London, UK: Dover Publications, Inc.
5. Wroblewski, S.V., *Ueber Die Natur der Absorption der Gase durch Flussigkeiten unter Hohen Drucken (in German).* Ann. d. Phys. u. Chem., 1879. **8**: p. 29-52.

6. Graham, T., *On the Absorption and Dialytic Separation of Gases by Colloid Septa.* Philos. Tran. R. Soc. Lond., 1866. **156**: p. 399-439.
7. Sturm, P., et al., *Permeation of Atmospheric Gases through Polymer O-Rings Used in Flasks for Air Sampling.* J. Geophys. Res., 2004. **109**(D4): p. D04309.
8. Guyon, E., et al., *Physical Hydrodynamics*. 2001, UK: Oxford University Press.
9. Chapman, S. and T.G. Cowling, *The Mathematical Theory of Non-Uniform Gases*. 3 ed. 1970, UK: Cambridge University Press.
10. National Institute of Standards and Technology, *Isothermal Properties for Water*. 2011, NIST Standard Reference Data: USA.
11. L.D.Landau and E.M.Lifshitz, *Fluid Mechanics*. 1966, UK: Pergamon Press Ltd.
12. Arkilic, E.B., *Gaseous Flow in Mirco-Sized Channels*, in *Department of Aeronautics and Astronautics*. 1994, Massachusetts Institute of Technology.
13. Loyalka, S.K., *Kinetic Theory of Thermal Transpiration and Mechanocaloric Effect. II.* J. Chem. Phys., 1975. **63**(9): p. 4054-4060.
14. Knudsen, M., *The laws of molecular and viscous flow through tubes (in German).* Ann. Phys. (Berlin), 1909. **28**: p. 75-130.
15. Smoluchowski, M., *To the kinetic theory of transpiration and diffusion of dilute gases (in German).* Ann. Phys. (Berlin), 1910. **33**: p. 1559-1570.
16. Cercignani, C., R. Illner, and M. Pulvirenti, *The Mathematical Theory of Dilute Gases*. 1994, Germany: Springer-Verlag GmbH.
17. Karniadakis, G., A. Beskok, and N. Aluru, *Microflows and Nanoflows from fundamental to simulation*. 2005, USA: Springer Science+Business Media, Inc.

18. Loyalka, S.K. and S.A. Hamoodi, *Poiseuille Flow of A Rarefied Gas in A Cylindrical Tube: Solution of Linearized Boltzmann Equation.* Phys. Fluids A, 1990. **2**(11): p. 2061-2065.

19. Lorenzani, S., *Higher Order Slip According to the Linearized Boltzmann Equation with General Boundary Conditions.* Philos. Trans. R. Soc. A, 2011. **369**(1944): p. 2228-2236.

20. Sharipov, F., *Data on Internal Rarefied Gas Flows.* J. Phys.Chem. Ref. Data, 1998. **27**(3): p. 657-706.

21. S.S.Lo and S.K.Loyalka, *An Efficient Computation of Near-Continuum Rarefied Gas Flows.* J. Appl. Math. Phys., 1982. **33**: p. 419-424.

22. Valougeorgis, D. and J.R. Thomas Jr, *Exact Numerical Results for Poiseuille and thermal Creep Flow in A Cylindrical Tube.* Phys. Fluids, 1986. **29**: p. 423-429.

23. Bhatnagar, P., E. Gross, and M. Krook, *A Model for Collision Processes in Gases. I. Small Amplitude Processes in Charged and Neutral One-Component Systems.* Phys. Rev., 1954. **94**(3): p. 511-525.

24. Golse, F., *From the Boltzmann Equation to the Incompressible Navier-Stokes Equations*. 2006, Lax-Nirenberg Conference.

25. X.Y. He and L.S. Luo, *Latticel Boltzamann Model for the Incompressible Navier-Stokes Equation.* J. Stat. Phys., 1997. **88**: p. 927-944.

26. Guo, Z., B. Shi, and N. Wang, *Lattice BGK Model for Incompressible Navier–Stokes Equation.* J. Comput. Phys., 2000. **165**(1): p. 288-306.

27. Granger, R.A., *Fluid Mechanics*. 1985, NY,USA: The Dryden Press.

28. Cha, C.Y. and B.J. McCoy, *Application of third-order constitutive relations to Poiseuille flow of a rarefied gas.* J. Chem. Phys., 1971. **54**: p. 4373-4383.

29. Brenner, H., *Navier–Stokes Revisited.* Physica A, 2005. **349**(1-2): p. 60-132.

30. Brenner, H., *Fluid Mechanics Revisited.* Physica A, 2006. **370**(2): p. 190-224.

31. Dongari, N., A. Sharma, and F. Durst, *Pressure-Driven Diffusive Gas Flows in Micro-Channels: From the Knudsen to the Continuum Regimes.* Microfluidics Nanofluidics, 2009. **6**(5): p. 679-692.

32. Bird, G.A., *Molecular Gas Dynamics and the Direct Simulation of Gas Flows*. 1994, UK: Oxford University Press, Inc.

33. Burnett, D., *The Distribution of Molecular Velocities and the Mean Motion in A Non-Uniform Gas.* Proc. London Math. Soc., 1935. **39**(2): p. 385-435.

34. Woods, L.C., *An Introduction to the Kinetic Theory of Gases and Magnetoplasmas*. 1993, UK: Oxford University Press.

35. Sharipov, F.M. and V.D. Seleznev, *Rarefied Gas Flow through a Long Tube at Any Pressure Ratio.* J. Vac. Sci. Technol. A, 1994. **12**(5): p. 2933-2935.

Chapter 4 Maxwell's Accommodation Coefficient and Nitrogen Flow Rate through Microtubes

Gas flows have been studied quantitatively for more than a hundred years and have modern relevance in fields such as the control of gas inputs to processes, the measurement of leak rates and the separation of gaseous species. In this chapter, a convenient formula for the flow of an ideal gas applicable across a wide range of *Kn*, theory of Cha and McCoy, has been introduced and extended using a recent finding by Arya et al. replacing the Smoluchowski factor. We measure the flow rate of nitrogen gas in a smooth walled silica tube across a wide range of Knudsen number from 0.0048 to 12.4583. This is the first time to study flow rates across all flow regimes in a well-defined microtube. We find that the nitrogen flow obeys the Cha and McCoy equation with a large value of α, unlike carbon nanotubes which show flows consistent with a small value of α. Silica capillaries are therefore not atomically smooth. The flow at small *Kn* has α = 0.91 and at large *Kn* has α close to one, consistent with the redefinition of accommodation coefficient by Arya et al., which also resolves a problem in the literature where there are many observations of α of less than one at small *Kn* and many equal to one at large *Kn*. Silica capillaries are an excellent choice for an accurate flow control system.

4.1 INTRODUCTION

Calculation and accurate control of the flow of gases in microtubes are important in many fields. In biology and botany, air flows in nanodimensioned tubes are of fundamental

importance in respiration and transpiration. Gas flows in microfluidic devices are used for sensing and many process control applications require an accurate knowledge of the flow of a gas. Nitrogen has been selected as it is representative of a noncondensable ideal gas, it is the majority constituent of air and the control of its flow is required in many processes. The use of a tube for obtaining a calibrated gas flow rate has the advantage that the kinetic rather than the thermal properties of the gas are important. Such a method would use a tube of known dimensions to control the flow by means of the pressure difference across it. The only property of the gas needed to specify the flow rate is then the molecular mass.

For the Smoluchowski equation (Eq.(28)), a value of α less than one gives a flow rate higher than the Knudsen value (Eq.(27)), with the flow rate diverging to infinity as α tends to zero. Until recently, there have been no well authenticated cases of Smoluchowski's equation being required (that is $\alpha < 1$) instead of Knudsen's equation ($\alpha = 1$) in the molecular flow regime. This is in contrast to the slip flow regime where values of α of less than one are frequently reported. Recent results for air flows in carbon nanotubes have found that the Knudsen equation seriously underestimates the flow in carbon nanotubes in the molecular flow regime, suggesting that the Smoluchowski result may apply with small α. Carbon nanotubes may be exceptional in having atomically smooth walls and diameters less than 2 nm [1]. Meanwhile, the flow of argon and helium in fabricated silicon tubes of similar dimensions has subsequently been found to follow Knudsen's equation even for very high values of Kn up to 10^7 [2].

In order to simplify the calculation of flow across all flow regimes, extended Navier-Stokes equations have been derived which match the Smoluchowski result at large

Kn and the Poiseuille result at small *Kn* and also appear to fit the intermediate regimes well with only one additional empirically determined parameter. A problem arose however, when Arya et al. [3] showed that the use of the Maxwell definition of α is not appropriate in the molecular flow regime. In practice, all collisions are partly diffuse and partly specular so that only the ensemble average of the diffuse component across all collisions is meaningful. Simulation [3] revealed that the use of the Maxwell α overestimates the flow rate except for the trivial case where α is equal to unity. This overestimation resolves the problem in the literature that only values of α close to one are observed.

There are three studies in the literature that measure the mass flow rate of nitrogen in tubes of micrometer dimensions. Ewart et al. studied nitrogen mass flows in 25 μm diameter fused silica tubes in the continuum and slip flow regimes [4]. Tison studied flows in 1.08 μm radius tubes of stainless steel in the slip flow regime [5]. Otani et al. studied the nitrogen mass flow rates in porous Vycor glass in the transition flow regime [6]. In the last case the tubes have an average diameter of 4.5 nm but have a tortuosity. Until now, experimental data has not been available for the same gas in the same well-defined tube across all flow regimes. Here we present results for a 25 μm diameter fused silica tube with exceptionally smooth surface without imperfections [7], covering Knudsen numbers in the range 0.0048 to 12.4583.

A motivation for this work was to validate the approach to the accommodation coefficient of Arya et al. [3] by experiment. A second motivation was to obtain a formula for the accurate calculation of nitrogen mass flow rates in a silica tube across all flow regimes by obtaining a precise value of the empirical parameter in the extended Navier-Stokes

method of Cha and McCoy [8]. The formula would then be useful in controlling nitrogen flows. Silica tubes are readily available with controlled diameters and have relatively smooth surfaces so it is of interest to compare flows in silica and flows in carbon nanotubes.

4.2 Pressure Driven Ideal Gas Flow in a Tube

4.2.1 The Continuum and Slip Flow Regimes

We consider two-dimensional isothermal flow through a cylindrical tube in the form of a tube of length L, radius r_c, as shown in Figure 4. We consider the case where $L/r_c >> 1$, which allows us to neglect end effects near the inlet and the outlet of the tube.

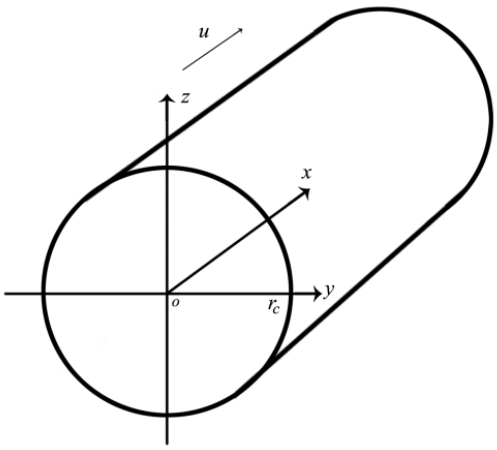

Figure 4 A cylindrical tube showing relevant variables. The flow direction is along x for which the flow velocity u is positive.

The flow is sustained by a pressure drop ΔP. For a cylindrical tube of uniform diameter, the Cauchy equation contains only the viscous drag force and the force arising from the pressure difference and becomes the Stokes equation (see Table 3). In cylindrical coordinates, the Stokes equation is:

$$-\frac{\partial P}{\partial x}+\frac{\mu}{r}\left(\frac{\partial u}{\partial r}+r\frac{\partial^2 u}{\partial r^2}\right)=0 \tag{43}$$

When the *no-slip* boundary condition is applied at the wall, the equation is solved to give the velocity as a function of r. The mass flow rate in the continuum is then given by the well known Poiseuille law (Eq.(42)) for an ideal gas:

$$\begin{aligned}\dot{m}_{continuum}=\dot{m}_P=\frac{\pi {r_c}^4\Delta P\rho}{8\mu L}\\ =\frac{\pi {r_c}^4\Delta P P_m m_m}{8\mu k_B T L}=\frac{\pi {r_c}^4 P_O^2 m_m}{16\mu k_B T L}(\Pi^2-1)\end{aligned} \tag{44}$$

where P_m is the mean pressure across the tube, we define $\Pi = P_i\,/P_o$ as the pressure ratio between inlet and outlet of the tube. It is useful to plot the mass flow rate against pressure ratio Π when the outlet pressure is constant.

In reality, the velocity of flow at the walls is not zero, but has a slip velocity, given by u_w. Reviews of the subject of slip velocity are given in Neto et al. [9] and Cao et al. [10]. Maxwell considered two limiting cases to take into account the collisions between the flowing molecules and the surface of the walls, each described by a value of the TMAC of α. If the surface of the wall is smooth on the molecular size scale, the reflection is perfectly specular. In this case, there is no momentum transferred from the molecules in the direction tangent to the surface of the walls, a case defined by $\alpha = 0$ where α is the average value of the ratio of the tangential momentum transferred to the surface divided by the initial momentum. It is easy to show that this average is also equal to the fraction of molecules that undergo diffuse reflection, if it is assumed that specular reflection and diffuse reflection are the only two options available to a molecule. If the surface of the wall is rough on the molecular scale, diffuse reflection occurs. A complete diffuse reflection transfers, on average, all of the tangential momentum of a molecule to the wall,

a case defined by $\alpha = 1$. In general, the TMAC is in the range of $0 \leq \alpha \leq 1$. Maxwell related α to the slip length that had been introduced by Helmholtz and Piotrowski [11] to refine the boundary conditions for fluid flows in the viscous flow regime involving the first order derivative of the velocity:

$$u_w = \pm \frac{2-\alpha}{\alpha} \lambda \frac{\partial u}{\partial r} \tag{45}$$

Here the mean free path λ is not the kinetic theory result (Eq.(12)), but an expression derived using the hard-sphere model [12]:

$$\lambda = \frac{\mu}{P} \left(\frac{\pi k_B T}{2m_m}\right)^{1/2} \tag{46}$$

This equation gives the previously quoted result for μ (Eq.(12)). Since the Knudsen number changes with pressure, its value in the tube will depend on the distance *x* along the flow direction. $Kn(x)$ is the local Knudsen number, $Kn(x) = \lambda(x)/d$ where $\lambda(x)$ is the local mean free path, defined as $\lambda(x) = \frac{\mu}{P(x)} \left(\frac{\pi k_B T}{2m_m}\right)^{1/2}$ and $P(x)$ is the local pressure. Using an approach in which the presence of a slip velocity is used to correct the Stokes equation, a mass flow rate equation for slip flow conditions can be obtained by integrating Eq.(43) over the cross section to give the flow at location x in the tube [13]:

$$\dot{m}_{slip} = -\frac{\pi {r_c}^4 m_m}{8\mu k_B T} \frac{dP}{dx} [1 + 8A_1 Kn(x)] \tag{47}$$

where $A_1 = \frac{\sigma_p}{k_\lambda}$, $\sigma_p = \frac{2-\alpha}{\alpha}$ is known as the first velocity slip coefficient and k_λ is a coefficient dependent on the assumed molecular interaction model (for example, $k_\lambda = \frac{\sqrt{\pi}}{2}$ for a hard sphere model [12], and $k_\lambda = 0.731$ for nitrogen for a "variable hard sphere" model [4]).

An improved expression for the first velocity slip coefficient is obtained by Albertoni et al.[14]:

$$\sigma_p = \frac{2-\alpha}{\alpha}(\sigma_p(1) - 0.1211(1-\alpha)) \tag{48}$$

where $\sigma_p(1) = 1.016$ is the first velocity slip coefficient when $\alpha = 1$.

In the case where the flow conditions do not change substantially in a tube, it is convenient to use a mean Knudsen number Kn_m to replace $Kn(x)$. A mean Knudsen number can be obtained from the relation $Kn_m = \lambda/d = \frac{\mu}{P_m}(\frac{\pi k_B T}{2m_m})^{1/2}$, where the mean pressure is $P_m = \frac{1}{2}(P_i + P_o)$. By integrating Eq.(47) with respect to x and replacing the integral of $K_n(x)$ by Kn_m, we obtain a convenient result for predicting the mass flow rates in the slip flow regime:

$$\dot{m}_{slip} = \frac{\pi {r_c}^4 \Delta p P_m m_m}{8\mu k_B T L}(1 + 8A_1 Kn_m) \tag{49}$$

This mass flow rate equation applies to the slip flow regime when first-order boundary conditions are used. The first order boundary conditions introduced by Maxwell can be extended by adding a series of derivatives of the high orders of velocities. The highest order of derivative specifies the order of the boundary condition. Where second-order and higher-order boundary conditions are used, a straightforward solution of the Navier-Stokes equations is no longer possible. The Burnett equations are then applicable but are much more difficult to solve. As an approximate method, a separate analysis of the Navier-Stokes equations for the interior region and the region near the walls has been used with higher order boundary conditions at the walls [15].

Maurer et al. [15] compared the use of first and second order boundary conditions with experimental data ranging from the slip flow to the transition flow regimes. In order to illustrate the effects of boundary conditions on the flow rates more clearly, it is useful to define a nondimensional normalised flow rate S defined as the ratio of mass flow rates under the slip boundary conditions to the mass flow rate under no-slip boundary conditions ($\dot{m}_{continuum}$):

$$S = \frac{\dot{m}_{slip-S}}{\dot{m}_{continuum}} = 1 + 8A_1 K_{nm} + 16A_2 ln\,\Pi\, Kn_m^2 \qquad (50)$$

where $\dot{m}_{slip-S}$ is the mass flow rate with second order slip flow boundary conditions, and A_2 is another dimensionless constant dependent on the molecular interaction model. For the hard sphere model $A_2 = \frac{\sigma_{2p}}{{k_\lambda}^2}\frac{\Pi-1}{\Pi+1}$ where σ_{2p} is the second velocity slip coefficient obtained from fitting to experimental data. For the variable hard sphere model [4]:

$$A_2 = (\frac{\sigma_{2p}}{{k_\lambda}^2} + \frac{1}{2{k_\lambda}^2})\frac{\Pi+1}{\Pi-1} \qquad (51)$$

Although the first and second order boundary conditions give somewhat different theoretical predictions, the experimental precision is not sufficient to discriminate between the predictions based on the different orders of boundary condition. Here we compare Eq.(49) for the first order boundary conditions and the mass flow rates for the second boundary conditions obtained from Eq.(50) with the experimental results from Ewart et al. [4] (see Figure 5).

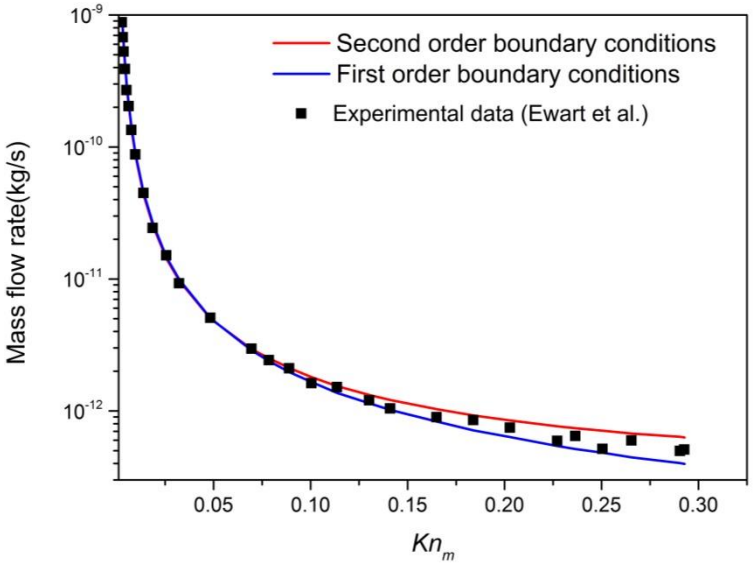

(a)

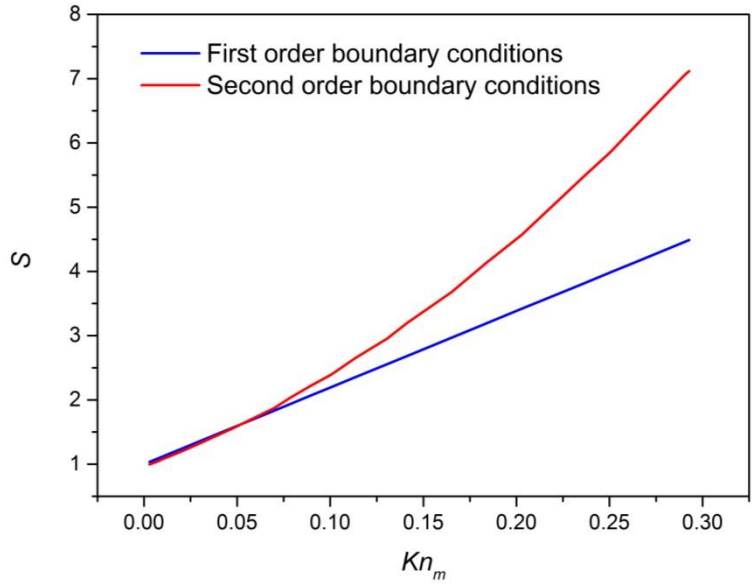

(b)

Figure 5 (a) The points show the experimental measurements of mass flow rate for nitrogen in a cylindrical tube of diameter 25 μm from [4] through the continuum regime, slip flow regime and part of the transition flow regime for a pressure ratio of 3, as a function of Knudsen number. The first order slip boundary conditions (lower curve, blue) and the second order slip boundary conditions (upper curve, red) are calculated from Eqs.(49) and (50); (b) shows the normalised nondimensional flow rate *S* defined in Eq.(50) as a function of the mean Knudsen number for the same two cases as in the theoretical curves in (a) to illustrate more clearly the difference caused by the choice of boundary conditions.

4.2.2 Extended Navier-Stoke Equations: Theory of Cha and McCoy

Cha and McCoy [8] developed equations for ideal gas flows based on the standard assumptions of Poiseuille flow, that the flow is laminar, independent of time, isothermal, that the end effects are negligible, the pressure is uniform in the plane normal to the flow and that the rate of pressure drop along the flow is constant. The approach of their work was to solve the Cauchy equation Eq.(39) by expanding the stress tensor in terms up to third order in velocity gradient and applying the Chapman-Enskog theory to the Krook equation to obtain the expansion coefficient. They required the resulting flow to approach the Smoluchowski equation (Eq.(28)) at large *Kn* and the Poiseuille law (Eq.(42)) at small *Kn*. They found a single adjustable numerical constant was required to match experimental data in the transition flow regime. Therefore, this equation is the extended Navier-Stokes equation we introduced previously which can work for all flow regimes.

For a steady flow, driven by a pressure gradient and in the absence of external body forces, the Cauchy relation Eq.(39) reduces to:

$$\nabla \cdot \boldsymbol{\sigma} = 0 \tag{52}$$

Evaluating the total stress in terms of contributions from pressure gradients and from the shear stress tensor $\boldsymbol{\sigma_s}$this can be written:

$$\nabla P - \nabla \cdot \boldsymbol{\sigma_s} = 0 \tag{53}$$

Expressing the shear stress tensor in terms of the velocity gradient including terms up to the third order in velocity gradient, a dimensionless nonlinear differential equation is obtained:

$$\frac{N^2}{r^*}\frac{d}{dr^*}\left\{r^*\frac{d}{dr^*}\left[\frac{1}{r^*}\frac{d}{dr^*}\left(r^*\frac{du^*}{dr^*}\right)\right]\right\} + \frac{1}{r^*}\frac{d}{dr^*}\left(r^*\frac{du^*}{dr^*}\right) = \beta \tag{54}$$

where $N = 4Kn/\sqrt{\pi}$, $r^* = r/r_c$ is a dimensionless radial coordinate, $u^* = (U - u)/U$ is the dimensionless velocity normalised to the centreline velocity U, and a function:

$$\beta = \frac{{r_c}^2 \Delta P}{\mu U L} \tag{55}$$

The solution to Eq.(54) is the reduced velocity profile [8]:

$$u^* = c_1 - c_2 J_0\left(\frac{r^*}{N}\right) - c_3 Y_0\left(\frac{r^*}{N}\right) + c_4 \ln\left(\frac{r^*}{N}\right) + \frac{\beta {r^*}^2}{4} \tag{56}$$

where c_1, c_2, c_3, and c_4 are constants determined by the boundary conditions and the limits at low and high Knudsen numbers, and J_0 and Y_0 are the Bessel functions of first and second kinds respectively of zero order. For the velocity in the centreline of the tube, $u^*(r^* = 0) = 0$; when r^* tends to zero, $Y_0\left(\frac{r^*}{N}\right)$ and $\ln\left(\frac{r^*}{N}\right)$ approach minus infinity. Using these two conditions, Cha and McCoy show that $c_1 = c_2$, $c_3 = c_4 = 0$. They also found that $c_1 = c_0 Kn\ tanhKn$ where c_0 is a numerical factor determined by empirical methods. The velocity profile for the continuum flow regime was then obtained from the Stokes equation (Eq.(43)):

$$u_{continuum} = \frac{{r_c}^2 \Delta P}{4\mu L}(1 - {r^*}^2) \tag{57}$$

Evaluating the centreline velocity ($r^* = 1$), we obtain a value of β in Eq.(55) for the continuum flow regime:

$$\beta_{continuum} = \frac{{r_c}^2 \Delta P}{\mu L U_{continuum}} = 4 \tag{58}$$

For the molecular flow regime, the boundary conditions are full slip, so the velocities are independent of r. The limiting conditions at large Knudsen number are:

$$\lim_{Kn\to\infty} u^* = 0$$
$$\lim_{Kn\to\infty} \left[1 - J_0\left(\frac{1}{N}\right)\right] = 0 \tag{59}$$

Therefore,

$$\lim_{Kn\to\infty} \beta = \beta_{molecular} 0 \tag{60}$$

Based on Eq.(58) and (60), the ratio of β in the continuum and molecular flow regimes is:

$$\frac{\beta_{molecular}}{\beta_{continuum}} = \frac{1}{1 + \epsilon Kn} \tag{61}$$

where ϵ is the dimensionless factor $\frac{2-\alpha}{\alpha}\frac{64}{3\pi}$,dependent on the TMAC α. Then the reduced velocity profile from Eq.(56) becomes:

$$u^* = c_0 Kn\ tanhK\ [1 - J_0\left(\frac{r^*}{N}\right)] + \frac{{r^*}^2}{1 + \epsilon Kn} \tag{62}$$

From Eq.(58) and the relation $\mu = \frac{\rho}{2}(\frac{8k_BT}{\pi m})^{1/2}\lambda$, the axial velocity is:

$$U = \frac{{r_c}^2 \Delta P}{\mu L \beta_{continuum}}$$
$$= [\frac{8}{3\sqrt{\pi}}\frac{2-\alpha}{\alpha} + \frac{\sqrt{\pi}}{8}\frac{1}{Kn}]\frac{r_c}{\rho}(\frac{m_m}{2k_BT})^{1/2}\frac{\Delta P}{L} \tag{63}$$

From Eqs.(62) and (63), the velocity profile $u(r_c)$ is evaluated. Integrating it gives the mass flow rate in cylindrical tube for all flow regimes:

$$\dot{m} = \int_0^{r_c} 2\pi r \rho u dr$$
$$= \frac{\pi {r_c}^3 \Delta P}{L}\left(\frac{m_m}{2k_BT}\right)^{\frac{1}{2}}\left[\frac{8}{3\sqrt{\pi}}\frac{2-\alpha}{\alpha} + \frac{\sqrt{\pi}}{8}\frac{1}{Kn}\right] \tag{64}$$
$$\times\left\{1 - c_0 Kn\ tanhKn\ \left[1 - 2NJ_1\left(\frac{1}{N}\right)\right] - \frac{1}{2(1 + \frac{2-\alpha}{\alpha}\frac{64}{3\pi}Kn)}\right\}$$

This equation has the correct asymptotic behaviour at small and large Knudsen numbers as required. A single empirically determined parameter, c_0 is required to ensure the correct behaviour in the intermediate flow regimes. At small Knudsen numbers, Eq.(64) gives the same result as the Poiseuille law (Eq.(42)) and at large Knudsen numbers, it gives the same results as the Knudsen equation (Eq.(27)) in the case where $\alpha = 1$. We will use the term Smoluchowski diffusivity for the fraction $\frac{2-\alpha}{\alpha}$.

Cha and McCoy used the nondimensional flow rate *G* to assist comparison with earlier theories where:

$$G = \frac{L}{\pi {r_c}^3 \Delta P} \left(\frac{2k_B T}{m_m}\right)^{1/2} \dot{m} \tag{65}$$

This definition of nondimensional flow rate has been used by other authors and will be referred to as the *reduced mass flow rate* or simply the *reduced flow rate*. *G* is analogous, except for the factor $\left(\frac{2k_B T}{m_m}\right)^{1/2}$, to the concept of *conductivity* in electrical property measurements, as it normalises for the length and the cross sectional area of the tube. Note that the other nondimensional flow rate *S* introduced earlier is useful mainly in the continuum and slip flow regimes, whereas *G* is useful across all flow regimes.

In the limit of large Knudsen numbers, the asymptotic value of *G* from Eqs.(64) and (65) is:

$$G = \frac{8}{3\sqrt{\pi}} \frac{2-\alpha}{\alpha} \tag{66}$$

Cha and McCoy's result for *G* as a function of Kn_m for three different choices of c_0 is shown in Figure 6 with a comparison with experimental data [16-18] and the Knudsen equation [18]. Theories without any empirical parameters based on a solution of the

Boltzmann equation by Cercignani and Daneri [19] and Loyalka and Hamoodi [20], that apply in the transition flow regime are also shown in Figure 6.

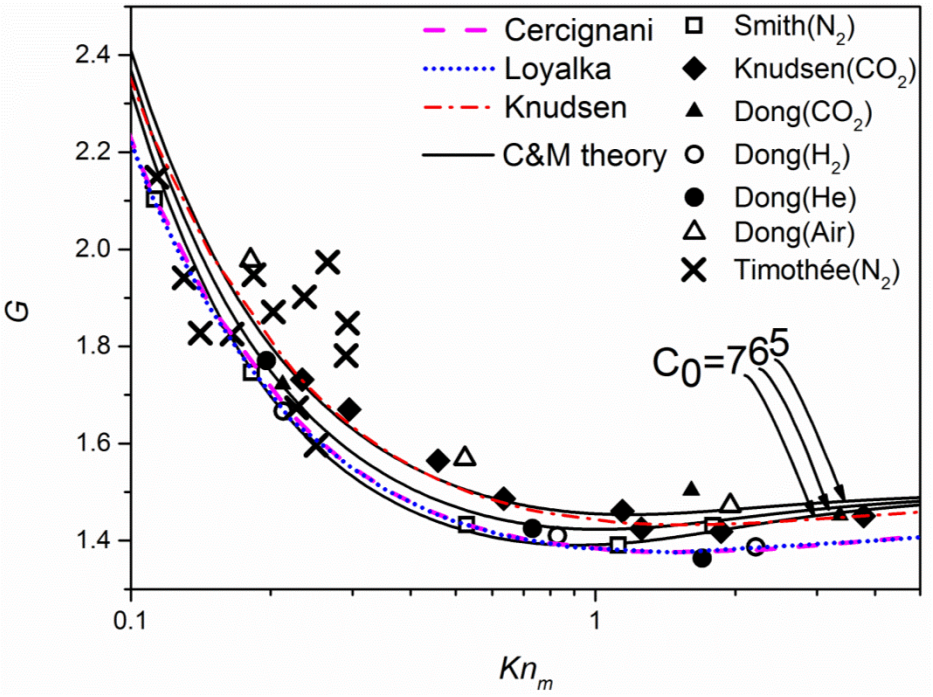

Figure 6 The reduced flow rate G in the transition flow regime for a cylindrical tube (d = 25 μm) as a function of the mean Knudsen number Kn_m showing theoretical predictions for the gases shown in the legend. The results of Cercignani and Daneri [19] and Loyalka and Hamoodi [20] are solutions of the BGK equation and the LBE equation respectively. The result of Knudsen is obtained with an assumption of α = 1[18]. The effect of varying the empirically determined number c_o in the theory of Cha and McCoy (C&M) [8] is shown. Experimental data shown as points for comparison are: Smith [6] and Tomothée for N_2 Knudsen [21]and Dong et al. [22] for CO_2 and Dong for H_2, He and air [22].

The theory of Cha and McCoy illustrates the Knudsen paradox, first enunciated by Knudsen in 1909 [18] which states that there is a minimum value of the mass flow rate per unit pressure difference when plotted as a function of Knudsen number. The occurrence of this minimum value happens when the diffusive flow begins to be dominant where it relates to the physical properties of the gas or vapour and the pressure ratio. In Cha and McCoy, this value shows when the *Kn* is around 1.43 for a cylindrical tube.[8].

There is another theory derived by Beskok and Karniadakis [23] that provides a similar type of formula with that of Cha and McCoy:

$$\dot{m} = -\frac{\pi {r_c}^4 P_m m}{8\mu k_B T}\frac{\Delta P}{L}(1 + aKn)(1 + \frac{4Kn}{1 - bKn}) \qquad (67)$$

Beskok and Karniadakis gave a relation for *a* derived from a fit to the experimental results of Tison [23]:

$$a = a_0 \frac{2}{\pi} tan^{-1}(a_1 Kn^{a_2}) \qquad (68)$$

where a_0 = 1.358, a_1 = 4.0 and a_2 = 0.4. We will use the parameter *b* as an adjustable parameter to fit our data later.

4.2.3 Comparison of Experiment with Theories That Cover All Flow Regimes

Here we compare several popular theories for mass flow rates and the reduced flow rate *G* covering all flow regimes in cylindrical tube. Figure 7 shows a comparison of the theories of Cha and McCoy [8], Lo and Loyalka [24], Loyalka and Hamoodi [20], Valougeorgis and Thomas [25] and Sharipov [26]. The theory of Lo and Loyalka and the theory of Valougeorgis and Thomas are solutions of the BGK equation for a cylindrical tube and the theory of Loyalka and Hamoodi is a solution of the linearised Boltzmann equation for a cylindrical tube. The theory of Graur and Sharipov is a solution of the BGK equation for an elliptical tube. Here we assume that the major and minor axes of an elliptical tube equals, which enable the theory of Graur and Sharipov to be applied for cylindrical tubes in order to allow comparison with other theories. From Figure 7, all the theories become almost consistent when *Kn* is larger than 0.1 for *G*. However, when *Kn* is small, only the theory of Cha and McCoy overlaps with the Navier-Stokes equations

which describe classical behavior in the continuum and slip flow regimes. The other theories are more advanced for the transition and molecular flow regimes as they have no empirical parameters. From Figure 7, it is clear that the reduced flow rate *G* allows a more discriminating comparison of the theories than does the mass flow rate itself.

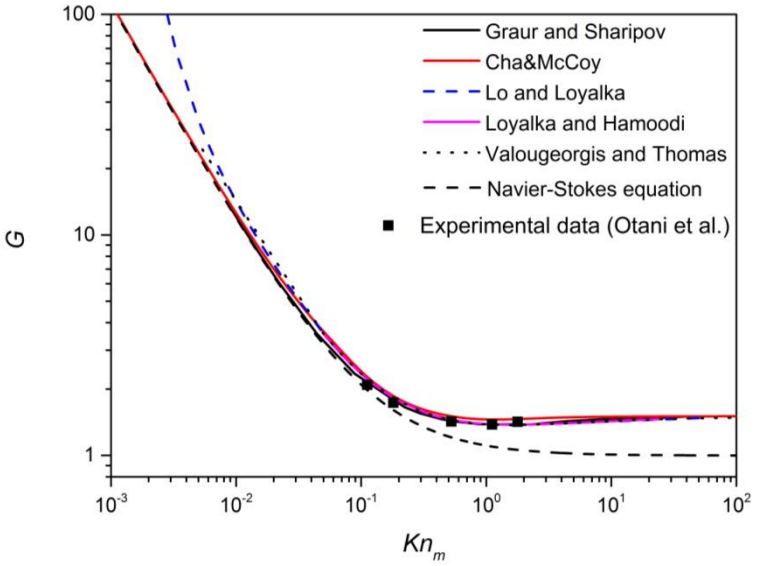

(a)

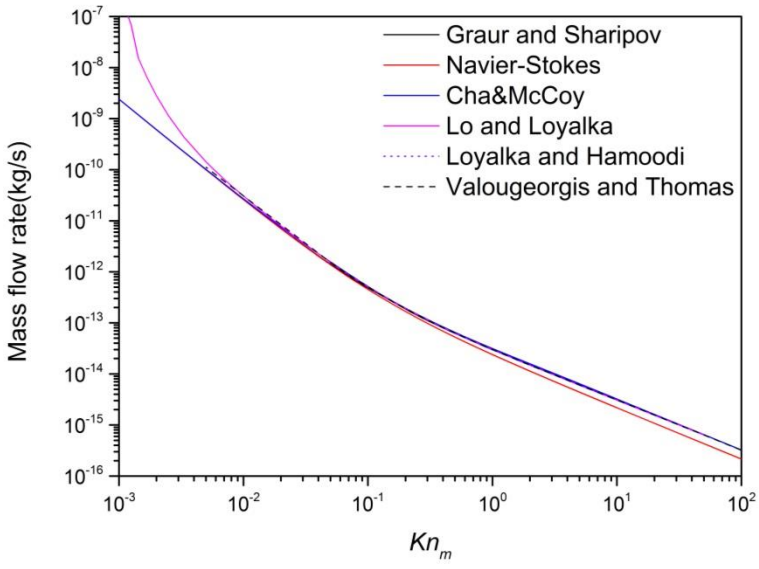

(b)

Figure 7 Comparison of experimental results with theories for helium mass flow rates in cylindrical tubes (d = 25 μm) across all flow regimes, including works by Graur and Sharipov [26], Loyalka and Hamoodi [20], Lo and Loyalka [24], Cha and McCoy [8] and Valougeorgis and Thomas [25]. Also shown is the result for the Navier-Stokes equation. (a) Comparison of theories mentioned above and the classical Navier-Stokes equations with

experimental results of Otani et al. [6] for the reduced flow rate *G*; (b) Comparison the same theories with (a) for mass flow rate.

4.3 Apparatus and Test Method

The experimental apparatus uses the "constant volume technique" [8, 11-13] or "two-chamber method" shown in Figure 8. Two test chambers of constant volume are connected by the microtube under test. The volumes of the test chambers are required to be much larger than the volume within the microtube in order to minimize pressure fluctuations in the chambers to less than 2%.

The volume of Chamber 2 was measured using an additional known volume reference, to obtain a result of 447.6234 ml with a standard error of 0.0098 ml. The pressure in Chamber 2 was measured by an appropriately selected MKS Capacitance Manometers (CM) with maximum pressure readings of 133 Pa, 1333 Pa, 13333 Pa or 133333 Pa. The accuracy of the capacitance manometer was better than 0.5% of the reading. The pressure in Chamber 2 was recorded as a function of time under isothermal conditions at 298 ± 2 K over a period of time using Labview software. The temperature of the surrounding air was logged together with the pressure.

The uncertainties of measurement in the constant volume technique arise principally from the exchange of gases with the walls of Chamber 2 while the test is running. The pressure in Chamber 1 was found to be stable over periods of hours at the operating pressure. The small outgassing of the walls is effectively balanced by the small outflow through the microtube. The leak rate of the two chambers was checked by helium leak detection (QMS 200) and was found to be less than the detection limit (~5.3×10^{-12} kg/s). The minimum measureable nitrogen flow rate was in the order of 10^{-16} kg/s established by the

outgassing rate of Chamber 2 (~1.23×10^{-12} kg/s). Nitrogen mass flow rates in the range of 1×10^{-10} to 2×10^{-15} kg/s were possible for measurement.

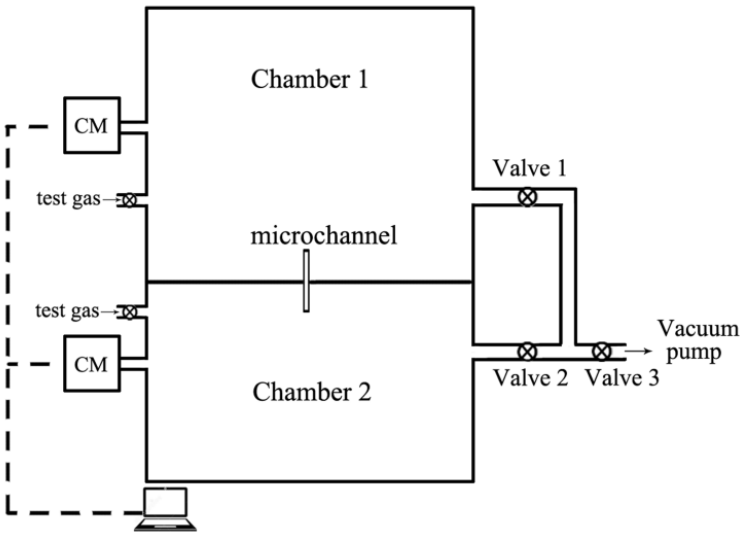

Figure 8 The apparatus consists of two chambers connected by the microtube under test. Chamber 1 is at the higher pressure and Chamber 2 has a known volume. After the test pressures are established, both chambers are isolated from inflows and outflows. The pressures in the chambers are monitored using capacitance manometers.

The silica microtube was from SGE Analytical Science Pty Ltd (Australia) of specified diameter 25 ± 0.5 μm and 20 cm length. The diameter was confirmed to an uncertainty of ± 3 μm using an image from an Axioplan 2 optical microscope Figure 9 (a) and a calibrated 50 μm reference length. The advancing contact angle of the tubes was measured to be 82° measured by optical microscope (shown in Figure 9 (b)). The measured contact angle is in agreement with the fabrication temperature of 1000°C reported by the manufacturer. Baking at these temperature is known to increase the water contact angle of silica [27, 28]. Limited by the saturation pressure of water vapor at a certain temperature, we can only obtain Knudsen numbers from the transition flow regime. Three tubes of length 1 cm were used in part of the transition flow regime ($0.1 < Kn < 10$) and for near the molecular flow regime ($Kn > 10$) 30 tubes of 1 cm length

were used. As the length of the tube is much larger than the diameter, end effects were neglected. The largest Reynolds number in this study was 2.26×10^{-5} ensuring laminar flow.

The measurement procedure of nitrogen mass flow rates is summarised below:

(1) Open valves 1 and 2 and pump Chambers 1 and 2 down to ~ 10^{-4} Pa;

(2) Close pump and fill Chambers 1 and 2 with nitrogen in high pressure, close valve 1;

(3) Open pump to decrease the pressure in Chamber 2 to low pressure, close valve 2;

(4) Start to record data of pressure change in Chamber 2.

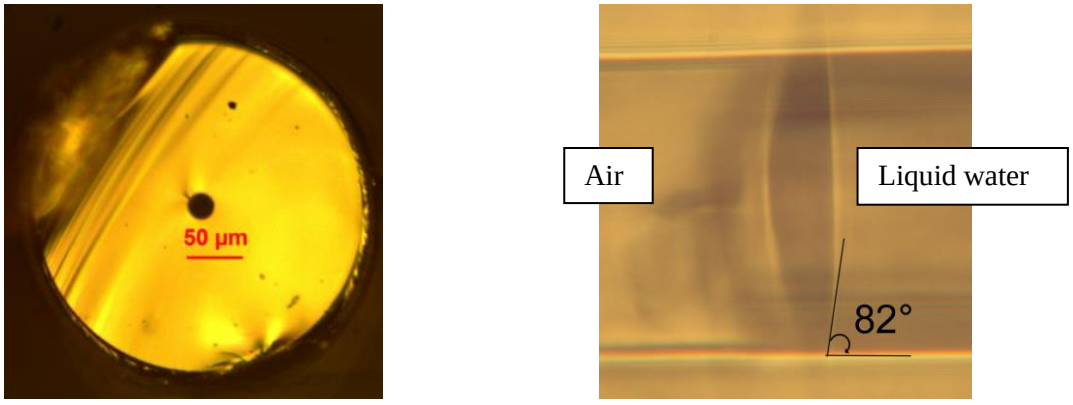

(a) (b)

Figure 9 (a) An optical microscope image of the 25 ± 0.5 μm diameter cylindrical microtube in cross section. (b) An optical microscope image of liquid water in the 25 μm channel. Water contact angle was measured as 82°.

4.3.1 Analysis of Uncertainty

For isothermal conditions, the ideal gas law applies:

$$P_o V_2 = m_m k_B T \tag{69}$$

where P_o is the pressure in outlet of the channel and V_2 are the pressure and volume of Chamber 2. From Eq.(69),

$$\frac{dP_o}{P_o} = \frac{dm}{m} + \frac{dT}{T} \tag{70}$$

We can obtain the mass flow rate by combining Eqs.(69) and (70):

$$\dot{m} = \frac{dm}{dt} = \frac{V_2}{k_B T}\frac{dP_o}{dt}(1-\delta); \quad \delta = \frac{dT/T}{dP_o/P_0} \tag{71}$$

If δ is much smaller than 1, an uncertainty estimate is obtained following Ewart et al. [4] For our experiments, the temperature variation is 2 K and pressure variation is 2%, giving a value of δ of the order of 0.34. In order to determine the mass flow rate, the only unknown parameter in Eq.(71) is $\frac{dP_o}{dt}$, obtained from a linear fitting of experimental data as a function of test time:

$$P_{0f}(t) = a't + b' \tag{72}$$

The uncertainty in the coefficient a' is ± 0.5% for our experiments. Thus, we can obtain a total uncertainty in mass flow rate of ± 3.24% ($\frac{\Delta V}{V}$ = ± 2.1%, $\frac{\Delta T}{T}$ = ± 0.67%, $\frac{\Delta a}{a}$ = ± 0.5%).

4.3.2 An Example of Recording Pressure Change

For nitrogen flow rate measurements (P_i = 71820 Pa, P_o = 23940 Pa), the pressure change in the outlet side of the tube is the red dots in Figure 10(a). The outgassing rate (black dots in Figure 10(a)) of the chamber results from natural adsorption of water vapour and other adsorbants. We measured the outgassing rate using two kinds of gauges with both showing a similar outgassing rate. The outgassing rate is stable at constant temperature and does not vary with nitrogen pressure since nitrogen absorbs weakly on stainless steel. We applied linear fitting to obtain rates of pressure rising for the outlet side of the tube

(black line) and the outgassing (red line), and then used the former one to reduce the latter one to gain a rate of dP_o/dt to calculate the mass flow rate using Eq. (71).

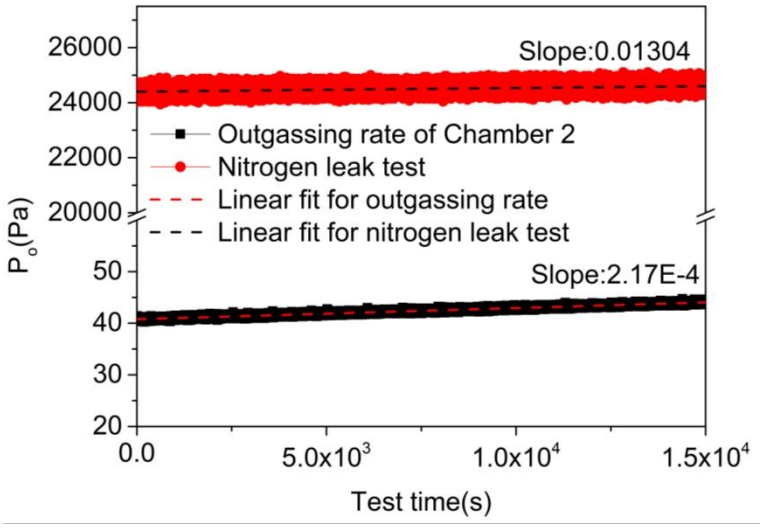

(a)

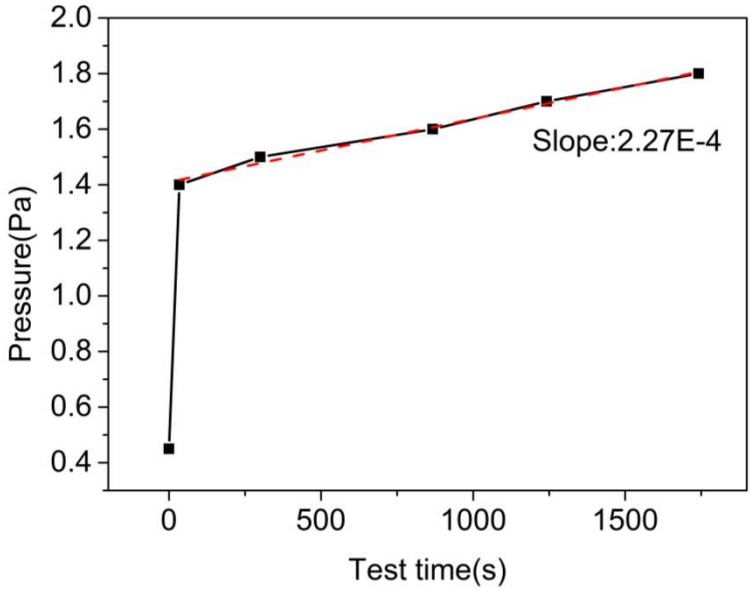

(b)

Figure 10 (a) An example of the pressure change in Chamber 2 with time during a flow test (red line). The inlet pressure is 71820 Pa and the outlet pressure is 23940 Pa. The black line shows the outgassing rate of Chamber 2 in the absence of a flow tube; (b) outgassing rate test using a hot cathode ionization gauge.

4.4 RESULTS AND DISCUSSION

The experimental values of the mass flow rate as a function of the inlet and outlet pressures are given in Table 4. Every value is a result of one measurement with ± 3.24% for uncertainty. The theory of Cha and McCoy fits the experimental results well across all of the flow regimes with $\alpha = 1$ (Figure 11). The value of the empirical parameter c_0 that gives the best fit is $c_0 = 6.5 \pm 1.5$.

We obtain a value of the empirical parameter b of 0.39 for the theory of Beskok and Karniadakis (Eq. (67)) which provides a good fit with our experimental data for the continuum and molecular flow regimes. However, it does not fit our data well for the slip and transition flow regimes as shown in Figure 11.

The use of G is necessary for comparison of our results with other authors (see Figure 12) as a variety of tube materials and diameters were used, each covering a limited flow regime. The results of Tison in Figure 12 were digitized from the conductance in his Figure 5 in $(\text{mole g})^{1/2}/\text{Pa/s}$, converted to a molar conductance and then to the reduced flow rate (Eq.(65)). The results of Ewart et al. were taken from their Table 9 and converted to G using the quoted pressure difference and tube dimensions (diameter 25 μm, length 5.3 cm). The results of Otani et al. were digitized from Figure 3 in Cha and McCoy, a plot of G as a function of r_c/λ. The values of λ were converted to Kn using Eq.(22). The results of all authors except for Tison agree well with our results. The results of Tison can be brought into alignment with all other results by multiplying the values of G by a scale factor of 1.64. The reason for the need for a scale factor for the Tison data is not known, but could be associated with turbulent flow near the inlet of his tube where

the high pressure gives a Reynolds number of ~ 10^5. Note that the theory of Beskok and Karniadakis provides a good fit only to the data of Tison.

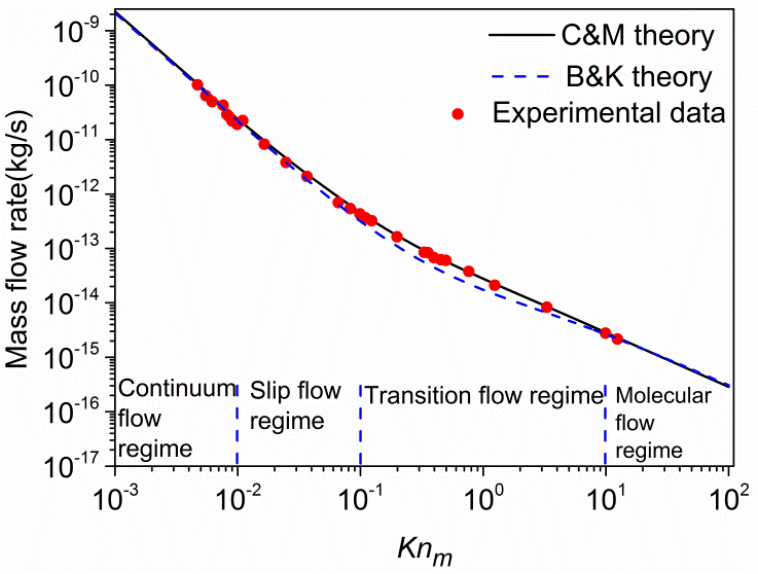

Figure 11 Experimental nitrogen mass flow rates as a function of mean Kn_m fitted with Cha and McCoy theory (c_0 = 6.5 ± 1.5). The data are for a pressure ratio P_i/P_o of 3.

Cha and McCoy assumed a value of α of unity after considering a wide variety of gases. Fitting our data to the Navier-Stokes equations with first order Maxwell boundary conditions only in the slip flow regime ($0.0048 < Kn_m < 0.1$) gives a value of α of 0.91 ± 0.051. Since the wall condition is constant throughout all flow regimes, it is noteworthy that we obtain a value of α of 1.000 ± 0.032 in the Knudsen regime (using our data for $Kn_m > 5$). This is a lower bound for α in our tube since G asymptotes from below at large Kn_m. The definition of α used by Maxwell and Smoluchowski has recently been shown to be inappropriate for the molecular flow regime by Atrya et al. who point out that each reflection has a diffuse component and a specular component [3], so that Maxwell's assumption that reflections are either fully diffuse of fully specular is not correct. Arya et al. [3] show by simulation that the use of Maxwell's definition for α

and the Smoluchowski diffusivity $(2-\alpha)/\alpha$ greatly overestimate the flow at large *Kn* and that the modified Smoluchowski diffusivity for the flow at large *Kn* should be:

$$D_{mS} = 1 - \frac{2\pi}{\ln \epsilon'} \frac{1-\alpha'}{\alpha'} \tag{73}$$

where α' is defined as the ensemble average of the diffuse fraction, and ϵ' is cutoff parameter of the order of 10^{-6} [3]. Therefore, our value of α of 0.91 ± 0.051 in the slip flow regime is consistent with the value of unity at large *Kn*. Our value of α in the slip flow regime agrees with that found by Maurer et al. [15] in silicon wafer microtubes (0.87 ± 0.03), by Ewart et al. [4] in fused silica microtubes (0.933 ± 0.037) and Porodnov et al. [29] in glass tubes (0.925 ± 0.014). Despite the relative smoothness of a silica glass surface, we conclude that the walls of our silica tube are not smooth on the atomic scale using either definition of accommodation coefficient and there is no similarity to the behaviour of a carbon nanotube. We note that in cases where the walls are smooth it will be necessary to modify the equation of Cha and McCoy (Eq.(64)) by replacing the Smoluchowski diffusivity $(2-\alpha)/\alpha$ by D_{mS} in Eq.(73).

Table 4 Experimental results for the mass flow rate as a function of the inlet and outlet pressures in the tube.

Kn_m	P_i(Pa)	P_o(Pa)	$\dot{m}$(kg/s)
0.0048	83790	27930	1.0197e-10
0.0055	71820	23940	6.4537e-11
0.0062	63840	21280	5.0081e-11
0.0077	51870	17290	4.2835e-11
0.0082	48279	16093	2.9126e-11
0.0085	46816	15428	2.7101e-11
0.0091	43890	14630	2.2145e-11
0.0099	39900	13300	1.9059e-11
0.0111	35910	11970	2.2550e-11
0.0166	23940	7980	8.2841e-12
0.0249	15960	5320	3.8325e-12
0.0369	10773	3591	2.1154e-12
0.0664	5985	1995	7.0232e-13
0.0831	4788	1596	5.4381e-13
0.0997	3990	1330	4.3421e-13
0.1103	3591	1197	3.6676e-13
0.1240	3192	1064	3.2460e-13
0.1979	1995	665	1.6441e-13
0.3584	1197	399	8.5155e-14
0.3559	1117.2	372.4	8.4312e-14
0.3987	997.5	332.5	6.8199e-14
0.4530	877.5	292.6	6.2654e-14
0.4983	798	266	6.0594e-14
0.7935	518.7	172.9	3.7940e-14
1.2458	319.2	106.4	2.1078e-14
3.3222	119.7	39.9	6.3057e-15
9.9666	39.9	13.3	2.7720E-15
12.4583	31.92	10.64	2.1695E-15

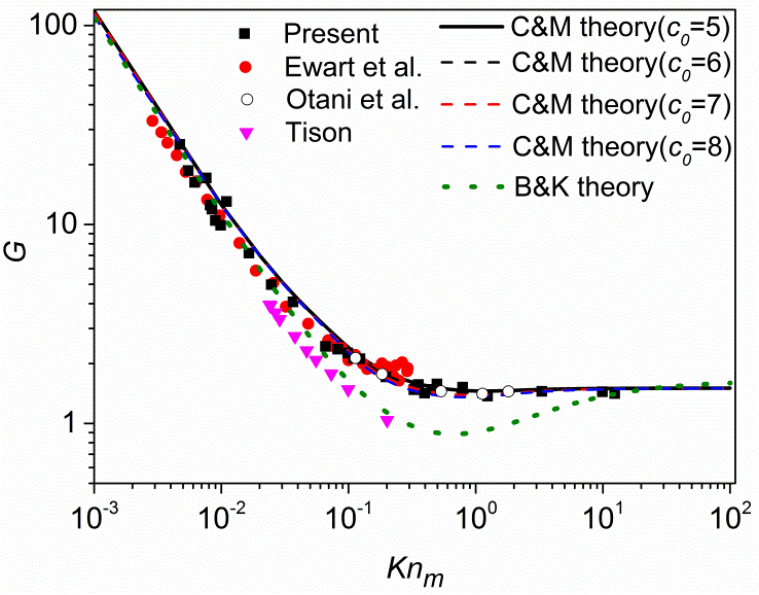

(a)

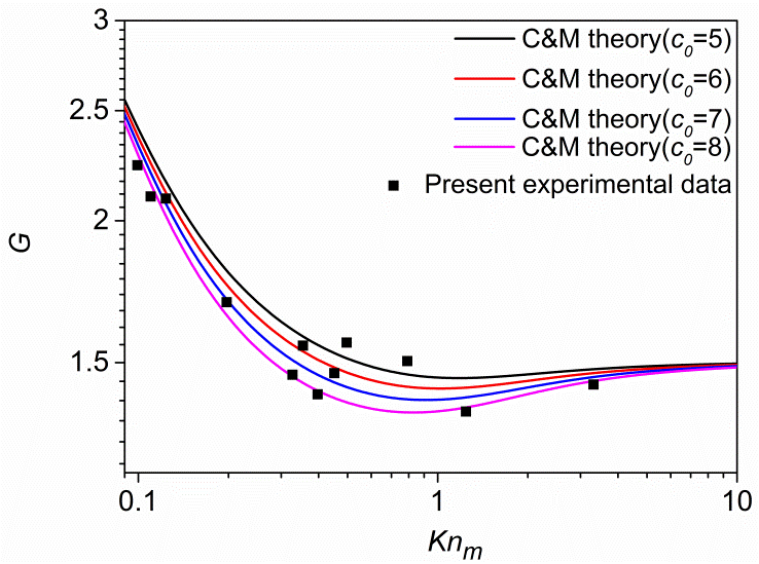

(b)

Figure 12 (a) The experimental results of this work for reduced nitrogen flow rates G compared to reported values in the literature. Red dots show data of Ewart et al. [4], circles show data from Otani et al. [6], and pink triangles show data from Tison. [5] The solid line is the theory of Cha and McCoy (C&M theory) (Eq. (64)); (b) enlargement showing the fitting of c_0 in the transition flow regime.

4.5 CONCLUSION

We have shown that the theory of Cha and McCoy with the value of c_0 of 6.5 ± 1.5 provides an excellent fit to experimental measurements across all flow regimes for the flow of nitrogen in a silica capillary. A silica capillary can be used to provide a calibrated mass flow rate that depends only on a knowledge of the capillary length, diameter and the pressure difference. Our result enables an accurate mass flow of nitrogen to be delivered to a process. If the process requires admission into vacuum or near vacuum, only the inlet pressure requires measurement.

The value we find of the Maxwell accommodation coefficient of 0.91 ± 0.051 agrees with all other measurements in the literature for nitrogen flow in silica. However, there will be cases for ultra-smooth walls where the Arya et al. [3] result for the diffusivity D_{mS} should replace the Smoluchowski diffusivity in the equation of Cha and McCoy (Eq. (64)).

REFERENCES

1. Holt, J.K., et al., *Fast mass transport through sub-2-nanometer carbon nanotubes.* Science, 2006. **312**: p. 1034-1037.
2. Gruener, S. and P. Huber, *Knudsen Diffusion in Silicon Nanochannels.* Phys. Rev. Lett., 2008. **100**: p. 064502.
3. Arya, G., H.-C. Chang, and E. Maginn, *Knudsen Diffusivity of a Hard Sphere in a Rough Slit Pore.* Phys. Rev. Lett., 2003. **91**: p. 026102.
4. Ewart, T., et al., *Mass flow rate measurements in gas micro flows.* Exp. Fluids., 2006. **41**: p. 487-498.

5. Tison, S.A., *Experimental Data and Theoretical Modeling of Gas Flows through Metal Capillary Leaks.* Vacuum, 1993. **44**: p. 1171-1175.

6. Otani, S., N. Wakao, and J.M. Smith, *Part II. Diffusion and flow in porous catalysts.* AIChE J., 1965. **11**: p. 435-445.

7. SGE Analytical Science. *LC PEEKsil Tubing*, *http://www.sge.com/products/gc-lc-supplies/lc-supplies/lc-peeksil-tubing3*. 2015.

8. Cha, C.Y. and B.J. McCoy, *Application of third-order constitutive relations to Poiseuille flow of a rarefied gas.* J. Chem. Phys., 1971. **54**: p. 4373-4383.

9. Neto, C., et al., *Boundary Slip in Newtonian Liquids: A Review of Experimental Studies.* Rep. Prog. Phys., 2005. **68**(12): p. 2859-2897.

10. Cao, B.Y., et al., *Molecular Momentum Transport at Fluid-Solid Interfaces in MEMS/NEMS: A Review.* Int. J. Mol. Sci., 2009. **10**(11): p. 4638-706.

11. Maxwell, J.C., *On stresses in rarified gases arising from inequalities of temperature.* Phil. Trans. R. Soc. Lond., 1879. **170**: p. 231-256.

12. Chapman, S. and T.G. Cowling, *The Mathematical Theory of Non-Uniform Gases.* 3 ed. 1970, UK: Cambridge University Press.

13. Graur, I.A., J.G. Méolans, and D.E. Zeitoun, *Analytical and Numerical Description for Isothermal Gas Flows in Microchannels.* Microfluidics Nanofluidics, 2005. **2**(1): p. 64-77.

14. Albertoni, S., C. Cercignani, and L. Gotusso, *Numerical Evaluation of the Slip Coefficient.* Phys. Fluids, 1963. **6**(7): p. 993-996.

15. Maurer, J., et al., *Second-Order Slip Laws in Microchannels for Helium and Nitrogen.* Phys. Fluids, 2003. **15**: p. 2613-2621.

16. W.Dong and L.A.Bromley. in *Transactions of 8th Vacuum Symposium and 2nd International Congress on Vacuum Technology*. 1961. New York.

17. Otani, S., N. Wakao, and J.M.Smith, *Significance of Pressure Gradient in Porous Media: Part II. Diffusion and Flow in Porous Catalysts.* AIChE Journal, 1965. **3**: p. 7.

18. Knudsen, M., *The laws of molecular and viscous flow through tubes (in German).* Ann. Phys. (Berlin), 1909. **28**: p. 75-130.

19. Cercignani, C. and A. Daneri, *Flow of a Rarefied Gas between Two Parallel Plates.* J. Appl. Phys., 1963. **34**(12): p. 3509-3513.

20. Loyalka, S.K. and S.A. Hamoodi, *Poiseuille Flow of A Rarefied Gas in A Cylindrical Tube: Solution of Linearized Boltzmann Equation.* Phys. Fluids A, 1990. **2**(11): p. 2061-2065.

21. Ewart, T., et al., *Mass flow rate measurements in gas micro flows.* Experiments in Fluids, 2006. **41**(3): p. 487-498.

22. Dong, W., *Internal Report (UCRL-3353)*. 1956: University of California.

23. Beskok, A. and G.E. Karniadakis, *Report: A Model for Flows in Channels, Pipes, and Ducts at Micro and Nano Scales.* Microscale Therm. Eng. , 1999. **3**(1): p. 43-77.

24. S.S.Lo and S.K.Loyalka, *An Efficient Computation of Near-Continuum Rarefied Gas Flows.* J. Appl. Math. Phys., 1982. **33**: p. 419-424.

25. Valougeorgis, D. and J.R. Thomas Jr, *Exact Numerical Results for Poiseuille and thermal Creep Flow in A Cylindrical Tube.* Phys. Fluids, 1986. **29**: p. 423-429.

26. Graur, I. and F. Sharipov, *Gas Flow through An Elliptical Tube over the Whole Range of the Gas Rarefaction.* Eur. J. Mech. B-Fluid 2008. **27**: p. 335-345.

27. Vigil, G., et al., *Interactions of silica surfaces.* J. Colloid Interface Sci., 1994. **165**: p. 367-385.

28. Zhuravlev, L.T., *The surface chemistry of amorphous silica. Zhuravlev model.* Colloids Surf., A, 2000. **173**: p. 1-38.

29. Porodnov, B.T., et al., *Experimental Investigation of Rarefied Gas Flow in Different Channels.* J. Fluid Mech., 2006. **64**: p. 417-438.

Chapter 5 Enhanced Water Vapour Flow in Silica Microtubes Explained by Maxwell's Tangential Momentum Accommodation and Langmuir's Adsorption

Maxwell introduced the TMAC in 1879 to describe boundary conditions in fluid flow [1]. Recent findings of anomalously high gas flow rates in carbon nanotubes show how smooth hydrophobic walls can increase specular reflection of molecules and reduce TMAC. Here we report the first measurements of water vapour flows in microtubes over a wide humidity range and show that for hydrophobic silica there is a range of humidity over which an adsorbed water layer reduces TMAC and accelerates flow. Our results show that this association between hydrophobicity and accelerated moisture flow occurs in readily available materials. We develop a hierarchical theory that unifies Maxwell's ideas on TMAC with Langmuir's ideas on adsorption. We fit the TMAC data as a function of humidity with the hierarchical theory based on two stages of Langmuir adsorption and derive total adsorption isotherms for water on hydrophobic silica that agree with direct observations. We propose structures for each stage of the water adsorption, the first reducing TMAC by a passivation of adsorptive patches and a smoothing of the surface, the second resembling bulk water with large TMAC. We find that leak testing of moisture barriers with an ideal gas such as helium may not be accurate enough for critical applications and that direct measurements of the water leak rate should be made.

5.1 INTRODUCTION

The study of water flows, especially over hydrophobic surfaces, is of importance in many areas of scientific and technological interest including permeation through membrane channels [2-5], through carbon nanotubes [6-9], the formation of micelles [10] and biological self-assembly processes [11, 12]. Recent findings for liquid water flows in channels lined with hydrophobic aquaporins [3, 4] and in carbon nanotubes [6-9] show that the boundary conditions lead to large slip lengths and higher than expected flow rates. The flow of water vapour as well as the flow of liquid water has become very important in the understanding of the penetration of moisture through encapsulations designed to protect sensitive electronic devices such as active implantable prosthetics ("bionic" ears and eyes). Therefore, there is a need to investigate water vapour flows in hydrophobic channels to determine whether such effects are reflected in changes in TMAC and whether they translate to strongly enhanced water vapour flows.

In the early years of the 20th century, the regime of free molecular flow, in which the mean free path is larger than the channel width, was investigated as an application of the kinetic theory of gases. Knudsen [13] developed a formula for an ideal gas flow under the assumption that all molecules suffer diffuse reflections from the walls, an assumption which has been confirmed many times by experiment when the gas is in the free molecular flow regime. Flows of a wide variety of gases have been carefully studied in the years since Knudsen's paper appeared, with one important exception: water vapour, the flow of which has received hardly any attention, probably because of the perceived experimental difficulty of controlling the adsorption of water to the walls of the flow channel. While Knudsen's formula for free molecular flow assumed α was equal to one,

Smoluchowski [14] allowed it to take any value between zero and one. More recently, it has been realized that the TMAC is a sensitive probe of molecule/surface interactions [15]. Flow rates of hydrogen [8], air [9], argon [8],[16], nitrogen [8],[16] and oxygen [8],[16] greatly exceeding Knudsen's prediction have been found in carbon nanotubes, leading to the idea that very smooth hydrophobic surfaces do in fact lead to very small values of α.

Silica glass was chosen for this study of the TMAC of water vapour because of its well-known water adsorption and its ability to show a transition from a hydrophilic to a hydrophobic surface by suitable heat treatment [17-20]. The hydrophobic form of silica glass is prepared directly from the melt or by heating above 600 K [21] and the hydrophilic form is obtained by hydroxylation of the hydrophobic form by reaction with acids or bases in aqueous solution. The water adsorption isotherms of the hydrophobic form differ significantly from those of the hydrophilic form [19]. Since adsorption destroys tangential momentum, it is conceivable that these adsorption observations could be linked with TMAC observations. A theoretical basis for linking Langmuir's adsorption theory with the boundary conditions for flow (including the Maxwell TMAC) has been attempted by Myong et al. [22, 23] but there are no observations of both adsorption and TMAC on a single surface to test these ideas. An intriguing result has been found by Seo et al. [15] [24] in which a layer of water and ocatadecyltrichlorosilane (OTS) adsorbed on the surface of silica glass greatly reduces the value of TMAC that applies to incident nitrogen molecules. For the paper on water adsorption modifying TMAC, the nitrogen TMAC for both hydrophilic and hydrophobic silica glass has been measured [15] at various humidity levels using an atomic force microscope. For hydrophobic silica there

is a range of humidities that causes the nitrogen TMAC to fall to as low as 0.2 before it rises again to 1 as the saturation pressure is approached, a result regarded as unexpected and unexplained by Seo et al. They also found that a small TMAC is caused by OTS adsorption. The OTS films provide a smooth layer on silica and the stiffness of OTS films also plays a role at low temperature. If such effects applied to incident water molecules colliding with the walls of a channel, then the water vapour flow would be greatly affected.

5.2 Adsorption and Condensation

There are three possible components to the flow of a condensable vapour in a tube: gas phase flow, surface flow and tube condensate flow (where liquid plugs the tube). Gas phase flow where it approximates ideal gas behaviour is described by the methods of the previous sections for non-condensable gases. Surface and tube flows represent new contributions to the mass flow rate and they can make a larger contribution to the total flow than gas phase flow under some conditions. For example, surface diffusion alone can account for the majority of the total mass flow of moisture in nano-dimensional tubes [25], and the presence of tube condensate also can have significant effects on reducing or enhancing the flow, depending on the conditions.

5.2.1 Adsorbed Layers

Condensable gases such as water initially form monolayers and then multilayers on the surfaces of tubes and pores under isothermal conditions, producing a layer thickness that is time dependent before reaching an equilibrium value depending on the pressure of the vapour relative to the saturation vapour pressure. An overview of adsorption is provided

in the book by Butt et al. [26]. A distinction between adsorbed layers and subsequent condensate is somewhat arbitrary, but can be made in terms of the strength of interaction with the surface. The thickness of the adsorbed layer determines the mass flow rate through the tube, strongly influencing surface and tube condensate flow. The relation between the vapour pressure above a surface and the number of adsorbed particles per unit area at a given temperature is the *adsorption isotherm*. The theory of Brunauer, Emmett, and Teller (BET) for isothermal adsorption builds upon the more basic theory for monolayer adsorption derived by Langmuir by describing the build-up of multilayers each of which is described by Langmuir theory for a single monolayer. In the BET theory, the heat of adsorption for the first layer Q_1 differs from that of all further layers Q_i which are all equal to the heat of condensation of the liquid; Q_1 and Q_i influence the rate of desorption. Adsorption and desorption processes are only allowed to take place between the vapour and the immediate surface in the model, and adsorbed molecules are not allowed to move from one layer directly to another.

The amount of adsorption at an interface is described by the function Γ which measures the number of molecules adsorbed per unit area. A plot of Γ versus the pressure *P* of vapour at constant temperature is an *adsorption isotherm*. Adsorption where the sublimation energy is lower than 50 kJ/mol is typically referred to as physisorption, whereas adsorption within typical sublimation energies of higher than 50 kJ/mol is referred to as chemisorption and involves chemical reactions [27]. Substances with sublimation energies < 20 kJ/mol effectively do not adsorb as the available energy (kT) is of the same order as the sublimation energy. Here we consider physisorption, rather than

chemisorption, since a water flow will be most strongly influenced by reversible adsorption.

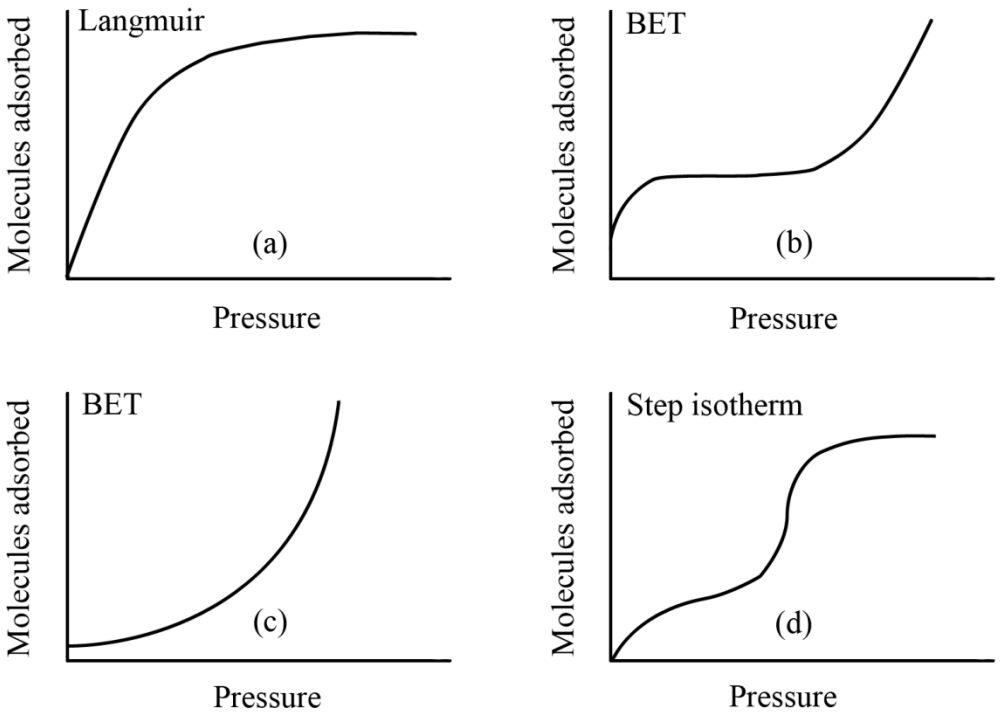

Figure 13 Classification of four common adsorption isotherms for condensation on surfaces. (a) Langmuir isotherm for a single monolayer, (b) BET isotherm (for high values of the parameter $\boldsymbol{C}$ - see Eq.(76)), (c) BET isotherm (for low values of the parameter $\boldsymbol{C}$), and (d) step isotherm, showing BET model at lower pressures and saturation at higher pressures, commonly seen in porous materials, which saturate when all pores have been filled. Reproduced with permission from Choi et al. [25].

All of the basic isotherms show an increase in the amount of adsorption as pressure increases. The normal Langmuir isotherm is a monolayer adsorption that forms the basis for the more complex behaviours. The BET adsorption isotherms show no saturation (Figure 13(b)) while the other type of BET isotherm (Figure 13(c)) shows saturation for high pressures. The BET isotherm in Figure 13(c) is relevant to porous materials. A feature of adsorption in porous solids is that on desorption, as pressure is reduced, *hysteresis* is often observed.

Experimental studies have been made of adsorbed water layers using ellipsometry [28] and atomic force microscope (AFM) [15] by measuring the thickness of the adsorbed layers. We will confine attention here to a range of materials having various affinities with water, as determined by the contact angles. For example, Tadros et al. [29] have studied water adsorption on polyethylene and have obtained the BET behaviour shown in Figure 13(c). Ellipsometry modeling of adsorption normally assumes a single adsorbed layer and therefore does not distinguish between a smooth layer conformal with the surface and an array of adherent droplets. We now discuss the mathematical description of the various adsorption isotherms.

(1) The Langmuir Adsorption Isotherm

A simple model to describe adsorption was presented by Langmuir in 1916 [30]. The model assumes that the surface contains a certain number of binding sites. Binding progresses until all sites are filled and the surface is saturated, with each site being able to be occupied once only, at which point a complete monolayer is reached. The amount of material adsorbed on the surface depends on the adsorption and desorption rates of the gas molecules from the surface binding sites: the adsorption rate is assumed to depend on both of the number of the vacant binding sites and the pressure, while the desorption rate is assumed to depend on the number of adsorbed molecules (the total number of binding sites reduce vacant ones). Equilibrium is reached when the adsorption and desorption rates are equal to one another. The particle number adsorption given by the Langmuir adsorption isotherm is:

$$\Gamma(\mathrm{P}) = \Gamma_{mon} \frac{K_L\, P}{1 + K_L P} \tag{74}$$

where Γ is the particle number adsorption per m^2, K_L is the ratio of adsorption to desorption rate, known as the Langmuir adsorption constant, and Γ/Γ_{mon} is the relative coverage, and Γ_{mon} is the particle number adsorption per square meter in a full monolayer. We will use this isotherm to develop a theory for TMAC in this Chapter.

(2) The BET Adsorption Isotherm

The expression for the BET isotherm takes the form:

$$\frac{\Gamma}{\Gamma_{mon}} = \frac{\boldsymbol{C}}{\left(1-\frac{P}{P_s}\right)\left[1+\frac{P}{P_s}(C-1)\right]}\frac{P}{P_s} \tag{75}$$

where P_s is the equilibrium saturation vapour pressure, and $\boldsymbol{C}$ is given by:

$$\boldsymbol{C} = \boldsymbol{C}_B e^{(Q_1-Q_i)/RT} \tag{76}$$

where R is the ideal gas constant and $\boldsymbol{C}_B$ is a constant that depends on the binding properties of the surface. Note that the ratio Γ/Γ_{mon} is a measure of the equivalent number of monolayers built up and becomes infinite as $P/P_s \to 1$, which is expected because condensation then continues unabated.

For large values of the parameter $\boldsymbol{C}$, the binding of vapour molecules from the vapour directly to the surface is strong compared with the intermolecular interaction (see Figure 13(b)). For small values of $\boldsymbol{C}$, the molecules prefer binding to themselves while the binding energy to the surface is lower (see Figure 13(c)). Therefore, in the case of low values of $\boldsymbol{C}$, the *first monolayer* only forms at relatively high pressures, and once it has formed, it is easier for the next molecules to adsorb.

By calculating the number of layers that build up, Γ/Γ_{mon}, it is possible to determine the overall thickness of the multilayer by multiplying the number of layers by the thickness of each layer. This is expressed as

$$t_l = (n/n_{mon})V_t/S_t \tag{77}$$

where V_t/S_t is the ratio of specific volume to the specific surface area of the tube.

5.2.2 Surface Flows

Surface flows primarily occur in small tubes and porous media in which case the transport of adsorbed molecules competes with transport in the gas phase. During the period from the 1940s to the 1980s, surface flows attracted many researchers [31-34]. The starting point is a two dimensional form of Fick's law [34] which for a cylindrical tube is:

$$\dot{n} = -2\pi r_c D_s \frac{d\Gamma'}{dx} \tag{78}$$

where D_s is the surface diffusion coefficient, Γ' is the surface concentration in particles per unit area of the condensed vapour. Compared to other flow modes, for example Knudsen flow, which has a dependence on ${r_c}^3$ and Poiseuille flow which has a dependence on ${r_c}^4$, the linear dependence on r_c of surface flows causes them to dominate in small tubes if both surface and vapour flow modes occur together.

Barrer [35] found that D_s is in practice not constant with concentration as for example in the case of condensed metal vapour spreading on tungsten but increases with C_S. Considerations arising from the confinement of flows to a surface are discussed in the work of Gilliland et al. [33] who made measurements on the flow of adsorbed SO_2, CO_2 and NH_3 and also found that the diffusion coefficient increases with C_S. Gilliland [33]

proposed that a second adsorbed layer will show higher diffusion than the first layer because it is less strongly bound to the surface (see Figure 13(b)). For P/P_s of less than 0.1 the slope of the isotherm for water on silica $\frac{d\Gamma}{dP}$ is small. The value of D_s is likely to be small for the first layers. A D_s for water vapour on mica has been reported of 3.85×10^{-16} m^2s^{-1} at a P/P_s of 0.14 using atomic force microscopy [36]. In order to obtain an upper limit for the contribution of surface flows at low P/P_s, the highest value from the range of reported values [33] gives a surface mass conductance of the order of 5×10^{-24} m s. This very small value can be safely ignored in comparison to the vapour phase flow for small P/P_s. However, when P/P_s exceeds approximately 0.6, condensation of liquid water dominates over the chain-like structure, $\frac{d\Gamma}{dP}$, increases sharply, as may D_s and surface flows are expected to play a role.

5.2.3 Laplace Pressure, the Kelvin Equation and Washburn theory

When adsorbed layers grow thick enough, they may be considered as a liquid phase with the properties of a bulk liquid. The distinction between an adsorbed layer and a liquid is not always clear, but for our purposes the distinction is based on the extent to which the internal structure of the layer is modified by the presence of the surface. In a porous medium, corners and small cavities will be filled, forming liquids with curved surfaces. In a cylindrical tube, the adsorbed layers on opposite sites may join to achieve local tube filling, bounded by a curved meniscus. Consider an interface in a partially filled tube between a wetting phase (in our case liquid water), and a non wetting phase (in our case a gas consisting of air and water vapour), surface curvature causes a pressure difference across the interface termed the Young-Laplace pressure [26]:

$$\Delta P' = \gamma \left(\frac{1}{r_1} + \frac{1}{r_2} \right) \tag{79}$$

where $\Delta P'$ is pressure difference across the interface between the two phases, also called Laplace pressure, γ is the surface tension of the interface, and r_1 and r_2 are the principal radii of curvature of the interface. The curvature of the interface is related to the contact angle between the liquid and the solid. For a tube of circular cross section of radius r_c, the two principal curvatures are the same and are related to the tube radius by:

$$r_1 = r_2 = \frac{r_c}{cos\chi} \tag{80}$$

where χ is the contact angle. The water vapour pressure in the gas phase is different from its value above a flat water surface and is determined by the Kelvin equation. A consequence of this is that the condensed phase appears at a lower pressure in a tube than for condensation at a flat interface. The Kelvin equation is:

$$ln\frac{P_c}{P_s} = -\gamma \frac{2m_m cos\chi}{\rho k_B T r_c} \tag{81}$$

where P_c is the vapour pressure above the curved interface (condensation pressure in a tube), for water vapour at 25°C, P_s = 3169.8 Pa and γ is surface tension of water (71.99 mN/m [26]).

The interior surface of a tube has a cylindrical curvature and from Eq.(81), condensation will begin to occur in a tube with radius $r_C$at a pressure given by:

$$P_c = P_s e^{-\frac{\gamma m_m}{\rho k_B T r_C}} \tag{82}$$

In a tube with surfaces of contact angle χ, a fully developed meniscus with spherical curvature becomes stable at the vapour pressure given by:

$$P_c = P_s e^{-\frac{2\gamma cos\chi m_m}{\rho k_B T r_C}} \tag{83}$$

The equation predicts that for the case where $2cos\chi > 1$ (contact angles less than 60°) the spherical meniscus becomes stable at lower pressures in vapour than in liquid coated cylindrical wall. For contact angles greater than 90°, the spherical meniscus is convex and the Laplace pressure will tend to expel the liquid from the tube.

Capillary filling occurs by Washburn flow [37] in which the unbalanced Laplace pressure of the single meniscus draws in the liquid from the outside reservoir against the frictional forces described by the Poiseuille law until the meniscus approaches its final position where it remains, allowing water to evaporate into the encapsulation. For short channels the meniscus will reach the outlet. For smaller channels the meniscus evaporation rate exceeds the mass flow rate for capillary filling so that the Washburn equation determines the flow rate:

$$l^2 = \frac{({r_c}^2 + 4\varsigma r_c)P}{4\mu} t \tag{84}$$

where l is the distance between the meniscus and the inlet of the tube (shown in Figure 14), ς is the *slip length*, a parameter determined empirically and described as the increase in tube radius required to give the observed flow. The parameter ς characterizes the hydrodynamic boundary condition of the liquid at the tube wall. An expression for the slip length in terms of microscopic parameters describing the nature of the wall has been derived from considerations of the friction at the interface by Bocquet and Barrat [38]. For the driving pressure P, in our case, is Laplace pressure only (Eq. (79)) or a net force with atmospheric pressure:

$$P = P_A + \frac{2\gamma}{r_c}\cos\theta \tag{85}$$

where P_A is the atmospheric pressure.

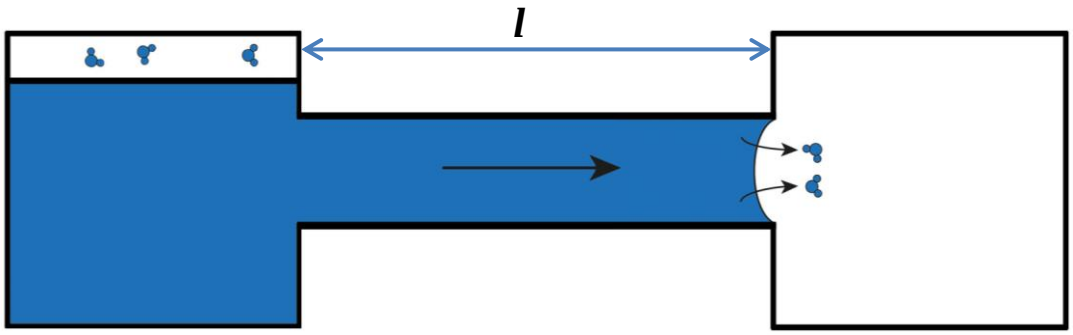

Figure 14 Schematic diagram for capillary filling that obey Washburn theory. The blue symbols are water molecules. One end of the channel is filled with liquid water, the other end of the channel is free of water. *l* could be the length of the channel (shown here) or smaller than it.

5.2.4 Two-Phase Flow

Two phase flows of water and humid air and water and water vapour (steam) in a tube have been reported [39, 40] for the case where there is a total pressure gradient. Various types of two phase flows in silica tubes have been observed using optical microscopy for 20, 25 and 100 μm air-water flows and 50 μm steam-water flows [40] (see Figure 15(a)). Many geometrical arrangements of liquid and gas were observed, including annular flows with water on the tube surface with a core of vapour, slug flows of liquid water with gas/vapour in the spaces between slugs and flows where there are bubbles of gas/vapour.

A recent example for two-phase flow in carbon nanotubes is reported by Rossi et al. [41]. A hydrophilic tube (water contact angle 5° and 15°) presents the interesting scenario that surface liquid coatings will be maintained on its walls and the tube will block with water liquid in several forms shown in Figure 15(b). The very high water conduction properties of the nanotubes are therefore maintained by surface flow. Such predictions are, however, based on the assumption that the microstructure of the liquid state when adsorbed in thin

layers remains the same as for bulk water and therefore the vapour pressure is predictable on that basis.

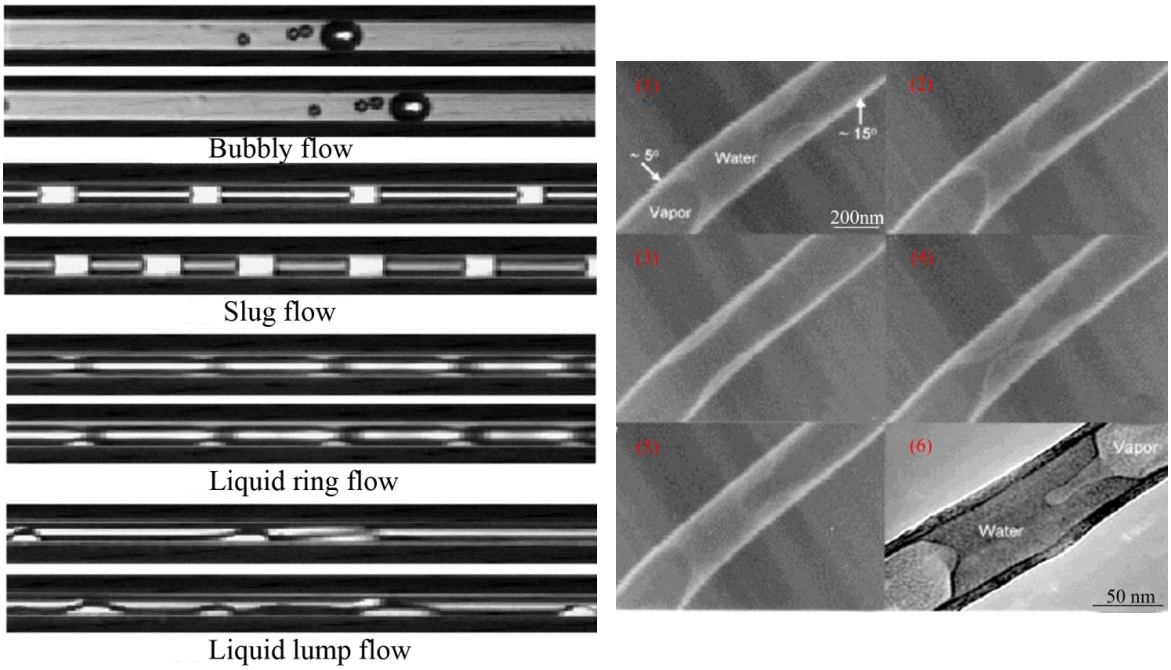

(a) (b)

Figure 15 Two phase flows in (a) 25 μm diameter silica tube at nearly atmospheric pressure of air from Serizawa et al. [40]; (b) 200-300 nm diameter carbon nanotubes at temperature of 4°C with pressures of water vapour of (1) 5.5 Torr, (2) 5.8 Torr, (3) 6 Torr, (4) 5.8 Torr and (5) 5.7 Torr, showing the dynamic behavior of a water slug close to the open end of the tube. A transmission electron microscopy (TEM) image (6) shows a similar slug shape in a closed carbon nanotube. Figures in (b) are reproduced from Rossi et al. [41].

For a two-phase flow as shown in Figure 16, the flow rates may be determined by a combination of theories for liquid flow rate, vapour flow rate and evaporation rate from a meniscus. Flow across a phase boundary (e.g. menisci and drops) was studied by Birdi and Vu [42] who measured the evaporation rate from the surface of water drops into a surrounding gas at a constant total pressure. The rate of evaporation was found to be determined by the rate of self-diffusion of the vapour away from the liquid surface rather than the much higher rate at which molecules cross the phase boundary, giving a mass flow rate of:

$$\dot{m} = 4\pi r_c m D \Delta c \quad (86)$$

where D is the self diffusion coefficient (m^2/s), c is the molecular concentration derived from the ideal gas law: $c = P/k_B T$ where P is the vapour partial pressure. For the case of water vapour interdiffusing into air, D is the self-diffusion coefficient of water vapour into air; for the case water diffusing into vacuum, D is the diffusion coefficient of water vapour into vacuum.

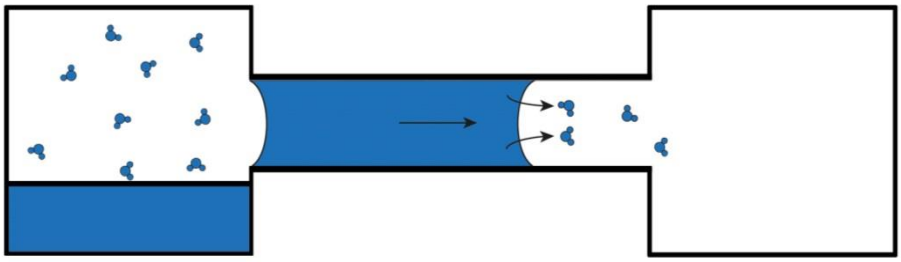

Figure 16 A schematic diagram of a two-phase flow with two menisci. The blue symbols represent water molecules. One end of the tube is provided saturated pressure of water vapour and the other end of the tube is exposed to an environment without water. Water vapour condensates on the meniscus proximal to the inlet and evaporates from the meniscus.

5.3 Test Apparatus and Procedure

We use the two-chamber method and mass loss method for studying water vapour flow rates. The two-chamber method we use here is the same with that we used for nitrogen flow rates. Either 3 or 30 identical parallel 25 μm diameter tubes were used. When this method applied to water vapour, it is necessary to carefully measure the net rate of adsorption or desorption from the surface of the second chamber that makes a contribution to the pressure change additional to that from the flow of vapour through the tube. Since the saturation pressure of water vapour at 295.5 K is 2702.3 Pa, the maximum input pressure was 2128 Pa. Water vapour mass flow rates in the range of 1×10^{-13} to 1×10^{-15} kg/s were possible for measurement.

For mass loss method, the glass vials (2 ml, Thermo Scientific, Australia) were charged with ~1.8 ml of water or mixture of water and glycerol, shown in Figure 17. We used aluminium sheet as lids for vials and punched it to make a little hole in the middle. Then put microtube samples through the hole and seal with epoxy resin (Selleys Araldite Super Strength, Australia). The lids with samples were sealed with epoxy resin onto the vials. After waiting for a curing period, we weighed to an accuracy of 100 μg. Three containers with different numbers of tubes formed an experimental set, together with the control having a resin seal and no tube. Mixtures of glycerol and water were made to vary the partial pressure of water vapour. We used 93.5% and 95% weight concentration of glycerol to mix with water to provide pressure of water vapour of 532 Pa and 425.6 Pa in the bottle [43]. For operation in vacuum the containers were placed in a vacuum chamber and slowly evacuated to less than 10^{-2} Pa. using a mechanical pump. The pressure in the vacuum chamber was measured using a manometer gauge. The silica microtubes were cut to 1 cm length for the measurements in this chapter.

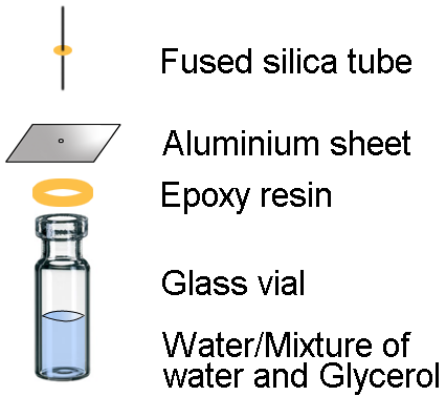

Figure 17 Schematic diagram of the mass loss method.

5.3.1 Measurement of adsorption rate

Water vapour adsorbs strongly on stainless steel walls. Because of adsorption of water vapour, pressures in chambers decreased once water vapour purged into the test chambers. Deitz and Turner have showed that water vapour obeys BET adsorption isotherms on stainless steel [44]. Since the pressure in Chamber 2 is much lower than the saturation pressure in our test, the adsorption occurs fast and then trends to a constant value.

For an example of water vapour experiments (P_i = 119.7 Pa, P_o = 39.9 Pa shown in Figure 18), Stage I. shows the case that adsorption rate is faster than the flow rate and Stage II. shows the flow rate is faster than the adsorption rate. There is also desorption in both stages, while here we consider the sum of adsorption and desorption as background "outgassing rate" which corresponds to the black dots in Figure 18. The flow rate starts to be counted after the initial decrease (red dots in Figure 18) and then reduce the "outgassing rate". Using this result, the exact flow rate is obtained using Eq.(71). Unlike the case for measuring outgassing rate for nitrogen tests, each input pressure of water vapour needs to be measured to obtain a corresponding "outgassing rate", since adsorption rate is dependent on the input pressure.

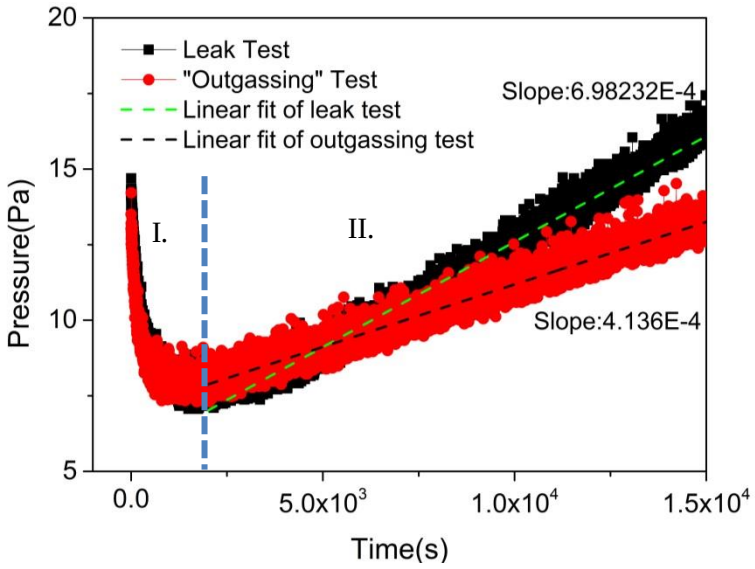

Figure 18 An example of the pressure change in Chamber 2 with time during a flow rate testing (red dots). The inlet pressure is 119.7 Pa and the outlet pressure is 39.9 Pa. The black line shows the outgassing rate of Chamber 2 in the absence of a flow tube.

5.4 Results and Discussion

We show in Figure 19 the results of our measurements of nitrogen and water vapour flows through the same silica tubes (see Figure 9) across a wide range of Knudsen number. The Cha and McCoy formula guides understanding of the water vapour flow results and a value of c_0 of 5.0 and a TMAC of 1.0 were used for the theory line for water vapour of Figure 19. The experimental measurements for water vapour obtained using the two-chamber method show significant departures from the theoretical curve for mean Knudsen numbers in the restricted range $8 < Kn_m < 25$. Data for the mass flow rate measured by the mass loss method for the same tube for Kn_m close to the saturation pressure limit (see Figure 19) show a very high mass conductance which we attribute to two phase and liquid flow modes. The mass loss results for values of Kn_m of 1.825 and 2.281 give flow conductances near the theory line of the Cha and McCoy formula, providing confirmation that there are two distinct ranges of Kn_m where the conductance

exceeds the theory line. To achieve this value of Kn_m it was necessary to reduce the water vapour pressure by using a glycerol-water mixture [43]. To assist the interpretation of the results for water vapour, we delineate in Figure 19 (b) the regions of relative mean water vapour pressure (relative humidity) P_m/P_s, where flows involving the liquid phase and where vapour-only flows occur. The region where P_m/P_s is close to unity is labeled "Two-phase and liquid flow". Elsewhere in Figure 19(b), the phenomena will be interpreted as the result of changes in TMAC, indicated in Figure 19 (b) as "Variable TMAC".

Surface flow could in principle contribute to conduction across the whole range of Kn. It takes place when there is an imposed concentration gradient on an adsorbed layer. The mass conductance of surface diffusion is obtained from Eq.(78):

$$C_{surface} = \frac{2\pi r_c D_s m}{L} \frac{d\Gamma}{dP} \tag{87}$$

For P/P_s of less than 0.6 the slope of the isotherm for water on silica $\frac{d\Gamma}{dP}$ is small. The value of D_s is likely to be small for the ice-like layers. A D_s for water vapour on mica has been reported of 3.85×10^{-16} m^2s^{-1} at a P/P_s of 0.14 using atomic force microscopy [36]. In order to obtain an upper limit for the contribution of surface flows at low P/P_s, the highest value from the range of reported values [33] gives a surface mass conductance of the order of 5×10^{-24} m s. This very small value can be safely ignored in comparison to the vapour phase flow for small P/P_s. However, when P/P_s exceeds approximately 0.6, condensation of liquid water dominates over the chain-like structure, $\frac{d\Gamma}{dP}$, increases sharply, as may D_s and surface flows are expected to play a role.

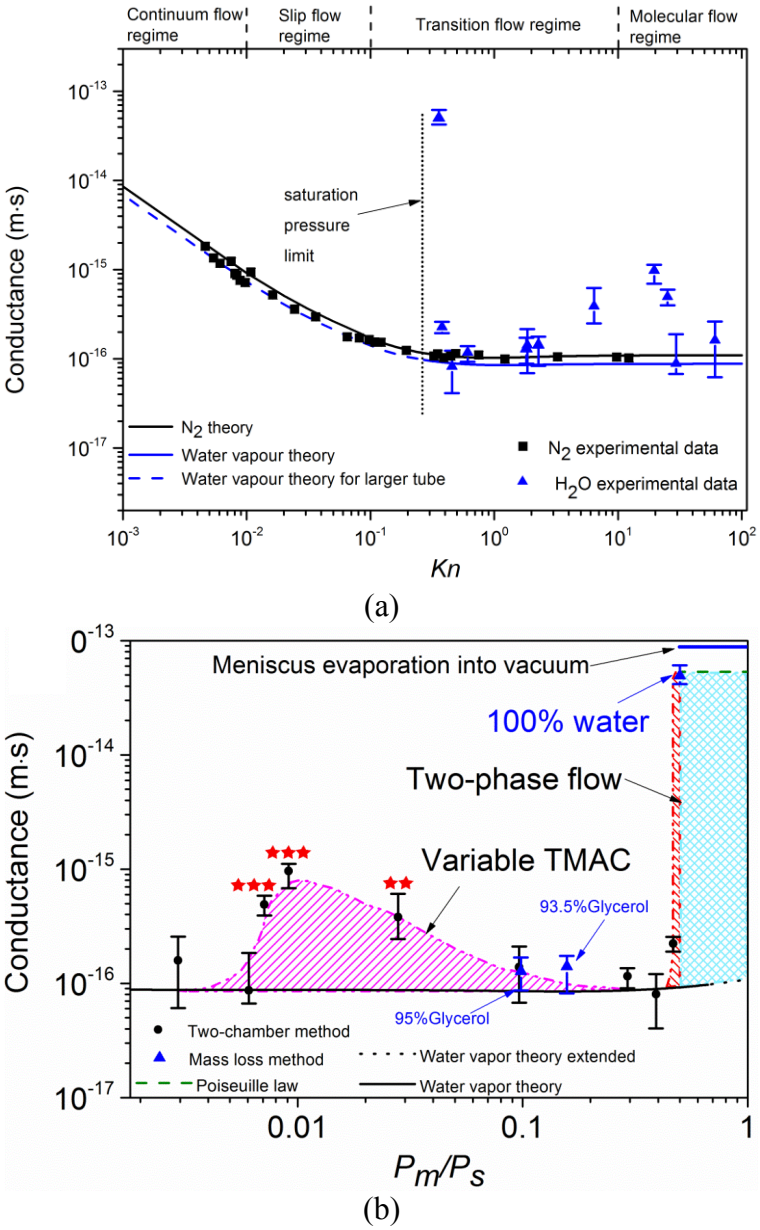

Figure 19 (a) The mass conductance of the 25 μm hydrophobic silica capillary for nitrogen at 298 K (black squares, same results with Chapter 4) and water vapour at 295.5 K (blue triangles) as a function of the mean Knudsen number Kn. The experimental data for nitrogen were measured using the two-chamber method [45], and the data for water vapour were measured by the two-chamber and mass loss methods. The solid curves are the theory of Cha and McCoy [46] for nitrogen (black) and water vapour (blue). The dashed curve is for water vapour flows that cannot be accessed at the test temperature (295.5 K) because of the formation of liquid water above the saturation vapour pressure. The pressure ratio is 3 for both nitrogen and water vapour for the two-chamber method. For the mass loss method, the outlet is under vacuum. Only three data points are shown for the mass loss method. (b) The same water vapour flow measurements and theory as in (a) are here shown as a function of P_m/P_s. The mass loss measurements are labeled with an arrow indicating the composition of the water/glycerol mixture used. The dashed line is a guide to the eye. The stars are results of a t test comparing theory and experiment (★★★ $p<0.001$, ★★ $p<0.01$). The experimental points lie above the theory curve in two regions labeled as "Variable

TMAC" and "Two-phase and liquid flow" as discussed in the text. The blue cross hatching indicates the region of liquid flow and the adjacent red hatching indicates two-phase flow.

5.4.1 Theory for Modifying TMAC with Water Vapour Pressure

We obtained TMAC results for water vapour on hydrophobic silica from our data by fitting to the Cha and McCoy formula (Eq.(64)) with α as the fitting parameter. The resulting TMAC dependence on P_m/P_s shows a strong reduction for very thin adsorbed water layers. We interpret this behavior as reflecting the properties of the adsorbed water. When any surface is exposed to water vapour, an adsorption takes place to produce a mass concentration Γ of water molecules that depends on the surface, the temperature, and the partial pressure P of water vapour. At constant temperature, for a fluid with a saturation vapour pressure of P_s, the dependence of Γ on the ratio P/P_s at constant temperature is an *adsorption isotherm*. For water, P_s is 2702 Pa at 295.5 K [47]. The adsorption isotherm for water on a hydrophobic silica surface has been measured in many works [17, 19, 20, 48-50]. Klier et al [19] obtained adsorption isotherms of water on silica glass with two different hydrophobicities, showing that progressive heating in vacuum removes hydroxyl groups and increases the hydrophobicity on the isotherms. Both surfaces show initial Langmuir-like adsorption, with the more hydrophobic surface, measured after treatment to 1073 K, more resistant to adsorption. At P/P_s of 0.4, the slope of the isotherm changes quickly, suggesting that a different adsorption mode (non-Langmuir) dominates from this humidity level.

We now develop a hierarchical model in which there are two adsorbed components. One component is unlike bulk liquid water and strongly bonded to the surface that acts as a passivation layer for subsequent adsorption. This layer is assumed to have a low TMAC

of α_1. The second component is a bulk-water-like one with a higher TMAC of α_2. The model is termed "hierarchical" because of the hierarchy of coverage, illustrated in (a). We use Langmuir adsorption for both components, following the work of Klier et al. [19] The dry surface of TMAC α_0 is covered by a Langmuir adsorption of TMAC α_1 onto the sites most attractive to water on the overall hydrophobic surface. These sites may be located at low points on the surface, and the effect of filling them is to smooth the surface for incoming water molecules, so that the TMAC of α_1 is imparted to an area larger than the area actually covered by water molecules. The smoothed area is larger than the adsorption area by an enhancement factor f, which can be determined by observation of the mass coverage at small P_m/P_s. The occupancy of these sites ensures that the surface retains the ability to grow a subsequent layer with bulk-water-like properties, which, at least in its initial stages, we describe by a second Langmuir adsorption. This adsorption covers both the previous adsorption and any uncovered original dry surface and imparts a TMAC of α_2 to the area it covers. We write the isotherms for the fractional covered areas by the two adsorptions in the Langmuir form:

$$\Gamma_1 = \frac{K_1 x}{1 + K_1 x}$$
$$\Gamma_2 = \frac{K_2 x}{1 + K_2 x} \qquad (88)$$

where x is the ratio P_m/P_s, and $K_1$and K_2 are the two Langmuir constants. The TMAC is then written as the weighted average of the three component TMACs where the weights are the exposed fractional areas determined by the hierarchical scheme of Figure 20 (a):

$$\alpha = (1 - \Gamma_1)(1 - \Gamma_2)\alpha_0 + (1 - \Gamma_2)\Gamma_1\alpha_1 + \Gamma_2\alpha_2 \qquad (89)$$

This expression was fitted to the TMAC data (Figure 20(a)) using the values of $\alpha_1, K_1,$ and K_2 as the fitting parameters. We assume a value of 1 for both α_0 and α_2, since we

find the dry surface and the fully wet surface both have a TMAC of 1. Other variables used here are obtained as well by fitting result as shown in Table 5. The fitting was carried out using an algorithm named Trust-Reqion.

Table 5 Fitting results for variables in Eqs.(88) and (89).

K_1	202.7
K_2	16.5
α_1	0.001

Using these data, we calculated the adsorption isotherms shown in Figure 20(c). The initial water layer applies for small water vapour pressures and water-like layers dominate after P_m/P_s larger than about 0.1. The values for α_1 are in agreement with Seo et al. [15] who describe an experiment in which nitrogen molecules in the presence of water vapour are reflected from silica glass. Within a narrow range of humidities, these authors found values of the nitrogen TMAC as low as 0.3, in agreement with our minimum value in Figure 20 (a). We used our values of the fitting parameters K_1 and K_2 to calculate a total adsorption isotherm of the form $\Gamma = S(\frac{1}{f}\Gamma_1 + \Gamma_2)$, where f is the enhancement factor for the smoothing effect and S is a scale factor determined by fitting to experiment as shown in Figure 20 (b). Using the observations of Klier et al. [19] for a silica surface with the same heat treatment as our tube, we chose f = 2.5 and S = 0.0002 to give a good fit. Other experimental observations by many authors for hydrophobic silica are shown for comparison in Figure 20 (b).

The structure of very thin adsorbed layers of water on hydrophobic silica are not known, but their sum-frequency vibrational spectrum suggests a structure unlike that of bulk liquid water [51, 52]. A strong tendency for hydrogen atoms to be directed towards the hydrophobic silica surface in a strongly-bonded initial adsorption has been described in

several works, some of which refer to an “ice-like” structure [52-54]. Figure 20 (c) and Figure 20 (d) show two proposed configurations for the initial water layer on hydrophobic silica. The principles illustrated by these structures are that the deeper (more concave) parts of the surface are most attractive to adsorbing water molecules and that the coverage is limited to a small fraction of the total area. We propose that the initial layer, by filling depressions in the surface first, imparts a smoothing effect to the whole of the surface. Two possible structures are patches (Figure 20 (c)) or chains (Figure 20 (d)) of water that form with hydrogen bonds directed to neighboring molecules as well as to the surface. The effect is a suppression of further adsorption, once the attractive sites are filled, as well as a reduction of the TMAC. The effect on TMAC is a type of passivation in which the interactions of the surface with incoming molecules are minimized. Chain-like configurations of water have been proposed in a mechanism for single file flow though small hydrophobic channels [55]. The chain-like configuration of Figure 20 (d) allows water molecules to line up in single file on the surface in such a way that one hydrogen atom on each water molecule interacts with an atom on the surface and the remaining hydrogen atom is directed towards the oxygen atom of its neighbor in the chain. The chains may branch in such a way that they have a smoothing effect by filling the low points on the silica surface as they wander over it. In a study of water adsorbed on silica using density functional theory, Ma et al. [56] show that chain-like water clusters on the silica surface are energetically favorable.

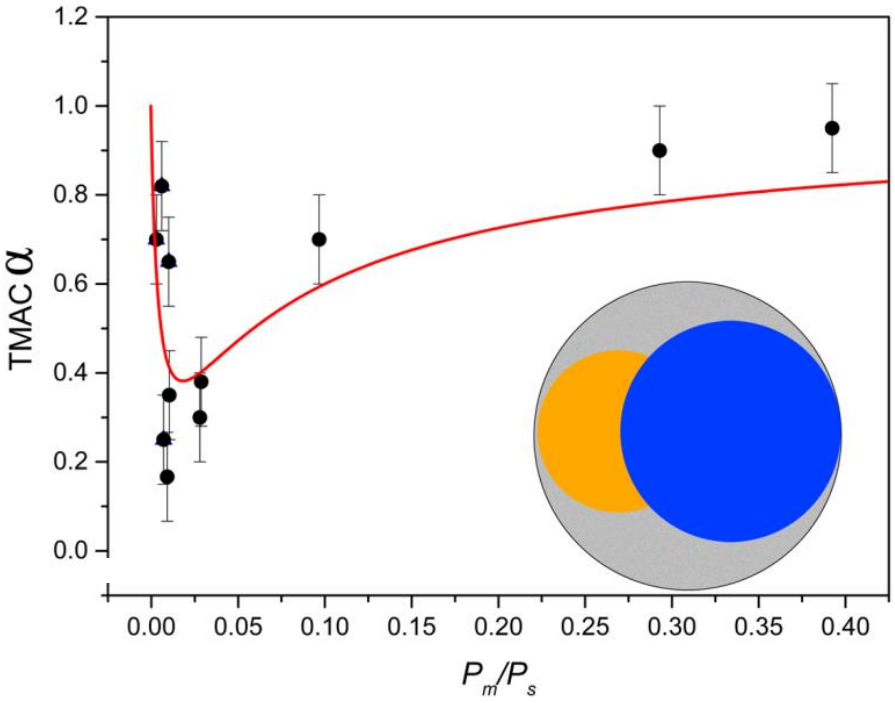
TMAC α
1.2
1.0
0.8
0.6
0.4
0.2
0.0
0.00
0.05
0.10
0.15
0.20
0.25
0.30
0.35
0.40
P_m/P_s

(a)

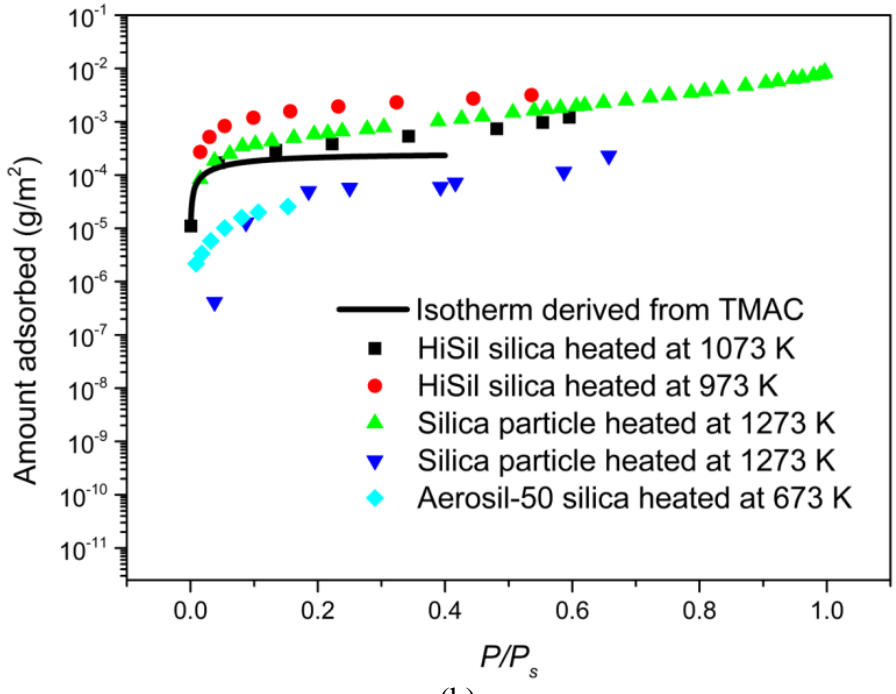
Amount adsorbed (g/m^2)
10^{-1}
10^{-2}
10^{-3}
10^{-4}
10^{-5}
10^{-6}
10^{-7}
10^{-8}
10^{-9}
10^{-10}
10^{-11}
0.0
0.2
0.4
0.6
0.8
1.0
P/P_s
Isotherm derived from TMAC
HiSil silica heated at 1073 K
HiSil silica heated at 973 K
Silica particle heated at 1273 K
Silica particle heated at 1273 K
Aerosil-50 silica heated at 673 K

(b)

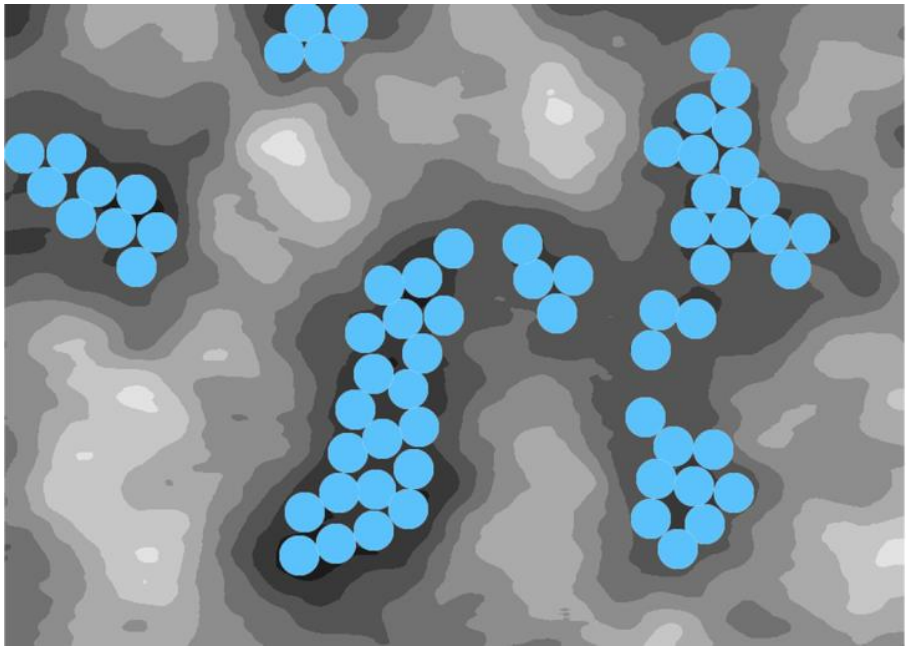

(c)

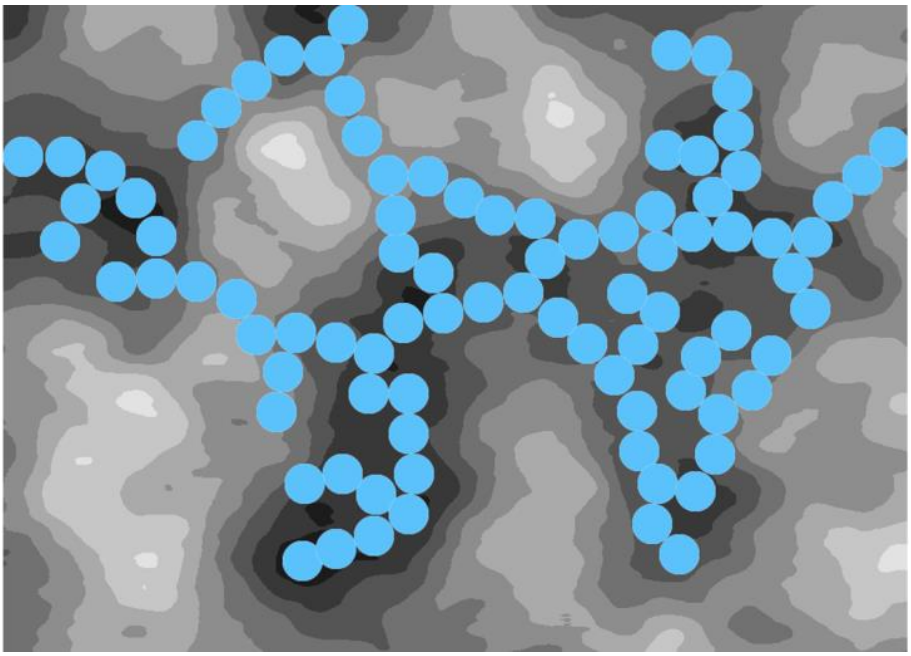

(d)

Figure 20 (a) TMAC obtained by fitting the Cha and McCoy theory (Eq.(64)) to the experimental data of water vapour in Figure 19. Also shown is the fitted line corresponding to the hierarchical two-component adsorption model of Eq.(89). The inset shows the adsorption hierarchy as overlapping circles. The yellow circle is the first Langmuir component that smoothes the surface and the overlapping blue component is the dominant water-like adsorption. (b) Adsorption isotherms of water on hydrophobic silica measured near room temperature by various authors (two heat treatments of HiSil silica from Klier et al.[19], silica particles (green) from Baker et al. [50], silica particles (dark blue) from Muster [20] and Aerosil-50 silica from Bolis et al. [49]). The solid line is our calculation based on the hierarchical adsorption theory, approximating the shape of the HiSil treated to 1073 K. (c) Schematic contour diagram of a

hydrophobic silica surface showing water molecules smoothing the surface by preferentially filling the depressions in a patch-like configuration. (d) The same contour diagram of (c) showing water molecules smoothing the surface by filling low points in a chain-like configuration.

The experimental results of the flow rates of water vapour (shown in Figure 19) are summarized in Table 6.

Table 6 Experimental results for the mass conductance as a function of the inlet and outlet pressures in the tube.

Kn_m	P_i(Pa)	P_o(Pa)	C(m s)
Three tubes			
0.45799	1596	503.272	1.1734e-16
0.6134	1197	385.9095	1.1574e-16
1.85872	399	123.5969	1.3912e-16
6.42011	119.7	31.6287	3.9274e-16
19.66863	39.9	11.9704	9.6260e-16
Thirty tubes			
0.38009	2161.25	394.345	2.2255e-16
6.25031	119.7	35.644	3.2450e-16
17.62432	39.9	15.1972	3.3356e-16
25.19975	31.92	6.6101	4.9044e-16
29.49893	27.93	4.9847	8.6896e-17
60.83638	11.97	3.99	1.5879e-16
mass loss method			
0.35934	2702.3	0	4.9414e-14
1.82509	532	0	1.2770e-16
2.28136	425.6	0	1.4082e-16

5.5 CONCLUSION

This work has demonstrated using two different experimental techniques that water vapour flow rates are measurable with good precision, provided that the effects of two-phase flows are understood and separated. The results show that hydrophobic silica walls enhance water vapour flows in a restricted range of relative humidity P_m/P_s by up to an order of magnitude. Application of extended Navier-Stokes theory interprets the cause of

the enhanced flows as a reduction of TMAC. The dependence of TMAC on humidity is explained by a model in which there is a hierarchy of adsorption of water on the hydrophobic silica. In such a hierarchical adsorption, the properties of the adsorbed layers are quite different, being distinguished by their effect on TMAC. The model shows how a measurement of TMAC and a measurement of the adsorption isotherm reveal different aspects of the same adsorption phenomenon.

Our work shows the usefulness of TMAC as a sensitive probe of the properties of adsorbed layers. The extent to which water flow enhancements apply in cases of other channel wall materials is not known, but we recommend a direct measurement of moisture penetration for a component under test rather than relying on a helium or other ideal gas test, to ensure the flows are not underestimated.

REFERENCES

1. Maxwell, J.C., *On stresses in rarified gases arising from inequalities of temperature.* Phil. Trans. R. Soc. Lond., 1879. **170**: p. 231-256.
2. Fu, D., et al., *Structure of a glycerol-conducting channel and the basis for its selectivity.* Science, 2000. **290**: p. 481-486.
3. Murata, K., et al., *Structural determinants of water permeation through aquaporin-1.* Nature, 2000. **407**: p. 599-605.
4. Sui, H.X., et al., *Structural basis of water-specific transport through the AQP1 water channel.* Nature, 2001. **414**: p. 872-878.
5. Nair, R.R., et al., *Unimpeded permeation of water through helium-leak-tight graphene-based membranes.* Science, 2012. **335**: p. 442-444.

6. Joseph, S. and N.R. Aluru, *Why are carbon nanotubes fast transporters of water?* Nano Letters, 2007. **8**: p. 452-458.

7. Majumder, M., et al., *Enhanced flow in carbon nanotubes.* Nature, 2005. **438**: p. 44.

8. Majumder, M., N. Chopra, and B. J.Hinds, *Mass transport through carbon nanotube membranes in three different regimes: Ionic diffusion and gas and liquid flow.* ACS Nano, 2011. **5**: p. 3867-3877.

9. Holt, J.K., et al., *Fast mass transport through sub-2-nanometer carbon nanotubes.* Science, 2006. **312**: p. 1034-1037.

10. Tanford, C., *The Hydrophobic Effect: Formation of Micelles and Biological Membranes*. 2nd ed. 1980, New York: Wiley.

11. Dill, K.A., *Dominant forces in protein folding.* Biochemistry, 1990. **29**: p. 7133-7155.

12. Chandler, D., *Interfaces and the driving force of hydrophobic assembly.* Nature, 2005. **437**: p. 640-647.

13. Knudsen, M., *The laws of molecular and viscous flow through tubes (in German).* Ann. Phys. (Berlin), 1909. **28**: p. 75-130.

14. Smoluchowski, M., *To the kinetic theory of transpiration and diffusion of dilute gases (in German).* Ann. Phys. (Berlin), 1910. **33**: p. 1559-1570.

15. Seo, D., D. Mastropietro, and W.A. Ducker, *Gas flows near solids coated with thin water films.* J. Phys. Chem. C, 2013. **117**: p. 6235-6244.

16. Cooper, S.M., B.A. Cruden, and M. Meyyappan, *Gas transport characteristics through a carbon nanotubule.* Nano Letters, 2004. **4**: p. 377-381.

17. Young, G.J., *Interaction of water vapor with silica surfaces.* J. Colloid Sci., 1958. **13**: p. 67-85.

18. Kawasaki, K., K. Senzaki, and I. Tsuchiya, *Adsorption studies of water vapor on porous glass.* J. Colloid Sci., 1964. **19**: p. 144-151.

19. Klier, K., J.H. Shen, and A.C. Zettlemoyer, *Water on silica and silicate surfaces. I. Partially hydrophobic silicas.* J. Phys. Chem., 1973. **77**: p. 1458-1465.

20. Muster, T.H., C.A. Prestidge, and R.A. Hayes, *Water adsorption kinetics and contact angles of silica particles.* Colloids Surf., A, 2001. **176**: p. 253-266.

21. Vigil, G., et al., *Interactions of silica surfaces.* J. Colloid Interface Sci., 1994. **165**: p. 367-385.

22. Myong, R.S., *Gaseous slip models based on the Langmuir adsorption isotherm.* Phys. Fluids, 2004. **16**: p. 104-117.

23. Myong, R.S., et al., *Velocity slip in microscale cylindrical Couette flow: The Langmuir model.* Phys. Fluids, 2005. **17**: p. 087105.

24. Seo, D. and W.A. Ducker, *In SituControl of Gas Flow by Modification of Gas-Solid Interactions.* Phys. Rev. Lett., 2013. **111**(17).

25. Choi, J.-G., D.D.Do, and H.D.Do, *Surface Diffusion of Adsorbed Molecules in Porous Media-Monolayer, Multilayer, and Capillary Condensation Regimes.* Ind. Eng. Chem. Res., 2001. **40**: p. 4005-4031.

26. Butt, H.-J., K. Graf, and M. Kappl, *Physics and Chemistry of Interfaces*. 2003, Germany: Wiley-VCH GmbH& Co. KGaA, Germany.

27. Rezac, M.E., T. John, and P.H. Pfromm, *Effect of Copolymer Composition on the Solubility and Diffusivity of Water and Methanol in A Series of Polyether Amides.* J. Appl. Polym. Sci., 1996. **65**: p. 1983-1993.

28. Malmsten, M., *Ellipsometry Studies of Protein Layers Adsorbed at Hydrophobic Surfaces.* J. Colloid Interface Sci., 1994. **166**: p. 333-342.

29. Tadros, M.E. and A.W. Adamson, *Adsorption and Contact Angle Studies I. Water on Smooth Carbon, Linear Polyethylene, and Stearic Acid-Coated Copper.* J. Colloid Interface Sci., 1974. **49**: p. 184–195.

30. Langmuir, I., *The Constitution and Fundamental Properties of Soilids and Liquids.* J. Am. Chem. Soc., 1916. **38**: p. 2221-2295.

31. Barrer, R.M., *Diffusion in and through Solids*. 1941, London, UK: Cambridge University Press.

32. Hill, T.L., *Surface Diffusion and Thermal Transpiration in Fine Tubes and Pores.* J. Chem. Phys., 1956. **25**(4): p. 730-735.

33. Gilliland, E.R., et al., *Diffusion on surface. I. Effect of concentration on the diffusivity of physically adsorbed gases.* Ind. Eng. Chem. Fundam., 1974. **13**: p. 95-100.

34. Hwang, S.-T. and K. Kammermeyer, *Surface Diffusion in Microporous Media.* Can. J. Chem. Eng. , 1966. **44**: p. 82-89.

35. Barrer, R.M., *Nature of the Diffusion Process in Rubber*. Nature, 1937. **140**: p. 106-107.

36. Xu, L., et al., *Wetting and capillary phenomena of water on mica.* J. Phys. Chem. B, 1998. **102**: p. 540-548.

37. Washburn, E.W., *The Dynamics of Capillary Flow.* Physical Review, 1921. **17**: p. 273-283.

38. Bocquet, L.r. and J.-L. Barrat, *Flow Boundary Conditions from Nano- to Micro-Scales.* Soft Matter, 2007. **3**: p. 685-693.

39. Fukano, T. and A. Kariyasaki, *Characteristics of Gas-Liquid Two-Phase Flow in a Capillary Tube.* Nucl. Eng. Des., 1993. **141**: p. 59-68.

40. Serizawa, A., Z. Feng, and Z. Kawara, *Two-Phase Flow in Microchannels.* Exp. Therm. Fluid Sci., 2002. **26**: p. 703-714.

41. Rossi, M.P., et al., *Environment Scanning Electron Microscopy Study of Water in Carbon Nanopipes.* Nano Letters, 2004. **4**: p. 989-993.

42. Birdi, K.S. and D.T. Vu, *A study of the evaporation rates of small water drops placed on a solid surface.* J. Phys. Chem., 1989. **93**: p. 3702-3703.

43. Glycerine Producers' Association, *Physical Properties of Glycerine and Its Solutions*. 1963: Glycerine Producers' Association, New York.

44. Deitz, V.R. and N.H. Turner, *Introduction of water vapor into vacuum systems and the adsorption by the walls.* J. Vac. Sci. Technol., 1970. **7**(6): p. 577-580.

45. Lei, W. and D.R. McKenzie, *Revisiting Maxwell's tangential momentum accommodation coefficient: A study of nitrogen flow in a silica microtube across all flow regimes.* Ann. Phys., 2014. **351**: p. 828-836.

46. Cha, C.Y. and B.J. McCoy, *Application of third-order constitutive relations to Poiseuille flow of a rarefied gas.* J. Chem. Phys., 1971. **54**: p. 4373-4383.

47. Lemmon, E.W., M.O. McLinden, and D.G. Friend, *Thermophysical Properties of Fluid Systems.* retrieved Novermber 13, 2014. **NIST Chemistry WebBook, NIST Standard Reference Database Number 69**: p. Eds. Linstrom, P. J. and Mallard, W. G., National Institute of Standard and Technology, Gaithersburg MD, 20899, http://webbook.nist.gov.

48. Shioji, S., et al., *Rehydroxylation of dehydrated silica surfaces by water vapor adsorption.* Adv. Powder Technol., 2001. **12**: p. 331-342.

49. Bolis, V., et al., *Hydrophilic and hydrophobic sites on dehydrated crystalline and amorphous silicas.* J. Chem. Soc. Faraday Trans., 1991. **87**: p. 497-505.

50. Baker, F.S. and K.S.W. Sing, *Specificity in the adsorption of nitrogen and water on hydroxylated and dehydroxylated silicas.* J. Colloid Interface Sci., 1975. **55**: p. 605-613.

51. Shen, Y.R. and V. Ostroverkhov, *Sum-frequency vibrational spectroscopy on water interfaces: Polar orentation of water molecules at inerfaces.* Chem. Rev., 2006. **106**: p. 1140-1154.

52. Isaienko, O. and E. Borguet, *Hydrophobicity of hydroxylated amorphous fused silica surfaces.* Langmuir, 2013. **29**(25): p. 7885-95.

53. Giovambattista Nicolas, P.G. Debenedetti, and P.J. Rossky, *Effect of surface polarity on water contact angle and interfacial hydration structure.* J. Phys. Chem. B, 2007. **111**: p. 9581-9587.

54. Giovambattista, N., P. Rossky, and P. Debenedetti, *Effect of pressure on the phase behavior and structure of water confined between nanoscale hydrophobic and hydrophilic plates.* Physical Review E, 2006. **73**: p. 041604.

55. Alexiadis, A. and S. Kassinos, *Molecular simulation of water in carbon nanotubes.* Chem. Rev., 2008. **108**: p. 5014-5034.

56. Ma, Y., A.S. Foster, and R.M. Nieminen, *Reactions and clustering of water with silica surface.* J. Chem. Phys., 2005. **122**: p. 144709.

Chapter 6 Interdiffusive Mass Flow Conductances of Water and Water Vapour through Micro- and Nano- Tubes in a Background of Air

In this chapter, we investigate the theory and measurement of the mass flow rate of water through a tube consisting of a uniform air filled tube and the flow in the same tube in the absence of air. Such a study has not yet been reported in the literature. The outcomes of this study are important to the design and testing of encapsulations for preventing moisture ingress as well as to the building of knowledge of all the possible modes of flow of water in the vapour phase, the liquid phase and combinations of the two in the presence of a background of air.

6.1 INTRODUCTION

Knowledge of the rate of diffusion of moisture (liquid water and water vapour) through a channel is of relevance in the assessment of leaks in device encapsulations, the science of moisture barriers, water purification and in the prediction of the rate of water diffusion through soils on earth and regoliths on planets and comets. In this age of bionic implants, electronic devices are required to operate reliably for long periods in environments that contain both air and water. As devices such as the bionic ear and eye become widespread, it is critical that the resistance of their encapsulations to water penetration is quantified and understood to protect against failure. The discovery of graphene oxide membranes [1] that are highly selective to water penetration while impervious to helium gas has, on the one hand offered the possibility of higher performance water purification membranes

while on the other raising questions about the use of traditional helium leak testing as a quality control measure for water penetration.

Water is present as ice on Mars and on the surface of comets where, as a result of low temperatures and pressures, it sublimes directly to the vapour. The rate at which water vapour penetrates the porous regolith determines how quickly it is lost to the vacuum of space. An understanding of how water is retained in these environments therefore depends on knowledge of the rate of flow of water vapour through pathways that may also contain other gases. From bionics to comets, there is a need to know how fast water penetrates channels especially when a background of air or another gas is present.

It appears that there is a substantial gap in knowledge surrounding the flow of water vapour and mixed flows of water vapour and liquid water in channels. The flow of a great many other gases and vapours has been studied and it is surprising that, given its importance, the measurement of the flow of water vapour has been so neglected and related theory untested. Interdiffusive flows in channels, defined as flows of moisture as the diffusing species in a background of another gas, are especially important but have not been measured in a channel of known dimensions, preventing an adequate test of theory.

6.2 THEORIES OF INTERDIFFUSIVE FLOW

When there are two components, species 1 (defined as the *permeant*) and species 2 (defined as the *background*) we are now concerned with the interdiffusive flows that occur when there is no total pressure gradient, but partial pressure gradients are maintained between the ends of the tube. The concentration gradients are such that

diffusion drives an intermixing of the components in the tube. Marrero and Mason [2] have discussed the calculation and measurement of the binary interdiffusion coefficients D_{12} defined in Eq.(19). It can be shown that the interdiffusion coefficients are symmetric in the two species in order to maintain a constant pressure in an interdiffusing binary mixture, so that:

$$D_{12} = D_{21} \tag{90}$$

The simplest case of binary interdiffusion, termed *interdiffusive flow* applies to a mixture of gases in a container where there are imposed partial pressure gradients along one direction x but no imposed total pressure gradients. It is not in principle possible to maintain a strictly constant total pressure in an isothermal interdiffusing binary mixture, since if the particles are different, the molecular velocities are in general not equal and collisions in the laboratory frame are in general not symmetric. A small pressure difference is in fact needed to maintain the equilibrium particle distribution. For example, one species will tend to diffuse more readily through the other, requiring a total pressure difference to establish an equal and opposite flux of the two species. Such pressure differences have been measured in tubes but can usually be neglected for larger containers (see Page 6 of Marrero and Mason [2]) and will be neglected here.

6.2.1 Knudsen Interdiffusive Flow

Here we consider three cases of binary gaseous interdiffusive flow, depending on the dimension of the tube and the mean free path of the molecules undergoing flow. For flows in which the critical dimension of the flow tube is smaller than the mean free path of the permeant in the background gas, a case known as *Knudsen interdiffusive flow* applies. The two gases diffuse independently of each other and the flow of the gas

specified as the permeant is given by the Knudsen formula for molecular flow. Knudsen interdiffusive flow obeys the same equation as ordinary Knudsen flow (Eq.(27)) since the background gas plays no role:

$$\dot{m}_{KI} = \frac{\pi {r_c}^2 D_K}{k_B T}\frac{\partial P_1}{\partial x} = \frac{4\sqrt{2\pi} r_c^3}{3}\sqrt{\frac{m}{k_B T}}\frac{\partial P_1}{\partial x} \qquad (91)$$

where P_1 is the partial pressure of the permeant vapour. This equation applies to flows in the regime specified by values of the Knudsen number Kn greater than 10. For example, for water vapour diffusing into air at atmospheric pressure for tubes smaller than approximately 120 nm, the mean free path in air at one atmosphere is comparable with the diameter of the tubes. The practical outcome is that for large tubes, the presence of air at atmospheric pressure will impede the diffusive flow of permeant, whereas for tubes smaller than 120 nm it will not provide any additional impedance.

6.2.2 Interdiffusive Flow in the Absence of Boundaries

In this case the flow is described by a diffusive process in which the boundaries are distant (mean free path between molecules is much smaller than channel diameter). The results of Section 3.1.2 can be used. From Eq.(19) deleting terms in the total concentration gradient and the temperature gradient, we obtain:

$$J_1 = -D_{12}\frac{\partial c_1}{\partial x} = -\frac{D_{12}}{k_B T}\frac{\partial P_1}{\partial x} \qquad (92)$$

There are several theoretical approaches to the calculation of D_{12}, as outlined in Chapman and Cowling P`258 [3], the simplest of which, described by Chapman and Cowling as a first approximation, applies to rigid elastic spheres:

$$D_{12} = \frac{3}{8P{d_{m12}}^2}\sqrt{\frac{(k_B T)^3}{2\pi}\left(\frac{1}{m_{m1}} + \frac{1}{m_{m2}}\right)} \tag{93}$$

where d_{m12} is the average molecular diameter given by:

$$d_m = \frac{d_{m1} + d_{m2}}{2} \tag{94}$$

where d_{m1} and d_{m2} are diameters of the two components respectively.

The mass flow rate is:

$$\begin{aligned} \dot{m}_1 &= -\frac{AD_{12}m_{m1}}{k_B T}\frac{\partial P_1}{\partial x} \\ &= -\frac{3\pi {r_c}^2 m_{m1}}{8P_T {d_{m12}}^2}\sqrt{\frac{k_B T}{2\pi}\left(\frac{1}{m_{m1}} + \frac{1}{m_{m2}}\right)}\frac{\partial P_1}{\partial x} \end{aligned} \tag{95}$$

where P_T is the total pressure. There are many works on the binary diffusion of water vapour in a background gas at atmospheric pressure, measured from the evapouration rate of the water (see Table 16 of Marrero and Mason's paper [2]). Bogatyrev and Nezovitina [4] have measured the experimental values of the interdiffusion coefficients for many pairs of gases at various pressures other than atmospheric pressure. For the binary mixtures studied, it was found from measurement that the interdiffusion coefficients are not dependent purely on *1/P* as implied in Eq.(93) since the product $D_{12}P$ shows a systematic decrease with increasing pressure, indicating that the actual value of D_{12} is less than that expected from Eq.(93) as pressure increases. Barajas et al. [5] and Bennett et al. [6] have presented a formula known as the Enskog-Thorne formula which applies to a binary mixture of hard spheres and gives an understanding of the behaviour of D_{12} as a function of pressure. While Thorne's theoretical derivations of his

generalisations of the original work of Enskog were never published, they have been quoted for a long time in the literature (see [3]).

6.2.3 Intermediate Interdiffusive Flow

For tubes that are too large to ensure Knudsen interdiffusive flow and too small to ensure distant boundaries as in ordinary interdiffusive flow, there is an intermediate case discussed by Remick and Geankopolis [7] and Ernst and Hemond [8]. These authors considered Knudsen interdiffusive flow as one limit and ordinary interdiffusive flow as the other limit, and then combined the two limits using two equations (Eqs.(23) and (93)) corresponding to the two kinds of flows. Remick and Geankopolis first confirmed the theory for binary flows in the transition regime with experiment and then took the composition of the binary gases into account for the diffusion coefficient in the transition region. From their experiments, the diffusion coefficient in the transition region is only affected slightly by the composition, and the theory worked well for the test gases they used, N_2 and He. Subsequently, Ernst and Hemond studied both monatomic and polyatomic molecules (Ar, benzene, and 1,1,1-trichloroethane) by mass spectrometer. Following Remick and Geankopolis's results, they used the combination for specific conductance of transition regime without considering composition. We convert the specific conductance given by Ernst et al. to a diffusion coefficient:

$$D_t = 1/(\frac{1}{D_K} + \frac{1}{D_{12}}) \qquad (96)$$

At high total pressures Eq.(96) approaches D_{12} since D_K is much larger than D_{12} and the ratio term dominates over the unity term. At low pressures Eq.(96) approaches D_K, but at intermediate total pressures Eq.(96) is used in regions of total pressure where it formally

does not apply. The formula is therefore a convenient interpolation derived empirically but at present has no rigorous foundation. This approach has been tested experimentally by Ernst and Hemond [8] who carried out a series of experiments using air as the background gas and argon, benzene, and 1,1,1-trichloroethane (TCA) as permeants. In the continuum flow regime, as expected, the experiment agrees with Eq.(96). The air injection initially caused advective flow of the permeants first in several seconds and then diffusive flow took place in opposite direction. In the transition flow regime corresponding to relatively low pressures, Knudsen diffusion is dominated. Eq.(96) works well for single atom molecules but overestimated for multiatoms molecules because multiatoms molecules have relatively high specific heats associated with their high internal energy storage capability. This capability makes their collisions less elastic, leading to less momentum transfer in each collision. In the slip flow regime corresponding to relatively high pressures, interdiffusive flow is dominant. In this case, Eq.(96) works perfectly for both monatomic and polyatomic molecules. This means inelastic collisions between multicomponent gases or vapours are only important in Knudsen diffusive flow. It is accurate to predict the diffusive mass flow rate for the monatomic gas helium irrespective of flow regimes, while the existing models have difficulties in predicting the diffusive mass flow rate of water vapour in the transition and molecular flow regimes.

6.2.4 Liquid Flows

The Poiseuille law (Eq.(42)) has an implicit assumption of no-slip boundary conditions which are not always obeyed. Neto et al. [9] have reviewed the literature on the conditions under which boundary slip occurs and have given examples of cases where the

boundary slip contributes significantly to an increase of flow. Extreme cases of boundary slip are the aquaporin hydrophobic tubes in cell walls [10] and carbon nanotubes [11]. While a positive correlation between the slip length and the contact angle has been reported in experimental studies [12, 13] as well as simulations [14, 15], some boundary slip can also occur at hydrophilic surfaces. The formula for liquid water flow with a slip length is:

$$\dot{m}_{P-modified} = \frac{\pi {r_c}^4 \Delta P \rho}{8\mu L}(1 + \frac{4\zeta}{r_c}) \quad (97)$$

6.2.5 Surface and Two-Phase Flows

Surface and two-phase flows will occur in interdiffusive flow and may enhance the flow rate when the inlet pressure is close to the saturation pressure. Equations for surface flow and meniscus flow rates are detailed in Section 5.2.2 and 5.2.4.

6.3 Experimental Methods

We use the mass loss method discussed in Chapter 5 to measure the interdiffusive flow rates. The set of containers (1, 2 and 3 tubes with a control vial samples) were placed in a desiccator containing silica gel desiccant and weighed every few days. Mixtures of 95%, 93.5%, 90%, 84%, 70% and 50% of glycerol by weight were used, corresponding to the partial pressure of water in the bottle 425.6 Pa, 532 Pa, 771.4Pa, 997.5 Pa, 1729 Pa and 2128 Pa respectively [16]. The silica microtubes were cut to 1 cm length for the measurements in this chapter. Three ways of using the vials are shown in Figure 21. The first one is that microtubes were not connected with liquid water in the vial, in which case, the inlet pressure depends on partial pressure of water vapour inside the vials. The second one is that microtubes were connected with liquid water at the inlet, therefore the

inlet pressure is Laplace pressure with additional 1 atm. The third one is that microtubes samples were connected with liquid water and the inlet pressure is the same with the former one. The experimental results were shown in Table 7.

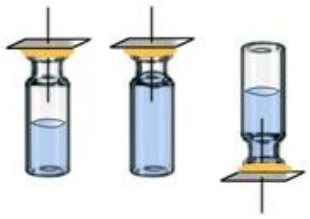

Figure 21 Schematic diagram for the mass loss method.

6.4 Results and Discussion

The results for the mass conductance for atmospheric interdiffusive flows for the 25 μm diameter tube as a function of the mean partial pressure of water vapour in the tube are shown in Figure 22(a) and as a function of the inlet partial pressure of water vapour are shown in Figure 22(b). Two plots are shown with different independent variables since the inlet partial pressure determines the likelihood of the formation of liquid water slugs inside the inlet of the tube, while the mean partial pressure more accurately determines the average Kn of the flow. Theoretical predictions for Poiseuille liquid water flow conductance and the interdiffusive water vapour conductance in air are shown as dashed and dashed-dotted lines respectively. When the inlet pressure approaches the saturation pressure of water, there is a possibility of two phase flows, since liquid water may condense at the inlet of the tube to form a liquid annular, slug flow or bubbly flow [17]. The presence of two phase flows with both liquid and air/vapour phases may be the reason that the experimental observation for interdiffusive flow of water vapour in air exceeds the theoretical prediction. At the highest value of P_i/P_s, the excess conductance is approximately two orders of magnitude higher than theory (see Figure 22(b)). When

the inlet water vapour pressure is reduced by the presence of 50% glycerol, the flow conductance is greatly reduced and is progressively further reduced by the presence of 84% and 95% glycerol. The theoretical result for flows of water vapour in the absence of air using the formula of Cha and McCoy is shown in Figure 22 as a solid line. Our observation of detailed plots of mass loss as a function of time reveals two different types of behaviors as shown in Figure 22 (c), only one of which gives a steady flow as a function of time as implied in the above description. In the second type of behavior, there are sudden increases or "jumps" in the mass loss at a certain times, due to small pressure or temperature changes of the environment. The experimental results of interdiffusive flow of water vapour are summarised in Table 7.

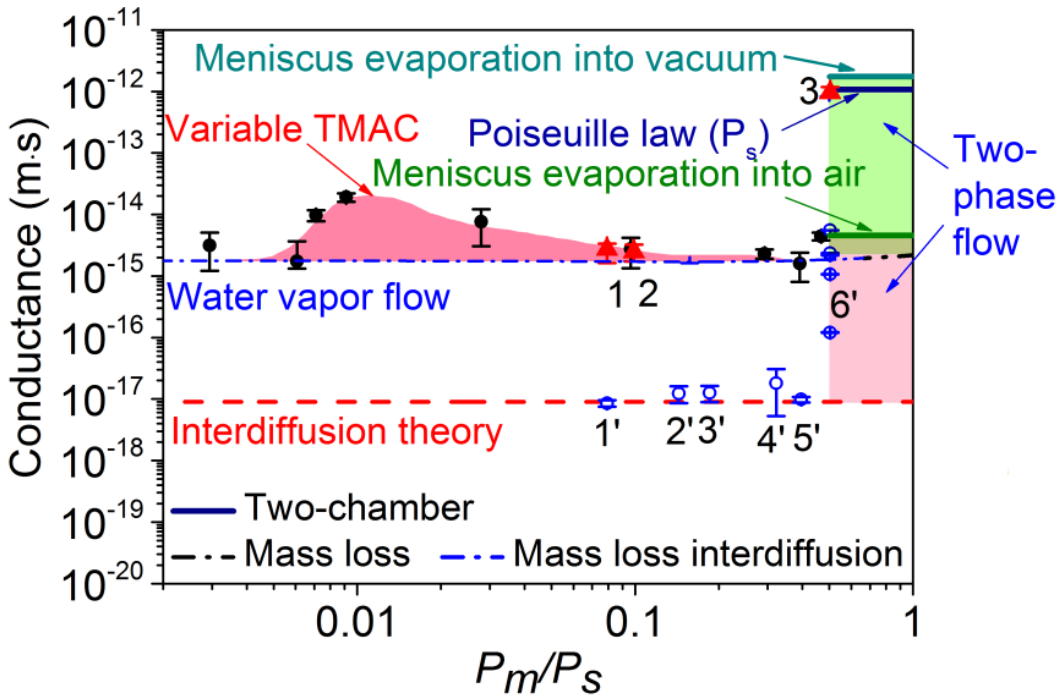

(a)

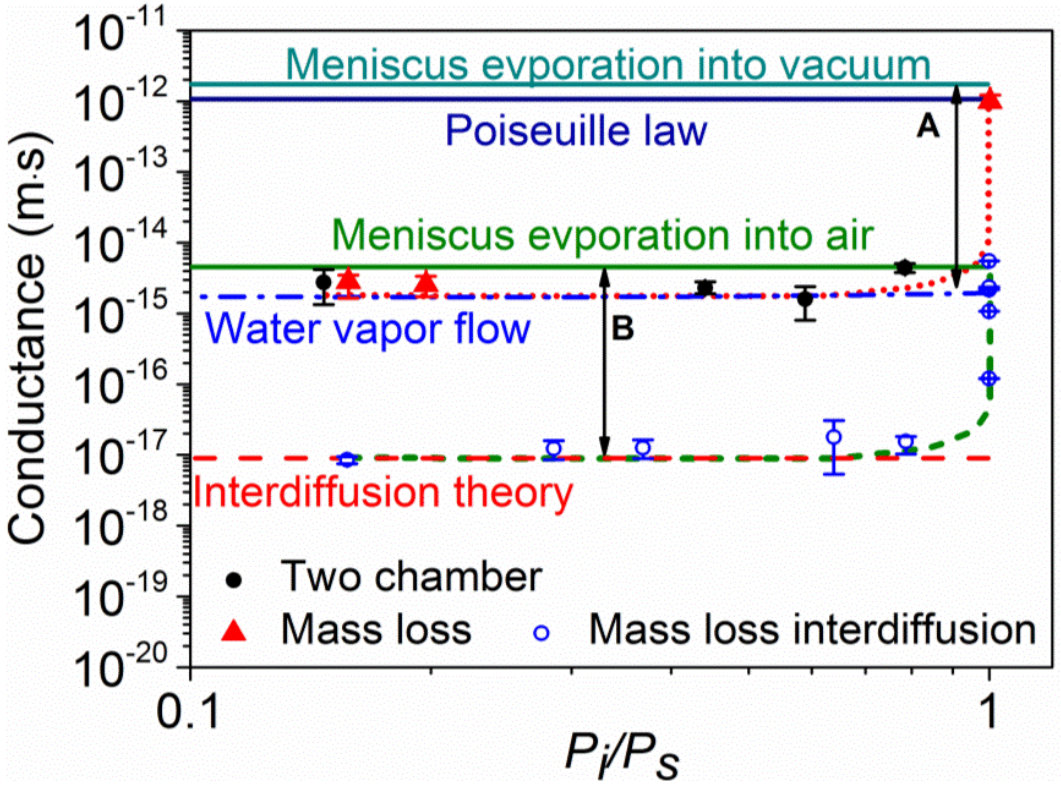

(b)

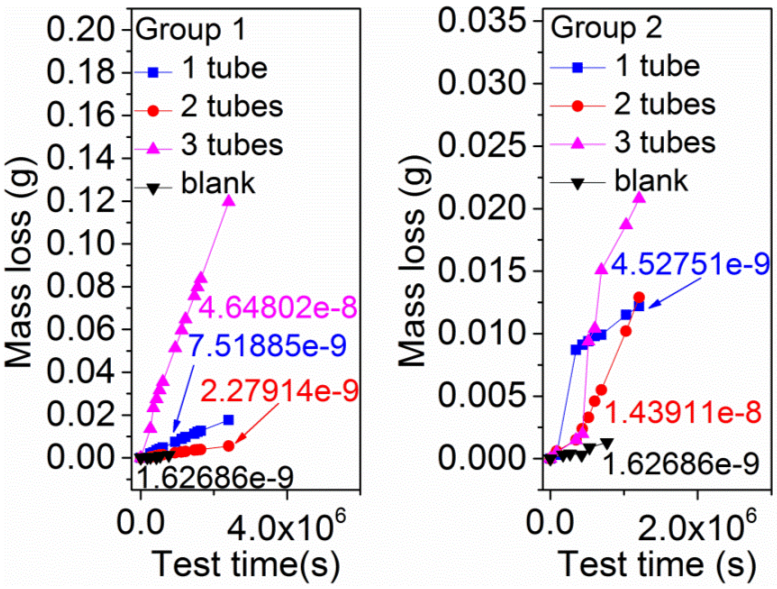

Figure 22 Water conductance in 25 μm silica tubes as a function of the ratios of (a) mean water vapour pressures to saturation pressure and (b) inlet water vapour pressures to saturation pressure. The data points for water vapour flows only are shown as solid symbols, while the data points for interdiffusive flows in air at one atmosphere are shown as hollow symbols. (a) The red patterned zone on the right is where two phase flows occur and the blue patterned zone is where tube filling is expected and Poiseuille flow will apply; (b) Arrow A indicates the excess flow caused by two phase flow for an interdiffusive flow situation (combination interdiffusive flow Eq.(96)). Arrow B indicates the excess flow caused by two phase flow for a water only situation (no background

of air). Excess vapour flow arising from reduced tangential momentum accommodation is shown as cross hatching. (c) Two examples of interdiffusive mass losses as a function of time for one, two and three tubes operating in parallel. The rapid mass loss increases "jumps" for two and three tubes shown in Group 2 are attributed to occasional ejection of liquid slugs.

Table 7 Experimental results for the mass conductance as a function of the partial pressure of water vapour at inlet and outlet of the tube.

Weight Concentration of Glycerol	P_i ***(Pa)***	P_o ***(Pa)***	C ***(m s)***
95%	425.6	0	8.48784e-18
90%	771.4	0	1.22641e-17
84%	997.5	0	1.257e-17
70%	1729	0	1.79752e-17
50%	2128	0	1.55146e-17
0	2702.3	0	2.18015e-15

The aim of a testing procedure is to detect the presence of flow paths through tubes that in practice might be described as "leaks". It is important to discriminate between tests done in the absence of air and tests done in the presence of air, since this determines whether interdiffusive flow applies. It is also important to determine whether the liquid water is likely to be present at the inlet by considering the partial pressure of water vapour in comparison to the tube condensation pressure P_c as determined by the Kelvin equation (Eq.(81)).

6.5 CONCLUSION

We have found using two different experimental methods, that water vapour flows in the presence of air have contributions from vapour flow and at least one flow mode involving the liquid phase. In applying the results of this work to the measurement of the moisture flow rates through very small leaks, it is important to recognize that the slip length for liquid water flows is the critical parameter in determining whether it is possible to estimate the flow from a gas penetration test using helium. Since the slip length for water

is not known from a helium penetration test, a significant recommendation of this work is that encapsulations requiring high levels of water hermeticity should be tested directly for their water leak rate rather than relying on a test using an ideal gas surrogate such as helium.

REFERENCES

1. Nair, R.R., et al., *Unimpeded permeation of water through helium-leak-tight graphene-based membranes.* Science, 2012. **335**: p. 442-444.
2. Marrero, T.R. and E.A. Mason, *Gaseous Diffusion Coefficients.* J. Phys. Chem. Ref. Data 1972. **1**: p. 3-118.
3. Chapman, S. and T.G. Cowling, *The Mathematical Theory of Non-Uniform Gases.* 3 ed. 1970, UK: Cambridge University Press.
4. Bogatyrev, A.F. and M.A. Nezovitina, *Interdiffusion Coefficients in Actual Gaseous Systems.* J. Eng. Phys. Thermophys., 2012. **85**: p. 1208-1214.
5. Barajas, L., L.S. García-Colín, and E. Piña, *On the Enskog-Thorne Theor for A Binary Mixture of Dissimilar Rigid Spheres.* J. Stat. Phys., 1973. **7**: p. 161-183.
6. Bennett, D.E., *Density Effects on the Transport Coefficients of Gaseous Mixtures.* J. Chem. Phys., 1969. **51**(7): p. 2811-2825.
7. Remick, R.R. and C.J. Geankoplis, *Binary Diffusion of Gases in Capillaries in the Trasition Region between Knudsen and Molecular Diffusion.* Ind. Eng. Chem. Fundam., 1973. **12**: p. 214-220.

8. Ernst, M.J. and H.F. Hemond, *Multicomponent Vapor Transport Model for Viscous, Transitional, and Molecular Flow.* J. Vac. Sci. Technol. A, 1995. **13**: p. 2962-2971.

9. Neto, C., et al., *Boundary Slip in Newtonian Liquids: A Review of Experimental Studies.* Rep. Prog. Phys., 2005. **68**(12): p. 2859-2897.

10. Sui, H.X., et al., *Structural basis of water-specific transport through the AQP1 water channel.* Nature, 2001. **414**: p. 872-878.

11. Holt, J.K., et al., *Fast mass transport through sub-2-nanometer carbon nanotubes.* Science, 2006. **312**: p. 1034-1037.

12. Cottin-Bizonne, C., et al., *Nanohydrodynamics: The Instrinsic Flow Boundary Condition on Smooth Surfaces.* Langmuir, 2008. **24**: p. 1165-1172.

13. Cottin-Bizonne, C., et al., *Boundary Slip on Smooth Hydrophobic Surfaces: Intrinsic Effects and Possible Artifacts.* Phys. Rev. Lett. , 2005. **94**(5): p. 0561021-0561024.

14. Huang, D.M., et al., *Water Slippage versus Contact Angle: A Quasiuniversal Relationship.* Phys. Rev. Lett. , 2008. **101**(22): p. 2261011-2261014.

15. Sendner, C., et al., *Interfacial Water at Hydrophobic and Hydrophilic Surfaces: Slip, Viscosity, and Diffusion.* Langmuir, 2009. **25**(18): p. 10768-81.

16. Glycerine Producers' Association, *Physical Properties of Glycerine and Its Solutions*. 1963: Glycerine Producers' Association, New York.

17. Serizawa, A., Z. Feng, and Z. Kawara, *Two-Phase Flow in Microchannels.* Exp. Therm. Fluid Sci., 2002. **26**: p. 703-714.

Chapter 7 Recommendations for Hermeticity Testing

Based on the theories for various leak types we discussed above, theory of Cha and McCoy (Eq.(64)) for ideal gas, Poiseuille flow (Eq.(42)) for liquid, meniscus evaporation into air and vacuum (Eq.(86)), Washburn theory for capillary filling (Eq.(84)), surface flow (Eq. (78)), we know that the flow rates for various type of leaks are different. To predict accurate flow rates for a known structure channel or material, it is important to confirm the leak type first. Channel size is another important factor to be considered, since unexpected phenomenon of moisture penetrating occurs in carbon nanotubes. In this chapter, we summarise the experimental results described in previous chapters and compare them with theories for a wide range of channel diameter (0.1 to 10^5 nm).

For making a bridge between our 25 μm channel and carbon nanotubes from literature, we measured flow rates for 1.7 μm channel (Polymicro Technologies, Australia) using mass loss method under three conditions (see Figure 21): channels above liquid water surface; one end of channels immerged in liquid water surface; channels immerged in liquid water and vials inverted.

In Figure 23, we show four types of leak (*a*-*d*) that allow moisture to penetrate an initially dry chamber that may contain air. These leak types are intended to represent real cases for an encapsulation operating in an environment such as the human body. The outside environment is either saturated humid air as in leaks *a* and *b*, or liquid water as in leaks *c* and *d*. Data from the literature is supplemented by our new experimental results in

Figure 23 to show the state of agreement between theory and experiment for the four kinds of water leaks. For purposes of comparison, we have converted the flow rate to that for a 1 mm channel.

Type a leaks are a flow of water vapour in a channel that may also contain air or other gases, with a possible contribution from a surface diffusive flow in which a very thin layer of adsorbed water molecules on the channel wall diffuses into the chamber.

Type b leaks have one or more slugs of liquid water condensed in the channel. Such slugs form readily in small channels, even when the vapour pressure at the inlet is less than the saturation pressure, as the Kelvin pressure for capillary condensation is always less than the saturation pressure. Without a total pressure gradient, the flow takes place by condensation onto the meniscus nearer the inlet and evaporation from the meniscus nearer the outlet. In the absence of a background gas, there is a pressure gradient in the slug caused by the vapour pressure gradient across the channel. In the presence of a background gas that maintains a constant total pressure on both sides of the slug, liquid flow could occur by drying and refilling of the slug. If the total pressure is not maintained constant, small "adventitious" pressure gradients arising from changes in atmospheric pressure or changes in ambient temperature can cause flow.

Type c leaks are driven by capillary filling from a reservoir of liquid water at the inlet. A single meniscus forms in the channel, with a continuous connection to the much larger volume of water outside. Water is drawn in by the Laplace pressure difference across the meniscus, a very large pressure for small channels. The channel fills, as described by the Washburn model [1] enabling water vapour to enter the encapsulation as the meniscus

nearer the outlet evaporates. Under some conditions the evaporating meniscus reaches the outlet as shown in Figure 23.

Type d leaks occur when there is a reservoir of liquid water at both inlet and outlet. This occurs when the encapsulation contains accumulated excess water that is present at the channel outlet. The channel is completely filled with liquid and both entrance and exit are connected to liquid reservoirs so that no meniscus forms in the channel. The flow is driven entirely by environmentally imposed or adventitious pressure gradients.

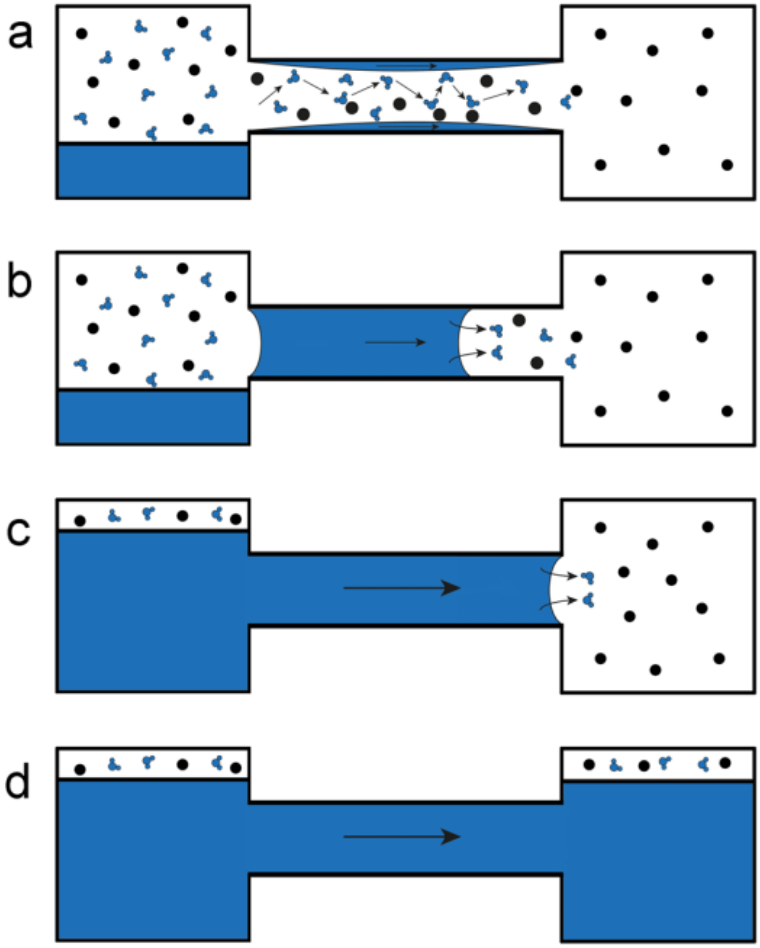

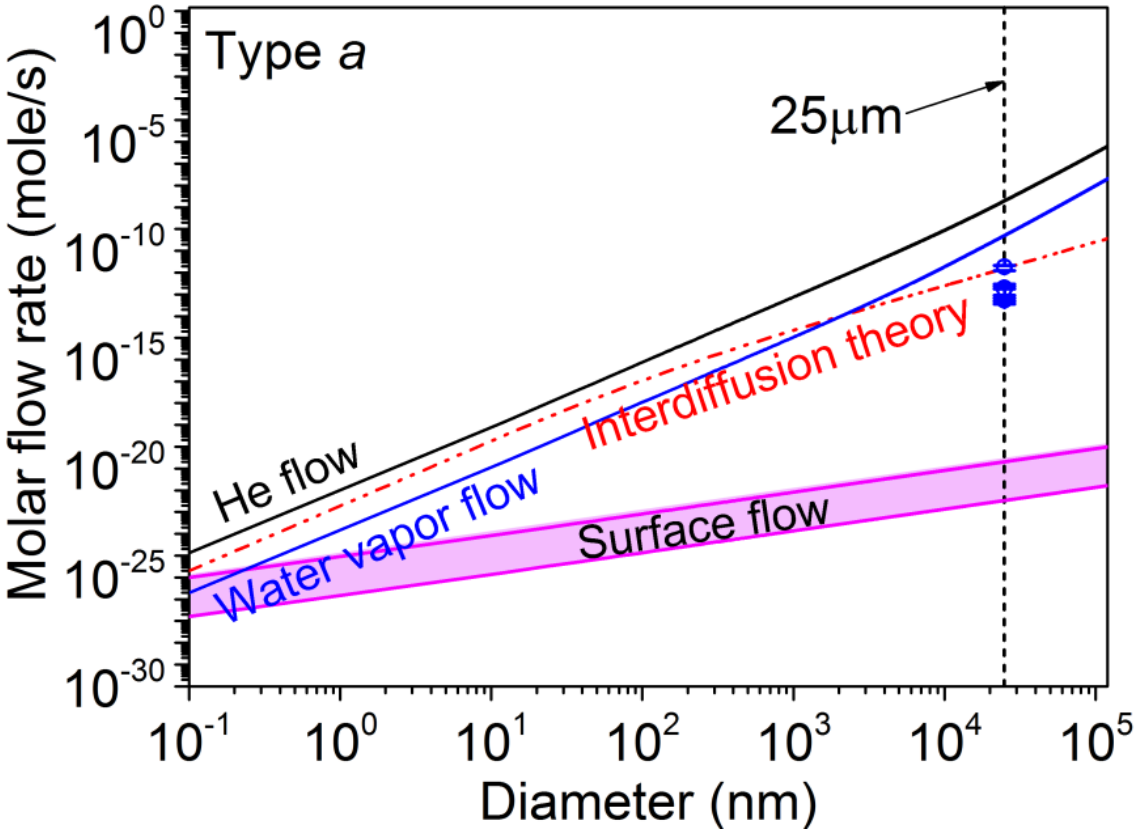
Type a
25μm
He flow
Water vapor flow
Interdiffusion theory
Surface flow
Molar flow rate (mole/s)
Diameter (nm)

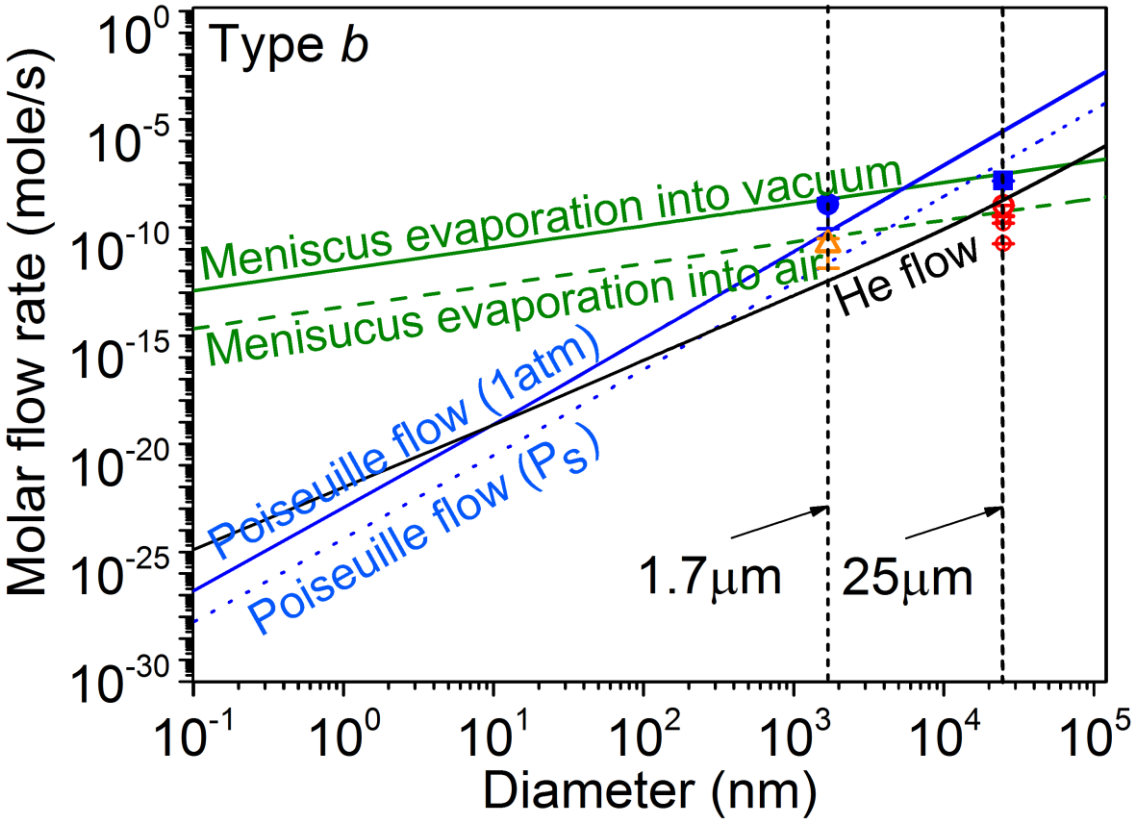
Type b
Meniscus evaporation into vacuum
Menisucus evaporation into air
Poiseuille flow (1atm)
Poiseuille flow (Ps)
He flow
1.7μm
25μm
Molar flow rate (mole/s)
Diameter (nm)

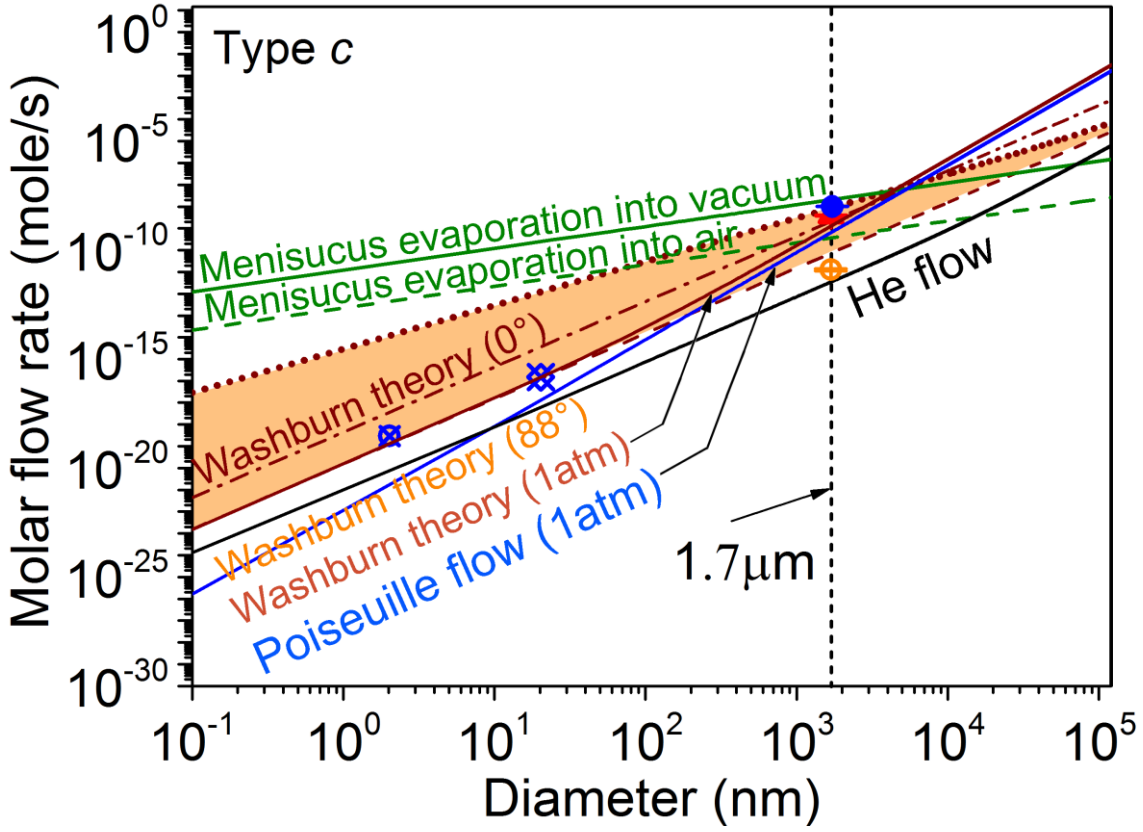
Type c
Molar flow rate (mole/s)
Diameter (nm)
Menisucus evaporation into vacuum
Menisucus evaporation into air
Washburn theory (0°)
Washburn theory (88°)
Washburn theory (1atm)
Poiseuille flow (1atm)
He flow
1.7μm

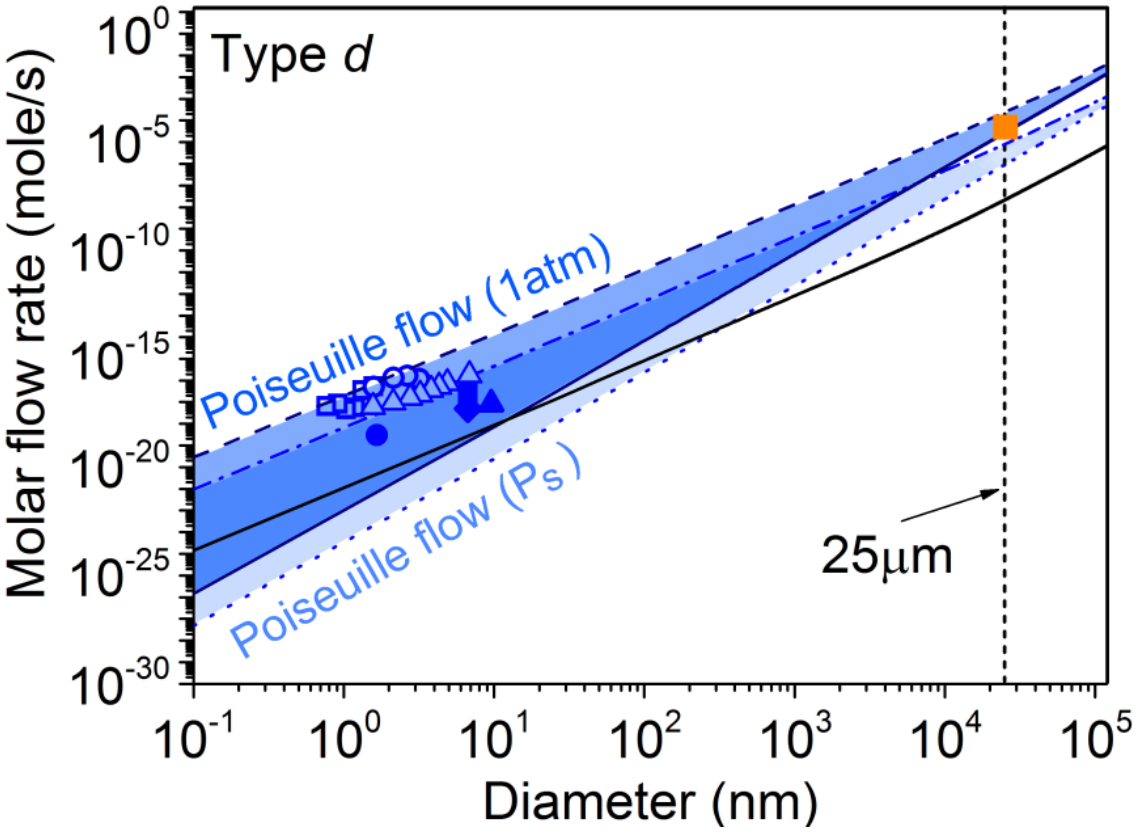
Type d
Molar flow rate (mole/s)
Diameter (nm)
Poiseuille flow (1atm)
Poiseuille flow (Ps)
25μm

Figure 23 Schematic diagrams of four types of moisture leak (*a*-*d*) and corresponding theory for the molar flow rate as a function of channel diameter for 1mm long channels. The points for type *a* leaks are our experimental results for water vapour interdiffusion into air (1 atm) at five relative humidities, matching interdiffusion theory; The points for type *b* leaks are our measurements for saturated air at the inlet. For the 25 μm channel, a meniscus is present that limits the flow; For channels smaller than 1.4 μm (pressure difference of 1 atm) or 4.4 μm (pressure difference of saturation pressure, P_s), Poiseuille flow will limit flow, as shown for our experimental point at 1 μm where evaporation is into air; The points for type *c* leaks for the 25 μm channel are for the case where air is present at 1 atm, limited by meniscus evaporation into air; for the 1 μm channel the points refer to the case when only water and its vapour are present, limited by meniscus evaporation into vacuum; the points for 2 nm and 20 nm channels are those of Lee and Hwang [2] and Tzevelekos et al. [3] respectively which agree with Washburn flow for 88° contact angle and no slip; The theory for type *d* leaks is Poiseuille flow, driven by either 1 atm pressure difference or saturation pressure difference, at slip length of 24.26 μm. The points for type *d* leaks at 25 μm and 1 μm are our measurements and the other points are for carbon nanotubes: theoretical simulation results from Li et al. [4] (squares), Thomas and McGaughey [5] (circles) and Thomas et al. [6] (triangles) and experimental results from Holt et al. [7] (filled circle), Majumder et al. [8] (filled square), Majumder et al. [9] (filled diamond) and Du et al. [10] (filled triangle).

For a Type *a* leak, the flow of moisture through the channel is driven by a concentration gradient of water vapour. The flow is carried partly by water vapour flow and partly by surface diffusion. Surface diffusion is important only for nanodimensioned leaks and its flow rate is described in Section 5.2.2. Surface flows with a surface diffusion coefficients of 0.2 m^2/s and 12 m^2/s is, which are the lowest and the highest values among those reported for various gases [11]. When air is present with no total pressure gradient, the flow is described by interdiffusion theory (Eqs.(91) (95) (96)). The mass flow rates of Eqs.(91) (95) (96)) are converted to molar flow rates of H_2O with saturated air outside the encapsulation and dry air inside, both at 1 atm. The results are shown in Figure 23. Water vapour flow in the absence of air and helium flow also in the absence of air (relevant for a helium leak test) are also shown. These latter two curves are calculated from the equation of Cha and McCoy (Eq.(64)). We use a value of α of 1 and 5 for c_0 for both water vapour and helium. The experimental points shown in Figure 23 for the type a leak are our results for a 25 μm silica tube at five relative humidities close to but less than P_s. The experimental points lie just below the theory line as expected.

For a Type *b* leak, we consider only the highest flow case, where the slug fills the channel. Without a total pressure difference, the flow consists of condensation of vapour onto one meniscus, classical Poiseuille flow in the slug and evaporation from the other meniscus. Interdiffusive flow across a phase boundary (e.g.: menisci and drops) was studied in Section 5.2.4 (Eq.(86)). In Figure 23 for type *b* leaks, the meniscus evaporation rate limits the flow. Evaporation takes place into vacuum or air depending on the application. The limiting flow rate for tubes larger than approximately 1.4 μm (pressure difference of P_s) and 4.4 μm (pressure difference of 1 atm) is given by Eq.(86), while for smaller channels the Poiseuille flow provides the limit. In Figure 23 two cases of Poiseuille flow are shown, depending on the driving pressure difference (1 atm or P_s). The meniscus may withdraw into the channel as evaporation takes place, whereupon Kelvin capillary condensation acts to refill the channel. An oscillatory solution for this type of flow has been discussed by Rand [12]. Changes in atmospheric pressure or changes in temperature cause this type of flow to "surge" as liquid slugs are ejected and reform, named "jumps" (Figure 22(c)). Our experimental results for the 25 μm channel are for evaporation into air and into vacuum and agree with the limit imposed by meniscus evaporation into air and vacuum. Our experimental results for the 1 μm channel are for evaporation into vacuum with relative large fluctuations because of jumps.

In the Type *c* leak, capillary filling occurs by Washburn flow [1] in which the unbalanced Laplace pressure of the single meniscus draws in the liquid from the outside reservoir against the frictional forces described by the Poiseuille law until the meniscus approaches its final position where it remains, allowing water to evaporate into the encapsulation. For short channels the meniscus will reach the outlet. For smaller channels the meniscus

evaporation rate exceeds the mass flow rate for capillary filling so that the Washburn equation (Eq.(84)) determines the flow rate. The Washburn flow rate is shown in Figure 23 as a function of channel diameter for contact angles of zero and 88^o (as an example for relatively hydrophobic channel) without slip ($\varsigma = 0$). A contact angle of zero gives a higher Washburn flow rate because the Laplace pressure difference across the interface depends on the surface curvature, highest for the smallest contact angles. The orange zone in the figure defines the most probable range of Washburn flow rates that would be encountered for a hydrophobic channel with contact angle of 88°. The lower limit is defined by zero slip length and the upper limit is defined by the largest observed slip length in carbon nanotubes [5] ($\varsigma = 24.26$ μm). Additional atmospheric pressure difference across the channel provides a higher flow rate when the diameter is larger than 4.5 μm while for small channels, the Laplace pressure is so large that the effect of an additional 1 atm pressure is not observable. For the channels larger than about 200 nm, Washburn theory with additional 1 atm is close to Poiseuille flow with 1 atm as a total pressure gradient. For our 1 and 25 μm channels, the experimental results, in the case where the channels immerged in liquid water (shown in Figure 21), may either from type *c* or type *d* leaks.

For the type *d* leak, viscous liquid (Poiseuille) flow applies (Eq.(42)). In the absence of a total pressure gradient, this leak would produce no flow, but if there were a total pressure gradient of 1 atm, the flow rate would occur. This flow rate is useful for comparison with the other leaks in cases since adventitious or environmentally imposed pressure gradients are common in applications: for example, 1 atm total pressure gradient could occur if the encapsulation were immersed under water to give an external pressure of 2 atm, while the

interior remained at 1 atm. In some channels, slip flow may apply, giving an accelerated flow determined by the slip length. The recent availability of nanodimensioned channels in the form of carbon nanotubes and carbon nanopipes has enabled measurements in very small channels of well-defined dimensions [7-10] that reveal flow rates of liquid water greatly exceeding the Poiseuille result with no slip. These results are shown in Figure 23 for type *d* leaks. For liquid water Poiseuille flows, the excess flow is attributed to slip flow against the smooth walls. In Figure 23 we show the Poiseuille flow as the blue regions (light blue: pressure difference of saturation pressure, dark blue: pressure difference of 1 atm) defined by a lower boundary with no slip boundary conditions and an upper boundary defined by a slip length of 24.26 μm that is the largest obtained from Thomas and McGaughey [5]. The experimental point for the 25 μm channel (the same with type *c*) is smaller than both the Washburn theory with additional 1 atm and Poiseuille flow (1 atm). The experimental point for 1 μm channel (the same with type *c*) agrees better with the limit imposed by Washburn flow than Poiseuille flow for evaporation into vacuum with an additional 1 atm imposed pressure.

It is clear from this work that a helium leak test has limitations for predicting moisture penetration rates. For a type *a* leak, the helium flow rate overestimates the flow of water at all scale sizes. The overestimation is most severe for large channels in the presence of air, where interdiffusive theory operates. For small channels in type *a* leak, the correction factor expected from Graham's law, namely 0.53 can be applied. For a type *b* leak, helium flow approximates water flow for channels large than about 1 μm, while for smaller channels, it ovestimates the Poiseuille flow that limits water flow, except if large slip length applies. For a type *c* leaks, He flow underestimates flow at all scale sizes. The

underestimation is most severe at small scale sizes, even when slip flow does not apply, but when it does apply, the water flow could be as much as 8 orders of magnitude higher. For type *d* leaks, helium flow underestimates water flow at large scale sizes and at small scale sizes in the presence of slip. The results of comparison between helium flow rate and moisture flow rates are summarized in Table 8.

Table 8 Flow modes that exceed He for a 1 mm length channel, for various channel diameters.

Diameter (nm)	Flow types	Flow modes exceeding He
<10	Type *b*	Meniscus evaporation into air/vacuum
	Type *c*	Washburn theory
	Type *d*	Poiseuille flow (1 atm/P_s) with slip length
10~350	Type *b*	Meniscus evaporation into air/vacuum
	Type *c*	Washburn theory
	Type *d*	Poiseuille flow (1 atm) with or without slip length, Poiseuille flow (P_s) with slip length
350~7×10^4	Type *b*	Meniscus evaporation into vacuum
	Type *c*	Washburn theory
	Type *d*	Poiseuille flow
> 7×10^4	Type *c*	Washburn theory
	Type *d*	Poiseuille flow

There is a straightforward comparison of water vapour and helium molar flow rates in the molecular flow regime corresponding to the elementary relation known as *Graham's Law*, giving the result for the ratio of the molar flow rate of water vapour to that of helium for the same mean pressure is given by $\sqrt{M_{He}/M_{H_2O}}$ =0.471. In our calculation on the basis of the theory of Cha and McCoy (Eq.(64)), the ratio of molar flow rate is 0.471 which for ideal gases is the same with the result of Graham. The only experimental measurement of the ratio of helium to water vapour flow rates available in the literature appears to be that of Lee and Hwang [2] for flows in porous Vycor glass at 70°C where the tube size was estimated to be 2 nm. From Figures 5 and 8 and Table V of their paper, it is possible to

obtain a value of 0.41 for the ratio of volume permeabilities of helium to water vapour at a temperature of 70°C. This compares well with the theoretically derived ratios.

In this chapter, we have defined four types of moisture leak and developed theory for predicting their water and helium gas flow rates, both in the presence and absence of a background gas. For nanoscale channels the theory has been validated by comparison with results in the literature. The behaviour of water in leaks is surprisingly diverse and in some cases remarkably efficient, so much so that the use of a simple helium leak test for predicting the hermeticity of an encapsulation is not adequate. In cases where Laplace pressure drives capillary filling, a helium leak test will severely underestimate flow and if slip boundary conditions also apply, the underestimation can be as high as 8 orders of magnitude. We conclude that helium is not a reliable reference for moisture testing. Encapsulations requiring high levels of water hermeticity should be tested directly for their water leak rate rather than relying solely on a test using an ideal gas surrogate such as helium.

REFERENCES

1. Washburn, E.W., *The Dynamics of Capillary Flow.* Physical Review, 1921. **17**: p. 273-283.
2. Lee, K.-H. and S.-T. Hwang, *The Transport of Condensible Vapors through a Microporous Vycor Glass Membrane.* J. Colloid Interface Sci., 1985. **110**(2): p. 544-555.

3. Tzevelekos, K.P., et al., *On the possibility of characterising mesoporous materials by permeability measurements of condensable vapours theory and experiments.* Adv. Colloid Interface Sci., 1998. **76-77**: p. 373-388.

4. Li, Y., J. Xu, and D. Li, *Molecular Dynamics Simulation of Nanoscale Liquid Flows.* Microfluidics Nanofluidics, 2010. **9**: p. 1011-1031.

5. Thomas, J. and A. McGaughey, *Water Flow in Carbon Nanotubes: Transition to Subcontinuum Transport.* Phys. Rev. Lett., 2009. **102**(18).

6. Thomas, J.A., A.J.H. McGaughey, and O. Kuter-Arnebeck, *Pressure-driven water flow through carbon nanotubes: Insights from molecular dynamics simulation.* Int. J. Term. Sci., 2010. **49**: p. 281-289.

7. Holt, J.K., et al., *Fast mass transport through sub-2-nanometer carbon nanotubes.* Science, 2006. **312**: p. 1034-1037.

8. Majumder, M., et al., *Enhanced flow in carbon nanotubes.* Nature, 2005. **438**: p. 44.

9. Majumder, M., N. Chopra, and B. J.Hinds, *Mass transport through carbon nanotube membranes in three different regimes: Ionic diffusion and gas and liquid flow.* ACS Nano, 2011. **5**: p. 3867-3877.

10. Du, F., et al., *Membranes of vertically aligned superlong carbon nanotubes.* Langmuir, 2011. **27**: p. 8437-43.

11. Gilliland, E.R., et al., *Diffusion on surface. I. Effect of concentration on the diffusivity of physically adsorbed gases.* Ind. Eng. Chem. Fundam., 1974. **13**: p. 95-100.

12. Rand, R.H., *The dynamics of an evaporating meniscus.* Acta Mech., 1978. **29**: p. 135-146.

Chapter 8 Conclusion

The subject of ultra-fast flows in nanotubes and new membrane materials such as graphene oxide has attracted many researchers and is developing quickly. Holt et al., Majumder et al. and Nair et al. all demonstrated enhanced water liquid flow in carbon nanotubes and Holt et al. also showed enhanced air flow rates. In contrast, Gruener and Huber did not find the enhanced flow rates in silicon nanotubes. This thesis provides understanding of water behaviour in micro- and nano-tubes theoretically and experimentally and fills the gap in knowledge of water vapour flows with and without air as background transporting through microtubes.

The main findings of this thesis are that (1) nitrogen flow obeys the theory of Cha and McCoy with different TMAC in slip flow regime and molecular flow regime. The extended theory based on the theory of Cha and McCoy with Arya's diffusivity should replace Smoluchowski's diffusivity for ultra-smooth channels. (2) Water vapour transporting in microtubes has close relation with the surface properties of the channel. Hydrophilic channels provide $\alpha = 1$ for water vapour because water molecules prefer to adsorb on the hydroxyl groups on the surface of the channel, which provides a diffusive reflection. Hydrophobic channels provide a small value of α because the groups on the surface of channel prefer to repel the incident water molecules. The repelled water molecules could gather into the lower topography on the surface and form chain-like groups to smooth the wall surface, which provides a specular reflection. This specular reflection only occur in a limited range of relative humidity since when the surface is fully covered with water molecules it will behave like a hydrophilic surface then. In this

limited range of relative humidity, enhanced flow rates of water vapour than expected from the theory of Cha and McCoy are obtained. When the relative humidity is close to 1, two-phase flow occurs, which provides another enhanced flow rates. (3) Interdiffusion theory has been tested for interdiffusive flow of water vapour. It shows that experimental results obeys the theory when the relative humidity is smaller than 1. Two-phase flow also occurs when the relative humidity is close to 1 as the case for water vapour flow only. (4) Four types of leaks has been developed. Theories for vapour phase, liquid phase and two-phase flows of water with and without atmospheric air as background gas have been plotted as a function of channel diameter. The comparison of flow rates from these theories and helium flow rates shows that helium leak testing as a commonly used method in industry underestimates moisture leak rates for type *c* and *d* leaks much (up to 8 orders) and part of type *b* leaks. Therefore, encapsulations requiring high levels of water hermeticity should be tested directly for their water leak rate rather than relying solely on a test using an ideal gas surrogate such as helium.

For further study, there are several areas can be further investigated:

(1) Test method: We used two test methods in this thesis: the two-chamber method and the mass loss method. They both have limitations which are that the outgassing rate of the chamber for the two-chamber method and accuracy of the microbalance for the mass loss method. Therefore, the methods we used cannot measure flow rates for small tubes (< 1 μm) during a proper period. To solve this problem, mass spectrometry will be a good method.

(2) Surface modification: The microtubes we used were heated to 1000°C during manufacture. This is one way of surface modification. If we could treat the surface

using other methods, such as plasma surface treatment or chemical solution immersing, we could obtain a comprehensive understanding on the relation between TMAC and surface conditions.

(3) Nanotubes: We only did theoretical predictions for nanochannels but no experiments. As far as we know, there are no studies on water vapour transport through nanotubes yet.

Appendix: Nomenclature

$\dot{m}$	mass flow rate	d_m	molecular diameter
A	cross sectional area of the aperture	P_{mass}	mass permeability
C	mass conductance	l	thickness of medium
ΔP	pressure difference	c_i	internal concentration in the inlet side of membrane
P_i	pressure on the inlet side of the membrane/tube	S_H	henry law solubility
P_o	pressure on the outlet side of the membrane/tube	P_{volume}	volume permeability
$\dot{n}$	particle flow rate	k	intrinsic Darcy's law permeability
m_m	molecular mass	μ	dynamic viscosity
$\dot{V}$	volume flow rate	J_1	particle flux of species 1
ρ	fluid density	D_{12}	mutual Fick's law interdiffusion coefficient
$\bar{v}$	average flow velocity	D_T	thermodiffusion coefficient
c	particle concentration	Re	Reynolds number
P_T	total pressure	d_h	hydraulic diameter
P_1 or P_2	partial pressure	p_w	wetted perimeter of the tube
V	volume	Kn	Knudsen number
n	number of particle	l_0	characteristic dimension of the tube
k_B	Boltzmann constant	h	height of rectangular tube
T	temperature	r_c	radius of a tube
c_1 or c_2	partial concentration	D_K	Knudsen diffusion coefficient
D_F	Fick's law diffusion coefficient		
$\bar{u}_m$	mean molecular speed		
λ	mean free path		

H	a shape dependent length ($2r_c$)	$\dot{m}_{slip}$	mass flow rate in slip flow regime
α	tangential momentum accommodation coefficient	σ_p	first velocity slip coefficient
$\boldsymbol{u}$	bulk velocity	k_λ	$\frac{\sqrt{\pi}}{2}$ (hard sphere model)
$\boldsymbol{v}$	particle velocity	Kn_m	mean Knudsen number
Q	collision term in Boltzmann equation	S	normalised flow rate
f	phase space distribution function	$\dot{m}_{slip-S}$	mass flow rate in slip flow regime with the second boundary conditions
f^0	absolute Maxwellian distribution function	A_1	$=\frac{\sigma_p}{k_\lambda}$
n_0	equilibrium number density	A_2	$=\frac{\sigma_{2p}}{{k_\lambda}^2}\frac{\pi-1}{\pi+1}$
$\mathrm{h}(\boldsymbol{r},\boldsymbol{v},t)$	perturbation distribution function	σ_{2p}	second velocity slip coefficient
f_{loc}	local Maxwellian distribution function	$\boldsymbol{\sigma_s}$	shear stress tensor
n_{loc}	local number density	N	$=4Kn/\sqrt{\pi}$
$\boldsymbol{g}$	gravitational acceleration	r^*	dimensionless radial coordinate
$\boldsymbol{\sigma}$	total stress tensor from pressure gradients and shear stresses	u^*	dimensionless velocity
L	tube length	U	centreline velocity in cylindrical tube
D_v	volumetric dilation	β	$\frac{{r_c}^2\Delta P}{\mu UL}$
$\dot{m}_P$	mass flow rate from Poiseuille law	c_1, c_2, c_3, c_4	constants determined by boundary conditions and the limits for low and high *Kn*
$\dot{m}_{continuum}$	mass flow rate in continuum flow regime	J_0, Y_0	Bessel functions of first and second kinds of zero order
P_m	mean pressure	c_0	empirical parameter in Cha & McCoy theory
Π	$P_i\ /P_o$		
u_w	velocity of flow at the walls		

$u_{continuum}$	velocity profile in continuum flow regime
ϵ	$\frac{2-\alpha}{\alpha}\frac{64}{3\pi}$
G	nondimensional flow rate
V_2	volume of Chamber 2
δ	$\frac{dT/T}{dP_2/P_2}$
$P_{0f}(t)$	linear fitting function
a'	slope of the linear fitting function
b'	intercept of the linear fitting function
D_{mS}	Smoluchowski diffusivity
α'	ensemble average of the diffusion fraction
ϵ'	cutoff parameter of Smoluchowski diffusivity
Q_1	adsorption heat of the first adsorbed layer
Q_i	adsorption heat of further adsorbed layers
Γ	amount of adsorption at an interface
K_L	ratio of adsorption to desorption rate
Γ_{mon}	particle number adsorption per square meter in a full monolayer
P_s	saturation pressure
$\boldsymbol{C}_B$	a constant depends on the binding properties of the surface
$\boldsymbol{C}$	a constant describing the binding condition between molecules and the surface
R	ideal gas constant
t_l	thickness of adsorbed multilayers
V_t	specific volume
S_t	specific surface area
D_s	surface diffusion coefficient
Γ'	surface concentration in particles per unit area of the condensed vapour
$\Delta P'$	Laplace pressure
γ	surface tension
r_1 and r_2	principal radii of curvature of the interface
χ	contact angle
P_c	condensation pressure in a tube
$\dot{m}_{meniscus}$	mass flow rate of evaporation from a meniscus
σ_c	condensation coefficient
P'	actual pressure above the meniscus
A_s	a constant for the equation for $\dot{m}_{meniscus}$
$C_{surface}$	mass conductance of surface diffusion
C_P	mass conductance of Poiseuille flow
Γ_1	first Langmuir adsorption

Γ_2	second Langmuir adsorption
K_1, K_2	Langmuir constants
α_0	TMAC for dry surface
α_1	TMAC for passivation layer
α_2	TMAC for bulk-water-like layer
f	enhancement factor for the smoothing effect
S	scale factor
$\dot{m}_{KI}$	mass flow rate of Knudsen interdiffusive flow
d_{m12}	average molecular diameter
D_t	total diffusion coefficient
$\dot{m}_{P-modified}$	mass flow rate for modified Poiseuille law
ς	slip length